

[REDACTED]

[REDACTED]

FACILITY FORM 602	<u>N66 30750</u> (ACCESSION NUMBER)	_____ (THRU)
	<u>169</u> (PAGES)	_____ (CODE)
	<u>CR-76254</u> (NASA CR OR TMX OR AD NUMBER)	<u>32</u> (CATEGORY)

[REDACTED]

**GENERAL DYNAMICS**  
*Convair Division*

[REDACTED]

A2136-1 (REV. 5-65)

GPU PRICE \$ \_\_\_\_\_

CFSTI PRICE(S) \$ \_\_\_\_\_

Hard copy (HC) # 5.00

Microfiche (MF) 1.00

**(GDDDD)****GENERAL DYNAMICS | ASTRONAUTICS****STUDY OF STABILITY OF UNPRESSURIZED  
SHELL STRUCTURES UNDER STATIC LOADING****FINAL REPORT  
VOLUME I****Contract Number NAS8-11181  
Request Number DCN 1-5-53-01067**

Prepared for the  
George C. Marshall Space Flight Center  
National Aeronautics and Space Administration  
Huntsville, Alabama

PREPARED BY George W. Smith  
George W. Smith  
Frank A. Dittoe  
Frank A. Dittoe

APPROVED BY E. H. Hausrath  
A. H. Hausrath  
Structures Group Engineer  
APPROVED BY D. J. Peery  
D. J. Peery  
Chief of Structural Analysis

Advanced Structures Group (Mail Zone 587-30)  
Research, Development and Engineering Department  
General Dynamics Convair Division  
Post Office Box 1128  
San Diego, California 92112

**REVISIONS**

NO.	DATE	BY	CHANGE	PAGES AFFECTED

ACKNOWLEDGEMENTS

This study was conducted at General Dynamics Convair Division by G. W. Smith and F. A. Dittoe under the technical direction of Dr. A. H. Hausrath, Group Engineer, Advanced Structures Group, who acted in the capacity of program leader. Programming for the digital computer was accomplished by Mrs. L. S. Fossum and Mrs. N. L. Fraser of the Technical Programming Group, and J. R. Anderson of the Guidance and Trajectory Programming Group.

Acknowledgement is made of the encouragement and advice furnished by E. E. McClure of the Advanced Structures Group.

Appreciation is expressed to H. R. Coldwater and H. L. Billmayer of the Structures Division, Propulsion and Vehicle Engineering Laboratory, Marshall Space Flight Center, for their support of the study. In the role of NASA Technical Representative, Mr. Billmayer provided valuable assistance in the definition and achievement of the study goals.

The entire report was typed by Mrs. F. C. Jaeger of the Convair Advanced Structures Group.

ABSTRACT

30750

This final report covers the work performed by General Dynamics Convair Division under NASA Contract NAS8-11181, "Study of Stability of Unpressurized Shell Structures Under Static Loading." The primary intent of this study was to employ orthotropic shell theory to develop practical working tools for the prediction of instability in stiffened circular cylindrical shells subjected to axial compression. Emphasis is on approximate analysis techniques to be used in preliminary sizing, rough checking, and the study of trends. Methods for the more stringent requirements of final analysis are also discussed and a digital computer program is provided for such applications. In addition to considering the overall buckling strength of the stiffened shell, curves are also presented for predicting the buckling of curved isotropic skin panels such as those found between stiffening elements. The report is divided into two distinct parts. Part I furnishes the theoretical and empirical foundations for the proposed methods while Part II gives concise procedures for the practical application of these methods.

CONTENTSVOLUME I

<u>Section</u>	<u>Title</u>	<u>Page</u>
	ACKNOWLEDGEMENTS	ii
	ABSTRACT	iii
	LIST OF FIGURES	ix
	LIST OF TABLES	xiv
	LIST OF SYMBOLS	xvi
	GLOSSARY	xxv
1	INTRODUCTION	1
2	CONCLUSIONS	6
3	LIMITATIONS	13
4	RECOMMENDATIONS	15

PART ITHEORETICAL AND EMPIRICAL FOUNDATIONS

5	BUCKLING OF ISOTROPIC SKIN PANELS SUBJECTED TO EDGE COMPRESSION	24
	5.1 General	24
	5.2 Buckling Criterion	26
	5.3 Comparisons Against Test Data	32
6	COMPRESSIVE BUCKLING OF LONGITUDINALLY STIFFENED CIRCULAR CYLINDERS	42
	6.1 General	42
	6.2 Buckling Criteria	42

CONTENTS (Cont'd)

<u>Section</u>	<u>Title</u>	<u>Page</u>
	6.2.1 Almroth Extension to Thielemann Solution	42
	6.2.2 Stuhlman-DeLuzio-Almroth Solution	54
	6.3 Fixity Factor for Longitudinally Stiffened Sections Between Rings	73
	6.4 Comparisons Against Test Data	78
	6.4.1 Longitudinally Stiffened Circular Cylinders	78
	6.4.2 Longitudinally Stiffened Circular Cylinders with Frames, Panel Instability Mode	93
7	GENERAL INSTABILITY OF ORTHOTROPICALLY STIFFENED CIRCULAR CYLINDRICAL SHELLS UNDER AXIAL COMPRESSION	98
	7.1 General	98
	7.2 Buckling Criteria	100
	7.2.1 Thielemann Solution	100
	7.2.2 Langley Solution	110
	7.3 Comparisons Against Test Data	119
8	INTERACTION BEHAVIOR	127
	8.1 General	127
	8.2 Axial Compression and Pure Bending	129
	8.3 Axial Compression and External Pressure	133
	8.4 Axial Compression and Internal Pressure	140
	8.5 Axial Compression and Shear	144

CONTENTS (Cont'd)

<u>Section</u>	<u>Title</u>	<u>Page</u>
9	INITIAL IMPERFECTIONS	147
	REFERENCES	159
<u>VOLUME II</u>		
	ACKNOWLEDGEMENTS	ii
	ABSTRACT	iii
	LIST OF FIGURES	ix
	LIST OF TABLES	xiv
	LIST OF SYMBOLS	xvi
<u>PART II</u>		
<u>APPLICATION</u>		
10	GENERAL	164
11	BUCKLING OF ISOTROPIC SKIN PANELS SUBJECTED TO EDGE COMPRESSION	166
	11.1 Procedures	166
	11.2 Design Curves	169
12	COMPRESSIVE BUCKLING OF LONGITUDINALLY STIFFENED CIRCULAR CYLINDRICAL SHELLS	187
	12.1 Procedures	187
	12.2 Design Curves for Bare 7075-T6 Aluminum Alloy	206
13	GENERAL INSTABILITY OF ORTHOTROPICALLY STIFFENED CIRCULAR CYLINDRICAL SHELLS SUBJECTED TO AXIAL COMPRESSION	274

CONTENTS (Cont'd)

<u>Section</u>	<u>Title</u>	<u>Page</u>
	13.1 Procedures	274
	13.2 Design Curves	285
14	INTERACTION BEHAVIOR	312
	14.1 Procedures	312 .
	14.1.1 Axial Compression Plus Pure Bending	312
	14.1.2 Axial Compression Plus External Pressure	314
	14.1.3 Axial Compression Plus Internal Pressure	316
	14.1.4 Axial Compression Plus Shear	316
	14.2 Design Curve	318
15	INITIAL IMPERFECTIONS	320
	15.1 Procedures	320
	15.2 Design Curves	320
16	BUCKLING OF MONOCOQUE CIRCULAR CYLINDERS	323
17	SAMPLE PROBLEMS	330
18	DIGITAL COMPUTER PROGRAMS	334
	18.1 Program for Buckling of Isotropic Skin Panels Subjected to Edge Compression	334
	18.2 Program for the Compressive Buckling of Longitudinally Stiffened Circular Cylindrical Shells	354
	18.3 Programs for General Instability of Orthotropically Stiffened Circular Cylindrical Shells Subjected to Axial Compression	370



CONTENTS (Cont'd)

<u>Section</u>	<u>Title</u>	<u>Page</u>
	18.3.1 Thielemann Solution	370
	18.3.2 Langley Solution	390
	18.3.3 $C_R$ Correction Factor	409
19	REFERENCES	417
Appendix		
A	SUPPLEMENTARY OPTIONS FOR ANALYSIS OF BUCKLING OF ISOTROPIC SKIN PANELS SUBJECTED TO EDGE COMPRESSION	A-1
	A.1 OPTION 2	A-1
	A.1.1 General	A-1
	A.1.2 Buckling Curves	A-2
	A.2 OPTION 3	A-18
	A.2.1 General	A-18
	A.2.2 Buckling Curves	A-18

LIST OF FIGURES

<u>No.</u>	<u>Title</u>	<u>Page</u>
1	Panel Instability	Vol. I, xx
2	General Instability	Vol. I, xxi
3	Anticlastic Bending of Beams	Vol. I, xxiv
4	Nondimensional Logarithmic Plot of Buckling Criteria for Isotropic Skin Panels	31
5	Buckling of Isotropic Skin Panels - Calculated vs. Test ( $\sigma_R$ from OPTION 1)	39
6	Buckling of Isotropic Skin Panels - Calculated vs. Test ( $\sigma_R$ from OPTION 2)	40
7	Buckling of Isotropic Skin Panels - Calculated vs. Test ( $\sigma_R$ from OPTION 3)	41
8	Equilibrium Paths for a Perfect Isotropic Circular Cylinder Subjected to Axial Compression	43
9	Thielemann Notation	45
10	Interaction of Twisting Moments in Wall of Monocoque Cylinder	57
11	Semi-Logarithmic Plot of $\tilde{N}$ vs $\alpha$ with $\eta_s$ as a Parameter	71
12	Buckling Curves for an Infinite Length Column Supported by Equally Spaced Deflectional and Rotational Springs	74
13	Alternative Method for Evaluating Rotational Spring Constant	76
14	Semi-Logarithmic Plot of $\bar{N}$ vs. $\gamma$	103
15	Alternative Ring Loading Conditions	104
16	Semi-Logarithmic Plot of $C_R$ Correction Factor	106

LIST OF FIGURES  
(Continued)

<u>No.</u>	<u>Title</u>	<u>Page</u>
17	Semi-Logarithmic Plot of Compressive Loading Coefficient for the General Instability of Stiffened Circular Cylinders	109
18	Example Interaction Curve	127
19	Combined Axial and Bending Loading Interaction Curve for Orthotropic Cylinders	132
20	Stability Interaction Results for Combined Axial Compression and External Radial Pressure	139
21	Stability Interaction Results for Combined Axial Compression and Internal Radial Pressure	143
22	Interaction of Pure Bending and Torsion for Stiffened Cylinders	146
23	Semi-Logarithmic Plot of $\Gamma$ vs. $R/t$ for Unstiffened Isotropic Cylinders Under Axial Compression	148
24	Load-Displacement Curve for Example Monocoque Cylinder	153
25	Load-Displacement Curve for Example Orthotropic Cylinder	153
26	Geometry of Isotropic Skin Panel	166
27	Buckling of Isotropic Panels	171-182
28	$\frac{b}{R}$ vs. $\frac{R}{t}$ for $\sigma_R = 2\sigma_p$	183-186
29	Fixity Factor vs. Rotational Stiffness Parameter	192
30	Minimization Factor $\tilde{N}$ vs. $\alpha$ and the Parameter $\eta_s$	193
31	Compressive Buckling Stress for Longitudinally Stiffened 7075-T6 Al Alloy Circular Cylinders	210-225
32	Compressive Buckling Stress for Longitudinally Stiffened 7075-T6 Al Alloy Circular Cylinders	226-241

LIST OF FIGURES  
(Continued)

<u>No.</u>	<u>Title</u>	<u>Page</u>
33	Compressive Buckling Stress for Longitudinally Stiffened 7075-T6 Al Alloy Circular Cylinders	242-257
34	Compressive Buckling Stress for Longitudinally Stiffened 7075-T6 Al Alloy Circular Cylinders	258-273
35	Design Curves for the Correction Factor $C_R$	276
36	Critical Compressive Loading Coefficient for the General Instability of Stiffened Circular Cylinders	287-311
37	In-plane Running Shear Load $N_{xy}$	317
38	Design Interaction Curve	319
39	Design Correlation (Knock-down) Factor for Pure Axial Load	321
40	Design Correlation (Knock-down) Factor for Pure Bending	322
41	$\frac{\sigma_{cr}}{E}$ vs. $\frac{R}{t}$ for Unpressurized Monocoque Circular Cylinders (Clamped Ends) Under Pure Axial Load; BEST FIT	324
42	$\frac{\sigma_{cr}}{E}$ vs. $\frac{R}{t}$ for Unpressurized Monocoque Circular Cylinders (Clamped Ends) Under Pure Axial Load; PROBABILITY = 90%, CONFIDENCE = 95%	325
43	$\frac{\sigma_{cr}}{E}$ vs. $\frac{R}{t}$ for Unpressurized Monocoque Circular Cylinders (Clamped Ends) Under Pure Axial Load; PROBABILITY = 99%, CONFIDENCE = 95%	326
44	$\frac{\sigma_{cr}}{E}$ vs. $\frac{R}{t}$ for Unpressurized Monocoque Circular Cylinders (Clamped Ends) Under Pure Bending Moment; BEST FIT	327
45	$\frac{\sigma_{cr}}{E}$ vs. $\frac{R}{t}$ for Unpressurized Monocoque Circular Cylinders (Clamped Ends) Under Pure Bending Moment; PROBABILITY = 90%, CONFIDENCE = 95%	328

LIST OF FIGURES  
(Continued)

<u>No.</u>	<u>Title</u>	<u>Page</u>
46	$\frac{\sigma_{cr}}{E}$ vs. $\frac{R}{t}$ for Unpressurized Monocoque Circular Cylinders (Clamped Ends) Under Pure Bending Moment; PROBABILITY = 99%, CONFIDENCE = 95%	329
47	Input Format - Program 3875.	335
48	Sample Input Data - Program 3875.	340
49	Sample Output Listing - Program 3875.	342-344
50	Flow Diagram - Program 3875.	347
51	Input Format - Program 3896.	355
52	Sample Input Data - Program 3896.	358
53	Sample Output Listing - Program 3896.	360
54	Flow Diagram - Program 3896.	362
55	Input Format - Program 3942.	373
56	Sample Input Data - Program 3942.	376
57	Sample Output Listing - Program 3942.	378
58	Flow Diagram - Program 3942.	381
59	Input Format - Program 3962.	393
60	Sample Input Data - Program 3962.	396
61	Sample Output Listing - Program 3962.	398
62	Flow Diagram - Program 3962.	403
63	Input Format - Program 3942I.	410

LIST OF FIGURES  
(Continued)

<u>No.</u>	<u>Title</u>	<u>Page</u>
64	Sample Input Data - Program 39421.	412
65	Sample Output Listing - Program 39421.	413
66	Flow Diagram - Program 39421.	415
67	Buckling of Isotropic Panels (OPTION 2)	A-5 - A-17
68	Buckling of Isotropic Panels (OPTION 3)	A-20 - A-34

LIST OF TABLES

<u>No.</u>	<u>Title</u>	<u>Page</u>
I	Buckling of Isotropic Skin Panels	36
II	Comparison of Calculations vs. Test Data of Ref. 22.	81
III	Comparison of Calculations vs. Test Data of Ref. 4.	83
IV	Comparison of Calculations vs. Test Data of Ref. 8.	86
V	Comparison of Fixity Factor Analyses With Panel Instability Data of Ref's. 28 and 29.	96
VI	Comparison of First-Iteration Calculations vs. Test Data of Ref. 29.	122
VII	Comparison of Second-Iteration Calculations vs. Test Data of Ref. 29.	123
VIII	Final Comparison of Calculations vs. Test Data of Ref. 29.	125
IX	Calculated Data for Interaction Example Configurations - Axial Compression and External Radial Pressure	137
X	Calculated Data for Interaction Example Configurations - Axial Compression and Internal Radial Pressure	143
XI	Buckling Coefficients for Isotropic Skin Panels Subjected to Edge Compression	167
XII	Table of Contents for the Design Curves "Buckling of Isotropic Panels"	169
XIII	Table of Contents for the Design Curves " $\frac{b}{R}$ vs. $\frac{R}{t}$ for $\sigma_R = 2\sigma_p$ "	170
XIV	Recommended Values for the Fixity Factor $C_F$	191
XV	Recommended Values for the Minimization Factor $\tilde{N}$	191

LIST OF TABLES  
(Continued)

<u>No.</u>	<u>Title</u>	<u>Page</u>
XVI	Recommended Formulas for the $A_{ij}$ 's, $D_{ij}$ 's, and $\bar{t}$ of Longitudinally Stiffened Circular Cylinders	199-205
XVII	Table of Contents for the Design Curves "Compressive Buckling Stress for Longitudinally Stiffened 7075-T6 Al Alloy Circular Cylinders"	207-209
XVIII	Recommended Formulas for the $A_{ij}$ 's and $D_{ij}$ 's of Circular Cylinders Having Both Longitudinal and Circumferential Stiffeners	281-284
XIX	Table of Contents for the Design Curves "Critical Compressive Loading Coefficient for the General Instability of Stiffened Circular Cylinders"	285-286
XX	Program 3875 Notation	345-346
XXI	Fortran Listing - Program 3875	348-353
XXII	Program 3896 Notation	361
XXIII	Fortran Listing - Program 3896	363-369
XXIV	Program 3942 Notation	379-380
XXV	Fortran Listing - Program 3942	382-389
XXVI	Program 3962 Notation	399-402
XXVII	Fortran Listing - Program 3962	404-408
XXVIII	Program 3942I Notation	414
XXIX	Fortran Listing - Program 3942I	416
XXX	Table of Contents for the Supplementary Curves "Buckling of Isotropic Panels" (OPTION 2).	A-2
XXXI	Table of Contents for the Supplementary Curves "Buckling of Isotropic Panels" (OPTION 3).	A-19



LIST OF SYMBOLS

THIS LIST OF SYMBOLS APPLIES TO ALL SECTIONS OF THE REPORT EXCEPT SECTIONS (7.2.2), (8.3), (8.4), AND (18.3.2), ALL OF WHICH RETAIN THE NOTATION OF REFERENCE 5. IN THE INTEREST OF CLARITY, THE SYMBOLS FOR THESE FOUR SECTIONS ARE DEFINED WHERE REQUIRED IN THE REPORT.

$A_r$	Cross-sectional area of ring (no basic cylindrical skin included).
$A_r'$	Cross-sectional area of ring (including effective width of basic cylindrical skin).
$A_s$	Cross-sectional area of stringer (no basic cylindrical skin included).
$A_{11}, A_{22}, A_{12}, A_{21}, A_{33}$	Elastic constants defined by equations (6-4); Computational formulas applicable to conventional configurations are tabulated in Sections 12.1 and 13.1.
$a$	Spacing between rings; Coefficient in quadratic equation (7-7); Postbuckling variable defined by Figures 24 and 25.
$a_e$	Effective width of basic cylindrical skin.
$b$	Spacing between stringers; Coefficient in quadratic equation (7-7); Postbuckling variable defined by Figures 24 and 25.
$b_e$	Effective width of basic cylindrical skin.
$b_s$	Thickness of integral longitudinal stiffener (see Table XVI).
$C$	Coefficient defined by equation (5-7); Symbol to identify clamped boundary condition; Deflectional spring constant (force per unit deflection).

LIST OF SYMBOLS  
(Continued)

$C_F$	Fixity factor.
$C_f$	Experimentally determined constant [see equation (7-1)].
$C_R$	Correction factor defined by equation (7-16).
$C_{11}$	Distance between middle surface of basic cylindrical skin and centroid of skin-stringer combination (positive for internal stringers).
$c$	Constant term in quadratic equation (7-7).
$D$	Diameter of middle surface of basic cylindrical skin.
$D_{11}, D_{22}, D_{12}, D_{21}, D_{33}$	Elastic constants defined by equations (6-4); Computational formulas applicable to conventional configurations are tabulated in Sections 12.1 and 13.1.
$E$	Young's modulus in compression.
$E_{tan}$	Tangent modulus in compression.
$F$	Eccentricity parameter defined by equation (6-17).
$G$	Shear modulus.
$G_{tan}$	Tangent modulus in shear.
$h$	Distance between middle surfaces of sandwich facings; Corrugation pitch $\div 4$ .
$h_s$	Depth of integral longitudinal stiffener (see Table XVI).

LIST OF SYMBOLS  
(Continued)

$I$	Centroidal moment of inertia.
$I_r$	Centroidal moment of inertia of ring cross section (no basic cylindrical skin included).
$I_r'$	Centroidal moment of inertia of ring cross section (including effective width of basic cylindrical skin).
$I_x$	Shell wall local moment of inertia per unit length of circumference, taken about the centroidal axis of skin-stringer combination (including all of the skin and stringer material).
$I_x'$	Same as $I_x$ except for effective width considerations [see note (p) of Table XVI].
$K$	Buckling coefficient for a flat plate; Rotational spring constant (torque per unit rotation); Parameter defined by equation (7-18).
$K_c$	Buckling coefficient for flat plate having loaded edges simply supported and longitudinal edges clamped.
$K_s$	Buckling coefficient for flat plate having all edges simply supported.
$L$	Overall length of entire cylinder.
$l_x$	Axial half-wavelength of buckle pattern.
$l_y$	Circumferential half-wavelength of buckle pattern.

LIST OF SYMBOLS  
(Continued)

$M$	Overall bending moment.
$M_x, M_y, M_{xy}, M_{yx}$	Stress resultants (see Glossary).
$m$	Number of longitudinal half-waves in buckle pattern.
$m_i$	Any particular selected value of $m$ .
$\bar{N}$	Thielemann parameter defined in equations (6-5).
$\tilde{N}$	Minimization factor defined by equation (6-30).
$N_s$	Number of stringers.
$N_x, N_y, N_{xy}, N_{yx}$	Stress resultants (see Glossary).
$(N_x)_{CL}$	Classical theoretical value for the critical longitudinal compressive membrane running load.
$(N_x)_{cr}$	Critical longitudinal compressive membrane running load.
$\left[ (N_x)_{cr} \right]_0$	Critical longitudinal compressive membrane running load for case of pure axial load (or pure bending moment) acting alone.
$(N_x)_{MIN}$	Minimum longitudinal compressive membrane running load for the postbuckling equilibrium path (see Figures 24 and 25).
$(N_x)_{wc}$	Wide-column critical longitudinal compressive membrane running load.
$\left[ (N_{xy})_{cr} \right]_0$	Critical in-plane running shear load for case of shear load acting alone.

LIST OF SYMBOLS  
(Continued)

$(N_y)_{cr}$	Critical circumferential compressive membrane running load.
$\left[ (N_y)_{cr} \right]_o$	Critical circumferential compressive membrane running load for case of external pressure acting alone.
$n$	Ramberg-Osgood parameter; Number of circumferential full-waves in buckle pattern.
$P$	Longitudinal force.
$Q_x, Q_y$	Stress resultants (see Glossary).
$R$	Radius to middle surface of basic cylindrical skin; Radius to centroid of ring (only when computing $C_R$ ).
$R_b$	Ratio of peak longitudinal compressive membrane running load from applied bending moment to the critical value under bending moment acting alone.
$R_c$	Ratio of longitudinal compressive membrane running load from applied axial load to the critical value under axial load acting alone.
$R_1$ or $R_2$	Ratio of applied load (or stress) to the critical value for that type of load (or stress) acting alone.
$SS$	Symbol to identify boundary conditions of simple support.
$T$	Torque.

LIST OF SYMBOLS  
(Continued)

$t$	Thickness of isotropic skin panel or isotropic cylinder.
$t'$	Effective skin thickness defined in note (o) of Table XVI.
$\bar{t}$	Effective thickness defined by equation (6-35).
$t_c$	Corrugation skin thickness.
$t_{eff}$	Equivalent thickness defined by equations (9-7) and (9-9).
$t_f$	Sandwich facing thickness.
$t_x$	Wall thickness for a monocoque circular cylinder of same total cross-sectional area as actual composite stiffened wall (including all of the skin and stringer material).
$t_x'$	Same as $t_x$ except for effective width considerations [see note (m) of Table XVI].
$t_y'$	Effective skin thickness defined in note (n) of Table XVI].
$U_b$	Flexural strain energy.
$U_m$	Membrane strain energy.
$\bar{u}$	Reference surface displacement in the x coordinate direction.
$V$	Total potential energy.
$\bar{v}$	Reference surface displacement in the y coordinate direction.

LIST OF SYMBOLS  
(Continued)

$W$	Discrete radial force depicted in Figure 15(a).
$\bar{w}$	Reference surface displacement in the $z$ coordinate direction.
$w_c$	Uniformly distributed running radial load depicted in Figure 15(b).
$X$	Variable defined by equations (7-5).
$x$	Longitudinal coordinate.
$Y$	Variable defined by equations (7-5).
$y$	Circumferential coordinate.
$z$	Radial coordinate.
$\alpha$	Parameter defined by equation (6-10).
$\beta$	Parameter defined by equation (6-7).
$\Gamma$	Correlation (knock-down) factor.
$\gamma$	Thieleman parameter defined in equation (6-5).
$\gamma_{xy}$	In-plane shear strain.
$\Delta_R$	Radial deflection for the points of load application shown in Figure 15(a).
$\Delta_x$	Deflection defined in note (j) of Table XVI.
$\Delta\theta$	Rotation defined in note (k) of Table XVI.
$\delta_R$	Radial deflection due to uniformly distributed running load shown in Figure 15(b).
$\delta_x$	Deflection defined in note (j) of Table XVI.
$\delta\theta$	Rotation defined in note (k) of Table XVI.

LIST OF SYMBOLS  
(Continued)

$\epsilon_x$	Strain in x direction.
$\epsilon_y$	Strain in y direction.
$\eta_p$	Thielemann parameter defined in equations (6-5).
$\eta_s$	Thielemann parameter defined in equations (6-5).
$\theta$	Half-angle between discrete load points shown in Figure 15(a).
$\nu$	Poisson's ratio.
$\rho$	Radius of gyration.
$\rho_{11}$	Effective local longitudinal radius of gyration of shell wall [see equations (6-33) and (6-34)].
$\rho_{22}$	Effective local circumferential radius of gyration of shell wall.
$(\Sigma d_i)$	Total peripheral length of corrugation center-line.
$\sigma$	Normal stress.
$\sigma_{cc}$	Crippling stress.
$\sigma_{cr}$	Critical buckling stress.
$(\sigma_{cr})_{CL}$	Classical critical stress.
$\sigma_{cy}$	Compressive yield stress.
$\sigma_o$	Critical value of uniformly distributed compressive stress, if acting alone.



LIST OF SYMBOLS  
(Continued)

$\sigma_{PL}$	Assumed proportional limit stress.
$\sigma_p$	Critical stress for buckling of a flat isotropic skin panel.
$\sigma_R$	Critical stress for buckling of an isotropic cylindrical shell.
$\sigma_{wc}$	Wide-column critical stress.
$\sigma_{.7}$	Ramberg-Osgood parameter.
$\tau$	Shear stress.
$\tau_o$	Critical value of torsional shear stress, if acting alone.
$\phi$	Parameter defined by equation (9-3).
$\Omega$	Potential energy of external loading.

NOTE: Subscripts which are preceded by commas denote partial differentiation with respect to the subscript variable. For example, the quantity

$\bar{w}_{,xy}$  is identical to  $\frac{\partial^2 \bar{w}}{\partial x \partial y}$

GLOSSARY

Buckling of Isotropic Skin Panel - The initial buckling of the monolithic skin whose boundaries are formed by the longitudinal and/or circumferential stiffeners. Buckling of the wall of unstiffened cylinders is a special instance of this mode of instability.

Local Buckling of Longitudinal Stiffener(Stringer) - The initial buckling of any leg or arc length of the cross-sectional shape of a longitudinal stiffener (stringer). Initial buckling of the outstanding flange of a Z-section stringer is an example of this mode of instability.

Crippling of Longitudinal Stiffener (Stringer) - The final ultimate compressive failure of a longitudinal stiffener which has a shaped cross section and is given sufficient support to prevent panel instability. The crippling stress is the ultimate average stress for such a stringer.

Panel Instability - This mode of instability manifests itself as a bowing of the longitudinal stiffeners (stringers) into one or more longitudinal half-waves as shown in Figure 1. The length of the half-wave

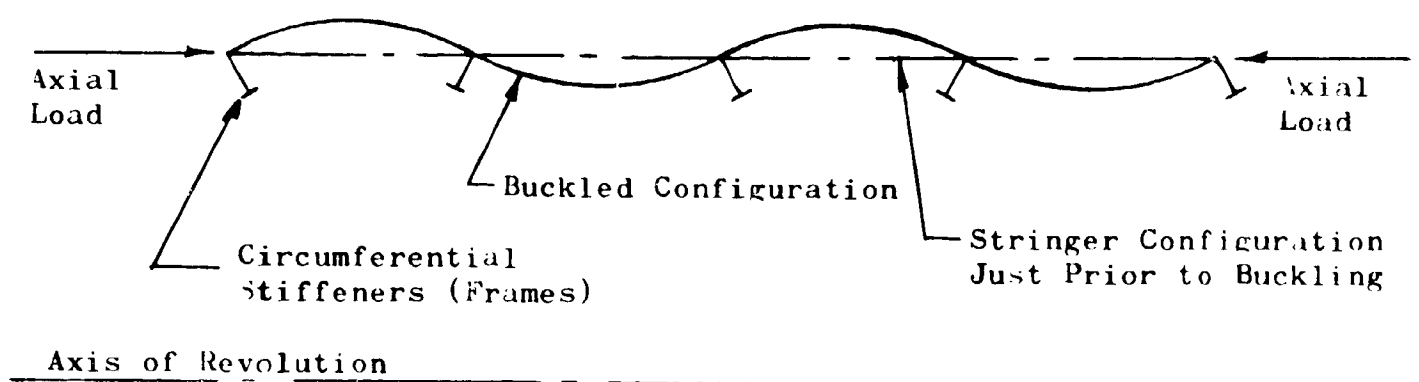


Figure 1 - Panel Instability

must not exceed the spacing between the circumferential stiffeners (frames). The frames do not participate in the radial bulging of the buckle pattern. This mode of instability may or may not be preceded by buckling of the isotropic skin panels and/or local buckling of the stringers. The identification "Panel Instability" is somewhat of a misnomer since this terminology could easily lead one to the erroneous conclusion that reference is being made to the mode which is identified above as "Buckling of Isotropic Skin Panel." A more suitable title could be selected but in the interest of maintaining consistency with the nomenclature usually found in the literature, the "Panel Instability" label has been retained in this report.

General Instability - This mode of instability involves the simultaneous radial displacement of both the longitudinal and circumferential stiffeners (stringers and frames). As shown in Figure 2, the axial half-wavelength

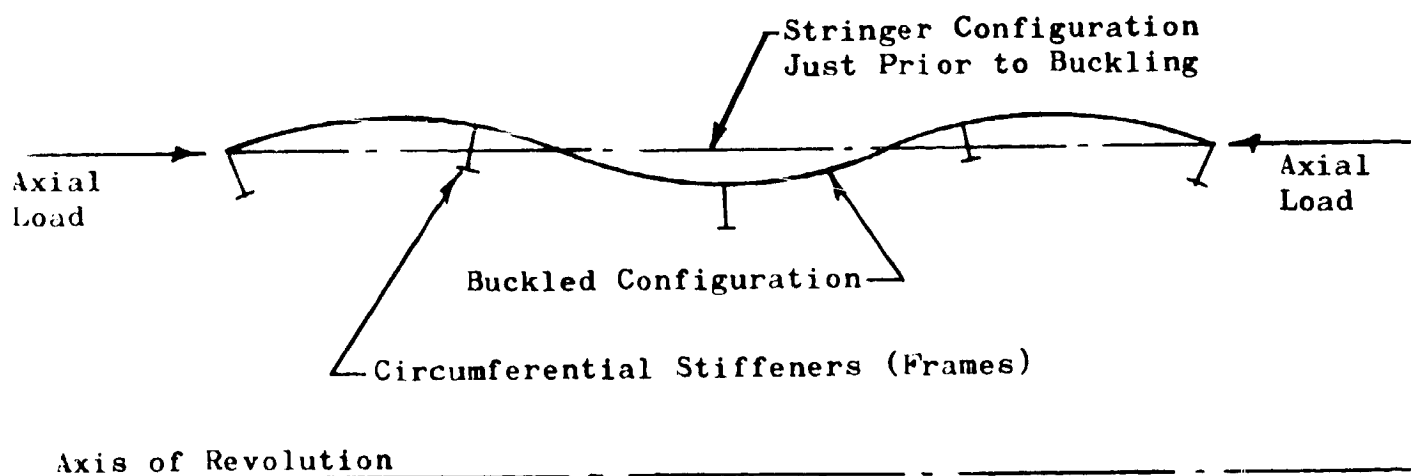


Figure 2 - General Instability

of the buckle pattern exceeds the spacing between frames. This phenomenon may or may not be preceded by buckling of the isotropic skin panels and/or local buckling of the stringers.

Stiffener Eccentricity - This is an internal structural characteristic which results from non-symmetry of the local cross section of the shell wall. The non-symmetry can be due to locating a stiffener on either the inside or outside surface of the basic shell skin.

End Moment - This is an external characteristic associated with the boundary load system. It can arise out of the introduction of longitudinal end load along a line of action which does not pass through the centroid of the skin-stringer combination.

Stress Resultants - The six quantities  $N_x$ ,  $N_y$ ,  $N_{xy}$ ,  $N_{yx}$ ,  $Q_x$ , and  $Q_y$  obtained by integration of the infinitesimal loads over the composite shell wall (including skin and stiffeners), and the four quantities  $M_x$ ,  $M_y$ ,  $M_{xy}$ , and  $M_{yx}$  obtained by integration over the composite shell wall (including skin and stiffeners) of the infinitesimal moments with respect to an arbitrary reference surface. The force stress resultants are expressed in units of force per unit length (lbs/in for example) while the moment stress resultants are expressed in units of moment per unit length (in-lbs/in for example).

Shell (or Shell Wall) - Throughout this report, repeated use is made of the terms "shell" and "shell wall". These terms are not meant to refer only to the basic cylindrical skin of the stiffened structure. They refer to the entire composite stiffener-skin combination. Whenever it is desired that reference be made solely to the basic monocoque cylinder which the stiffeners augment, the word "skin" will actually be included in the identification.

Monocoque - This term comes from the French word meaning "shell only" and is used here to identify these configurations which do not incorporate any stiffening members (integral or non-integral). Note, however, that a monocoque configuration can have orthotropic properties.

Anticlastic Bending - Bending into a deflected shape for which principal radii of curvature have opposite signs. Bending of an initially flat plate into a saddle shape is an example. In addition, for beams, the Poisson effect results in anticlastic bending as depicted in Figure 3.

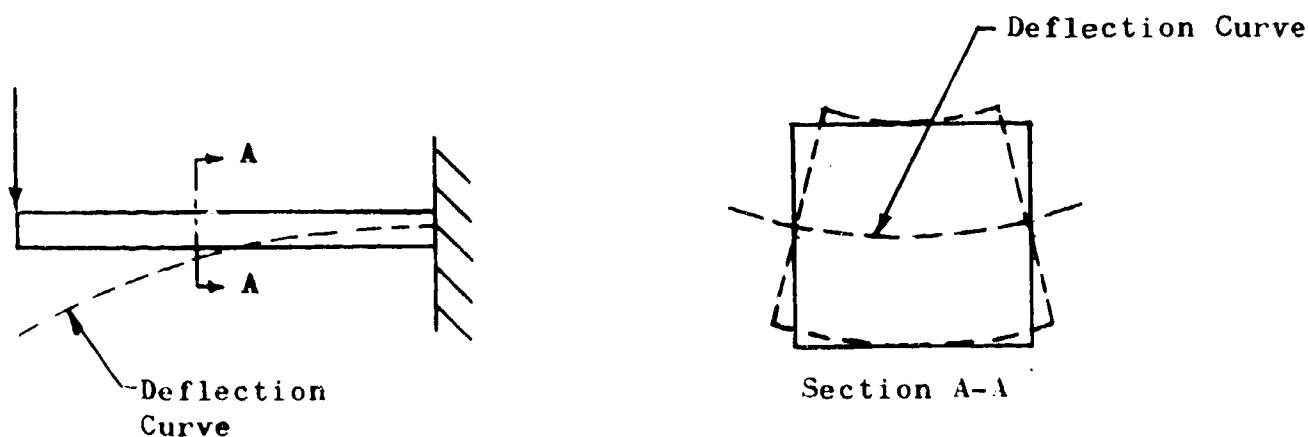


Figure 3 - Anticlastic Bending of Beams

## 1.0 INTRODUCTION

The structural components of aerospace vehicles are usually subjected to a wide assortment of loading conditions which frequently include loads of the following types:

- (a) Axial compression due to longitudinal acceleration and/or drag effects.
- (b) Overall bending moment due to aerodynamic disturbances and/or transverse inertia effects.
- (c) Transverse shear due to aerodynamic disturbances and/or transverse inertia effects.
- (d) External pressure.

Although dynamic phenomena are involved in some of these loads, many related practical problems can be treated on the basis of equivalent static loading. The particular types of loading cited here share a common characteristic in that each can cause a structural instability to occur. Such an instability manifests itself in the phenomenon commonly referred to as buckling. A structure is said to buckle whenever a small increase in the applied load results in disproportionately large deflections for reasons other than reduction in the slope of the stress-strain curve for the material. This behavior can initiate deformation processes which lead to total collapse of the structure. Such failures often occur very rapidly with little or no advance warning. Obviously, the engineer must be equipped with workable analytical tools for the prediction of such conditions if he is to properly design lightweight structures to support loads of the types enumerated above.

In designing cylindrical shell structures for aerospace applications, stability considerations will often lead to the use of stiffened configurations. In the past, analysis of the stiffeners has frequently been accomplished by neglecting the fact that they are actually components of a shell which provides a variety of interacting restraints to deformation. For example, in the design and analysis of longitudinal stiffeners (stringers), it has commonly been assumed that only the so-called wide-column strength can be attained. In the past few years, however, attention has been directed to the need for a more realistic approach, partly because of the prominent role which eccentricities have been found to play in the buckling of stiffened cylinders. The importance of eccentricity is shown in the experimental findings of references 1, 2, 3, and 4 which clearly demonstrate that longitudinally stiffened circular cylindrical shells with external stringers can have much higher critical compressive loads than other cylinders which are identical in all respects except for locating the stringers on the inside of the basic shell skin. The only hope for an accurate analytical assessment of this phenomenon rests in the application of shell theory to the problem. A similar situation also exists with regard to cylindrical structures which are subjected to end moments in combination with any of the loading conditions listed earlier.

In addition to the foregoing points, it should also be noted here that engineers have long been faced with a need for improved methods for the determination of circumferential stiffening requirements. Designing

for the prevention of general instability in frame-stringer constructions usually centers around the choice of suitable dimensions for the frames. Over the years, a number of crude empirical and rule-of-thumb techniques have been employed for this purpose. Such procedures, used in conjunction with generous safety factors and extensive proof testing, have proven adequate for most applications of the past. However, the requirements of the aerospace program become increasingly more stringent and it is now required that an approach be taken which properly identifies all the important variables related to the problem and provides a reasonably accurate numerical evaluation of their influences. Here again, one must resort to the use of shell theory to come up with suitable criteria.

The intent of this report is to provide the engineer with workable analytical tools for the prediction of instability in unpressurized, stiffened, circular cylinders, based upon orthotropic shell theory. In addition, methods are given for predicting buckling of the isotropic skin panels of such cylinders. In general, the emphasis is on approximate techniques which are primarily of use in preliminary sizing, rough checking, and the study of trends. These techniques constitute simplifications which are not meant to provide final detailed analysis. The simplifications were necessary to restrict the design curves to a reasonable number and to retain a sufficient degree of clarity for the



early phases of design and analysis. In particular, the approximate methods presented ignore the influences of several of the usually less crucial stiffnesses inherent in the orthotropic shell. In addition, as presented here, the simplified approach deals only with cases which do not include any eccentricities or end moments. However, the approach could be extended to include eccentricity influences without an undue amount of difficulty, particularly in the case of cylinders which incorporate only longitudinal stiffening. It should be noted that the neglect of certain of the existing stiffnesses should result in conservatively low predictions of critical loads. This is borne out in the test data comparisons shown in the report.

Although a clear need exists for simplified analysis methods which minimize the degree of complicating detail, it is likewise recognized that more rigorous means must be provided for the final analysis of selected configurations. Methods of this type are also discussed in the report and recommendations are made concerning their use. One of these is a digital computer program which was developed using the orthotropic shell solution of reference 5. This solution includes the influences of both longitudinal and circumferential stiffener eccentricities. The program provides a powerful tool which should enjoy a wide scope of application. The input and output of the program are fully discussed to facilitate its ready use.

The report is organized into two separate parts, the first of which presents the theoretical and empirical foundations that form the basis for the proposed methods. Part II then gives detailed procedures for the application of the methods. These procedures are presented in such a manner that they may be employed without extensive knowledge of the material in Part I. However, for full appreciation of the problem and to best interpret the analysis, it is recommended that, wherever possible, the user be familiar with the entire report.

Although both the approximate and the more rigorous methods cited in this report have general applicability to a wide variety of stiffened circular cylinders, it is anticipated that the most important applications will be for the assessment of the capabilities of current aerospace vehicles and to the future design of large aerospace structures including those of the reusable type.

## 2.0 CONCLUSIONS

(a) All objectives set forth in Exhibit A of NASA Contract NAS8-11181 have been met. In broad terms, these objectives were as follows:

- (1) Using the Schapitz criterion [6]\*, develop buckling curves for curved isotropic skin panels subjected to edge compression.
- (2) Using orthotropic shell theory, develop buckling curves and analysis methods for both panel instability and general instability in stiffened circular cylinders subjected to axial compression.
- (3) Test the applicability of the developed methods by comparing predictions against experimental data.

(b) The major portion of the results from this study are in the form of simplified analysis methods for use in preliminary sizing, rough checking, and the study of trends. More rigorous methods are also presented for detailed final analysis purposes. Both types of solutions are essential to the design and development process.

(c) The criterion used for the determination of critical stresses for the buckling of isotropic skin panels was adapted to include lower-bound predictions in cases where the stringer spacings are large and full-cylinder behavior is approached. As the panel size decreases and flat-plate behavior is approached, the test data show considerable scatter on either side of the predicted values. Hence, caution must be

---

\*Numbers in brackets [ ] in the text denote references listed in Section 19.

exercised in the interpretation of predictions in this latter regime. However, one should consider that, as flat-plate behavior is approached, the postbuckling load will increase and it might be possible to tolerate initial buckling depending, of course, upon the particular application. Further work is recommended to improve the reliability of the predictions in this area. This is discussed more fully in Section 4, "Recommendations".

(d) The curves which have been developed for the buckling of longitudinally stiffened circular cylinders provide conservative predictions for their intended application to configurations which have no eccentricity. The conservatism is due to the neglect of certain stiffnesses in the simplified theory employed. However, even this simplified approach constitutes a significant advance over methods which either neglect the shell-type redundancies or do not recognize the influences manifested in the minimization factor  $\tilde{N}$ .

(e) Although a basically sound method has been proposed for the determination of fixity factors, considerable uncertainty still remains in connection with the computation of required spring constants. Until further work is accomplished to resolve this uncertainty, it is recommended that the value  $C_F = 1.0$  be employed for the design of longitudinally stiffened sections which lie between rings. Any further work undertaken in this area should couple the circumferential width of the anticipated buckle pattern into the computation.

(f) The curves which have been developed for the general instability of stiffened circular cylinders provide conservative predictions for their intended application to configurations which have no eccentricities. The conservatism is due to the neglect of certain stiffnesses in the simplified theory employed. However, even this simplified approach accounts for many more interacting influences than does the so-called Shanley criterion [7] that has enjoyed widespread popularity for over fifteen years.

(g) It is concluded that the theory of monocoque orthotropic shells can be successfully applied to predict the buckling of circular cylinders with discrete longitudinal and/or circumferential stiffening by means of the "smearing-out" technique. This involves the mathematical artifice of converting the discrete stiffness values into equivalent uniformly distributed stiffnesses. However, certain precautions must be taken as pointed out in the procedures presented in Part II of this report.

(h) It is possible to adapt monocoque orthotropic shell theory to a wide variety of stiffener configurations by properly computing the so-called elastic constants. For shaped longitudinal stiffener configurations such as hats, Z's, etc., it is important to account for the possibility that crippling might occur.

(i) The methods presented in this report can be readily extended to analyze configurations which tolerate buckling of the isotropic skin panels or local buckling of longitudinal stiffeners prior to the catastrophic modes of instability. In such instances, iterative computations are required which include effective width considerations and reduction of the in-plane shear stiffness of the skin panels based upon their postbuckling characteristics.

(j) As one might intuitively expect, and as shown by test [8], the buckling stress for corrugated cylinders which do not incorporate any intermediate circumferential stiffeners will often be essentially equal to the Euler column value of an individual corrugation. The accordion-like flexibility in the circumferential direction minimizes the shell-type restraint to buckling. Analytically, this situation manifests itself through a severe reduction in the minimization factor  $\tilde{N}$ .

(k) The available test data for stiffened cylinders generally were obtained from specimens which incorporate eccentricities. Since the simplified analysis methods presented in this report apply only to cases with no eccentricity, auxiliary computations were required to assess the magnitudes of eccentricity influences when making comparisons of theoretical predictions versus the test data. From this work, it is concluded that the eccentricities often play a dominant role in the buckling process. Clearly there is a need for the engineer to be equipped with workable techniques for the numerical evaluation of this influence. This is discussed more fully in Section 4, "Recommendations".

(1) Although some of the design information presented in this report is limited in application to a particular material, there is nothing inherent in the proposed methods which prohibits direct extension to other materials by proper choice of input material properties. Similarly, extension to elevated or cryogenic temperature applications can be readily accomplished by adjustment of these properties.

(m) The Thieleman equation which provides the basis for the general instability analysis of this report [see equation (7-2)] was evaluated for applicability to sandwich configurations. Based on results obtained from the analysis of six arbitrary cylinder geometries, it is concluded that this equation essentially agrees with the classical small-deflection theory of reference 9 whenever the transverse shear stiffness of the core can be assumed to be infinite. Since for practical sandwich configurations this assumption will frequently be inappropriate, the referenced Thieleman equation will have very limited application to this type of construction. In addition, the general instability design curves of Section 13.2 are based upon the simplifying assumption that certain of the stiffnesses ( $D_{12}$  and  $D_{33}$ ) involved in the Thieleman equation are each equal to zero. These particular stiffnesses will probably be more crucial to sandwich configurations than they are to discretely stiffened designs. Hence, in general, neither equation (7-2) nor the general instability design curves of Section 13.2 should be considered applicable to sandwich construction.

(n) For external loading combinations of

- (1) Axial compression and shear
- (2) Axial compression and external pressure
- (3) Axial compression and pure bending

straight-line interaction curves having vertical and horizontal intercepts of unity are given as a practical expediency for preliminary estimates. Unlike the practice followed for isotropic cylinders, the proper presentation of interaction effects for combinations (1) and (2) above would require the use of multiple plots which are geometry dependent. It appears that the recommended straight line will furnish a lower bound to these families. For improved analysis of combination (2), a digital computer program presented in the report should be used. This same program may also be used to obtain interaction estimates for the case of axial compression and internal pressure. However, both in this instance and for combination (2) above, one must keep in mind that none of the methods of this report account for the pre-buckling discontinuity-type deformations which result from the presence of pressure differentials across the shell wall.

(o) The influence of imperfections will usually be of lesser importance to stiffened cylinders than they are to monocoque cylinders. Generally speaking, stiffened configurations will have higher effective wall thickness values so that their  $\left( R/t_{\text{eff}} \right)$  values will be lower.

GENERAL DYNAMICS  
Convair Division



Nevertheless, considerable uncertainty still exists relative to this entire question. At the present time, the best that can be done in the way of obtaining a numerical assessment of the imperfection influence is to employ a correlation (knock-down) factor derived on the basis of monocoque test data. This factor must be considered to be a function of an  $\left(R/t_{\text{eff}}\right)$  variable.

(p) A reliable orthotropic cylinder analysis method is needed for situations where the shell boundary restraint is other than classical simple support. The methods of this report employ an approximate engineering approach for evaluation of this effect.

### 3.0 LIMITATIONS

Wherever necessary to guard against misuse of the methods presented, attention is drawn to detailed limitations throughout the report. The following constitutes a listing of only those limitations which have broad implications:

(a) All of the results presented in this report are based on small-deflection theory. Imperfections are handled in an approximate manner by means of a correlation (knock-down) factor derived on the basis of monocoque test data.

(b) In general, pre-buckling bending deformations of the shell wall are not included in the analysis methods. Hence, in general, consideration is not given to the effects of end moment and the non-cylindrical deformations due to either pressure differentials or restraint to Poisson-ratio hoop growth. Although the digital computer program of reference 10 can account for pre-buckling bending deformations, it is presently too highly specialized in application to be regarded as a general working tool.

(c) The analysis methods that make use of the design curves are simplified approaches which do not account for stiffener eccentricities. The only means provided in this report for evaluation of eccentricity influences is a digital computer program based on the solution of reference 5.

(d) In accordance with the specification of NASA Contract NAS8-11181, the design curves furnished for the compressive buckling of longitudinally

stiffened circular cylinders apply only to 7075-T6 aluminum alloy cylinders.

(e) The design curves furnished for both the compressive buckling of longitudinally stiffened circular cylinders and the critical compressive loading coefficient for the general instability of stiffened circular cylinders are all based on the simplifying assumption that  $\eta_p = 0, (D_{12} = D_{33} = 0)$ .

(f) Throughout the entire report, it is assumed that transverse shearing deflections of the shell wall are negligible.

#### 4.0 RECOMMENDATIONS

The studies performed by Convair under NASA Contract NAS8-11181 have led to a recognition that several extensions and applications of this work would be quite useful and would add to the benefit derived from the effort already expended. The main objective of this supplementary effort would be to keep the designer and analyst abreast of the most recent advances concerning the structural stability of stiffened shells and to furnish practical means for incorporating these findings into the structural analysis. The specific tasks which are recommended at this time are as follows:

Parametric Studies and Weight-Strength Analysis (Including Eccentricity Influences) - This task includes the performance of parametric studies involving various spacings, stiffener shapes, eccentricities, diameters, etc., in order to provide measures of the relative importance of these various geometrical features. For example, a study would be included which explored the importance of stiffener eccentricity over wide ranges of stringer and frame stiffness values. In addition, investigations would be conducted to establish relative efficiencies between designs which tolerate buckling of the isotropic skin panels and those configurations which preclude such behavior.

This task would also include the development of weight-strength analysis methods which could assist in the selection of candidate designs for proposed applications. For this purpose, a digital computer program would be developed which provides both output listings

GENERAL DYNAMICS  
Convair Division

and automated plotting of a variety of curves. Separate families of curves could be plotted which show total weight versus an independent variable and a parameter, both of which could be chosen by the user from among a pre-determined selection of optional variables.

All work performed under this task would be based on orthotropic shell theory and would account for eccentricities of both longitudinal and circumferential stiffeners.

Supplementary Empirical Refinement - The results obtained by Convair under NASA Contract NAS8-11181 include a series of curves for the prediction of critical compressive edge loads for curved isotropic skin panels. These curves are based upon the approach proposed by Schapitz in reference 6. This criterion recognizes two regimes of response for the curved skins. One of these is primarily a region of transition between flat-plate behavior and that of a full cylinder. The second regime is encountered when the spacing between longitudinal stiffeners becomes sufficiently large for the panel to behave in essentially the same manner as a complete monocoque cylinder of the same radius and thickness. For this second regime, experimentally determined lower-bound correlation (knock-down) factors were applied to the results from classical small-deflection theory to arrive at appropriate predictions. Since the transition region is forced to blend into the full-cylinder behavior, it would be expected that comparisons against

test data would show that, as the size of the panel increases, the prediction curves tend toward a lower bound to the data. The results presented in this report show that this is indeed the case. However, it has also been observed that, as the panel size decreases and flat-plate behavior is approached, the transition criterion does not yield predictions which are consistently conservative. That is, for these panels, the test data show considerable scatter on either side of the predicted values. It is therefore recommended that an improved expression be developed for the transition curve such that lower-bound predictions are obtained throughout all regimes. A possible exception might be allowed for those situations which approach flat-plate behavior so closely that one may safely rely upon the existence of adequate post-buckling strength for the panel.

In addition to the foregoing effort related to the isotropic skin panels, this "Supplementary Empirical Refinement" task would also include further consideration of the composite cylinder. In this connection, supplementary test data reduction would be accomplished to more completely exhaust the remaining available sources. The additional information obtained from this effort would be reflected back into the proposed stability analysis procedures to provide improved techniques of increased reliability.

Plotting of Supplementary Design Curves - Under NASA Contract

NAS8-11181, Convair has developed a series of design curves showing predicted compressive buckling stresses for longitudinally stiffened 7075-T6 aluminum alloy circular cylinders. It is recommended that additional curves of this type be generated for other materials of interest to current and future aerospace programs. It is further recommended that a study be conducted to determine the feasibility of generating lesser numbers of curves, on a non-dimensional basis, which would have general applicability to all materials. If this should prove feasible, these too should be plotted.

The curves which have already been plotted for the 7075-T6 longitudinally stiffened cylinders require that the user establish the appropriate magnitude of a minimization factor  $\tilde{N}$ . Curves have been developed from which this value can be determined in cases which involve no eccentricity. It is recommended that these curves be supplemented by additional families that are applicable in the presence of eccentricity.

All of the shell buckling curves developed by Convair under NASA Contract NAS8-11181 are founded upon the usual thin-shell assumptions. As a result, transverse shearing deflections of the shell wall are completely neglected. For most types of practical stiffened shell structures currently used in the aerospace industry, these shearing deflections are sufficiently small to justify their neglect. However,

for certain important configurations, such as sandwich constructions, these shearing deflections are not negligible and they do play a significant role in the buckling process. It is therefore recommended that additional buckling curves be developed which account for the transverse shearing deflections, where important. Such curves would enable the engineer to consider the use of sandwich-type cylindrical walls augmented with longitudinal and/or circumferential stiffeners. This could prove to be a configuration of interest in situations where the sandwich wall would be desirable for insulating purposes, meteoroid protection, etc.

Extended Interaction Study - The studies conducted by Convair under NASA Contract NAS8-11181 included a limited effort in connection with interaction effects for stiffened circular cylinders subjected to the following combinations of applied loading:

- (a) Axial compression and shear.
- (b) Axial compression and internal pressure.
- (c) Axial compression and external pressure.

In the course of this investigation it was discovered that for any of these combinations a single interaction curve is not sufficient to describe the behavior of stiffened cylinders. Hence the primary interaction analysis tool which emerged from this study is in the form of a digital computer program developed for the buckling solution of reference 5. Since this solution is limited to cases involving no



externally applied shear forces, it is recommended that extensions be developed to properly include this variable in the final formulation. It is also recommended that further study be undertaken which would make use of dimensional analysis techniques to establish suitable parameters for the presentation of multiple interaction curves applicable to stiffened circular cylinders.

None of the effort recommended in this task would include consideration of influences due to discontinuity-type deformations that will usually be of importance in cases that involve pressure differentials. These influences are separately discussed in the next task to be recommended.

Pressure Effects - Most of the work performed by Convair under NASA Contract NAS8-11181 and most of the foregoing recommendations are applicable only in the absence of any pressure differential across the shell wall. The only considerations which have been given to pressure effects relate solely to the development of interaction curves without recognition of any influence from the discontinuity-type deformations. It is therefore recommended that an extensive program be undertaken to develop practical methods for the proper evaluation of all influences due to pressure. This evaluation should recognize two basic areas of interest. The first of these relates to the stress problems which arise out of the longitudinal and circumferential bowing created by the

presence of stiffeners. Secondly, one must consider the effects which these pre-buckling deformations have on the critical buckling load. Throughout both phases of this investigation, attention must be given to coupling effects between radial displacements and both the longitudinal and circumferential membrane loads.

Extension of Stuhlman Digital Computer Program - It is recommended that the digital computer program of reference 10 be modified to permit the input of hand-calculated elastic constants. This would provide a detailed-analysis tool of much greater versatility than the present program whose input format limits the application to one particular type of wall cross section.

(This page intentionally left blank)

PART I  
THEORETICAL AND  
EMPIRICAL FOUNDATIONS

## 5.0 BUCKLING OF ISOTROPIC SKIN PANELS SUBJECTED TO EDGE COMPRESSION

### 5.1 General

Buckling of the isotropic skin panels which are bounded by the stiffening elements of an orthotropic cylinder is a localized mode of compressive instability. Reliable means for prediction of such compressive strength is essential to optimum design although buckling of the isotropic skin panels may not necessarily be the limiting factor in the collapse of the structure; i.e., it is possible to design a structure employing stiffening elements so that buckling of the isotropic skin panels is permitted prior to either the so-called panel instability (ref. Glossary) or general instability loads. On the other hand, it may be desirable to prevent buckling of the skins at loads below the panel instability or general instability levels if such buckling adversely affects the integrity of the structure in other ways (fatigue, excessive deformations, etc.). Whether or not the design criteria will permit buckling of the isotropic skin panels, it is important that sufficiently reliable means for determination of their critical loads be available to the designer and analyst.

The Schapitz criterion [6] forms the basis for the analysis procedures presented here and supplies the means for evaluating the effects of skin panel geometry as the transition is made from wide panels behaving like monocoque cylindrical shells to smaller panels which approach flat plate behavior.

Three empirical analysis techniques were prepared for the case where longitudinal stiffeners are widely spaced giving panel behavior similar to that of a cylindrical shell. One of the techniques results in typical strength predictions for comparison with test data while the other two give design levels of high reliability recognizing scatter which exists in actual strengths. The recommended design procedure is consistent with that of NASA Space Vehicle Design Criteria [11] for monocoque cylinders.

For the limiting case of flat plate behavior for isotropic skin panels bounded by closely spaced longitudinal stiffeners, conventional flat plate theory is employed in the Schapitz criterion. While it is widely recognized that test data in flat plates also exhibit considerable scatter, they can continue to support steadily increasing loads well into the post-buckling regime. This is in contrast to the sudden drop-off in load usually observed for monocoque cylinders. As a consequence of postbuckling load-carrying capability, the full theoretical buckling level is utilized for the isotropic skin panel as the boundary case of flat plates is approached. As a result, caution must be exercised in employing the Schapitz criterion in the transition region where unconservative predictions may result due to the possibility of the post-buckling behavior of the curved plates being more severely influenced by cylinder mechanisms than assumed by the Schapitz criterion.

In this section, the results of the investigation are presented in terms of analytical expressions. Procedures and curves are given in Section 11 of Part II.

## 5.2 Buckling Criterion

The buckling criterion for isotropic skin panels is based on equations derived by Schapitz [6] which constitute extensions to the theory presented by Timoshenko [12]. The results of these extensions are embodied in the following criterion for buckling of curved isotropic panels:

$$\text{When } \sigma_R \leq 2\sigma_p \quad (5-1)$$

$$\text{then } \sigma_{cr} = \sigma_p + \frac{\sigma_R^2}{4\sigma_p} \quad (5-2)$$

and

$$\text{when } \sigma_R > 2\sigma_p \quad (5-3)$$

$$\text{then } \sigma_{cr} = \sigma_R \quad (5-4)$$

where,

$\sigma_p$  = Critical stress for buckling of a flat isotropic skin panel.

$\sigma_R$  = Critical stress for buckling of an isotropic cylindrical shell.

$\sigma_{cr}$  = Critical stress for buckling of a curved isotropic skin panel.

Equation (5-2) supplies the transition relationship for skin panels whose geometry results in behavior somewhere between that of a flat plate and that of a cylindrical shell. The two bounding conditions are then:

- (a) The spacing of the longitudinal stiffeners is very small so that the effect of curvature becomes negligible and the skin panel may be considered to be flat. Fixity along the longitudinal edges has marked influence on the critical buckling load.
- (b) The spacing of the longitudinal stiffeners is large so that the skin panel behavior is like a cylindrical shell and the fixity effect at the longitudinal edges is negligible.

For condition (a), the familiar theoretical flat plate buckling stress governs and  $\sigma_p$  becomes:

$$\sigma_p = K_s [c] \frac{E}{(1-\nu^2)} \left( \frac{t}{b} \right)^2 \quad (5-5)$$

where

- $K_s$  = Buckling coefficient (a function of aspect ratio) for flat plate having all edges simply supported.
- $K_c$  = Buckling coefficient (a function of aspect ratio) for flat plate having loaded edges simply supported and longitudinal edges clamped.
- $E$  = Young's Modulus.
- $\nu$  = Poisson's ratio.
- $t$  = Thickness of isotropic skin panel.
- $b$  = Spacing between stringers.



For condition (b), the buckling stress for an isotropic cylindrical shell governs and although theoretical levels are generally accepted for flat plate behavior, it is well known that practical cylindrical shells buckle under longitudinal loadings significantly below theoretical levels and that considerable scatter exists in the available test data. Because of this variation from theory, three semi-empirical approaches were examined for the determination of  $\sigma_R$  as follows.

OPTION 1) The lower bound approach of Seide, et al. [13]:

$$\sigma_R = CE \frac{t}{R} \quad (5-6)$$

$$\text{where } C = 0.605 - 0.546 \left( 1 - e^{-\frac{1}{16} \sqrt{\frac{R}{t}}} \right) \quad (5-7)$$

$R$  = Radius of isotropic skin panel

OPTION 2) The "best-fit" or "mean-expected" relations [14]

which may be rewritten in terms of the parameters of interest here as:

$$\frac{a}{b} \frac{b}{R} < 1.0 \rightarrow \sigma_R = 11.28 \left( \frac{R}{t} \right)^{-1.6} + 0.109E \left( \frac{R}{t} \frac{a}{b} \frac{b}{R} \right)^{-1.3} \quad (5-8)$$

$$\frac{a}{b} \frac{b}{R} \geq 1.0 \rightarrow \sigma_R = 11.28 \left( \frac{R}{t} \right)^{-1.6} + 0.109E \left( \frac{R}{t} \frac{a}{b} \frac{b}{R} \right)^{-1.3} - 1.418 \left( \frac{R}{t} \right)^{-1.6} \log_e \left( \frac{a}{b} \frac{b}{R} \right) \quad (5-9)$$

where  $a$  = longitudinal length of isotropic skin panel;

frame spacing

$b$  = width of isotropic skin panel; stringer spacing

OPTION 3) The statistical level [14] which represents 90% probability with 95% confidence; i.e., there is 95% confidence that 90% of specimens tested would exceed the buckling levels given by:

$$\frac{a}{b} \frac{b}{R} < 1.0 \rightarrow \sigma_R = 8.01E \left( \frac{R}{t} \right)^{-1.6} + 0.076E \left( \frac{R}{t} \frac{a}{b} \frac{b}{R} \right)^{-1.3} \quad (5-10)$$

$$\begin{aligned} \frac{a}{b} \frac{b}{R} \geq 1.0 \rightarrow \sigma_R = & 7.52E \left( \frac{R}{t} \right)^{-1.6} + 0.072E \left( \frac{R}{t} \frac{a}{b} \frac{b}{R} \right)^{-1.3} \\ & - 1.418 \left( \frac{R}{t} \right)^{-1.6} \log_e \left( \frac{a}{b} \frac{b}{R} \right) \end{aligned} \quad (5-11)$$

OPTION 1 is the recommended procedure for the determination of  $\sigma_R$  because of its simplicity and its inherent high reliability due to the fact that equation (5-7) represents a lower bound to test data. However, the test data were gathered over somewhat limited parameter ranges and panel length effects would be neglected using OPTION 1. OPTION 1 is the same method as that employed for isotropic cylinders in reference 11.

OPTIONS 2 and 3 were investigated because of their inferred length effect and because OPTION 2 would give "mean-expected"  $\sigma_R$

strengths for comparisons of the Schapitz criterion with test data. OPTION 3 was investigated because of the known high reliability of the analysis and inclusion of length effects.

It was found that for usual configurations involving both longitudinal and circumferential stiffening, OPTIONS 1 and 3 give essentially the same results for  $\sigma_R$ .

In order to permit representation of the buckling criteria of equations (5-1) through (5-4) in graphical form, equation (5-5) was written as

$$\sigma_p = K_s[c] \frac{E}{1-\nu^2} \frac{1}{\left(\frac{R}{t}\right)^2 \left(\frac{b}{R}\right)^2} \quad (5-12)$$

Using  $\sigma_R$  as determined by equations (5-6) and (5-7) with  $\sigma_p$  from equation (5-12), it is thus possible to arrive at families of curves of  $\sigma_{cr}$  or  $\sigma_{cr}/E$  versus  $R/t$  for various  $b/R$ , and  $K$  values. For practical purposes, it is prudent to consider the loaded edges of the panels to be simply supported and neglect the influence of fixity there. This might be expected to result in conservative estimates of  $K$  for equation (5-12). With the assumption of all edges simply supported ( $K_s$ ) or simply supported loaded edges and clamped longitudinal edges ( $K_c$ ),  $K$  becomes a function of the aspect ratio  $a/b$  [15]. Thus the relevant parameters are selected to be  $\sigma_{cr}/E$ ,  $R/t$ ,  $b/R$ ,  $a/b$ , and the type of support afforded to the longitudinal edges.

If  $\sigma_R$  is determined by OPTIONS 2 or 3, the length parameter  $a/R$  becomes significant but since this can be expressed in terms of  $\frac{a}{b} \frac{b}{R}$ , no additional parameters are required. However, many more families of curves are required to describe desired parameter ranges for OPTIONS 2 and 3 than for OPTION 1.

On a logarithmic plot, the buckling criterion of equations (5-1) through (5-4) may be represented nondimensionally as shown in Figure 4. The transition curve, equation (5-2), becomes tangent to the cylinder curve when  $\sigma_R = 2\sigma_p$ . For all  $R/t$  greater than that of the tangency point, the skin panel behaves as a cylindrical shell whereas for smaller  $R/t$ , the transition relation, equation (5-2), applies.

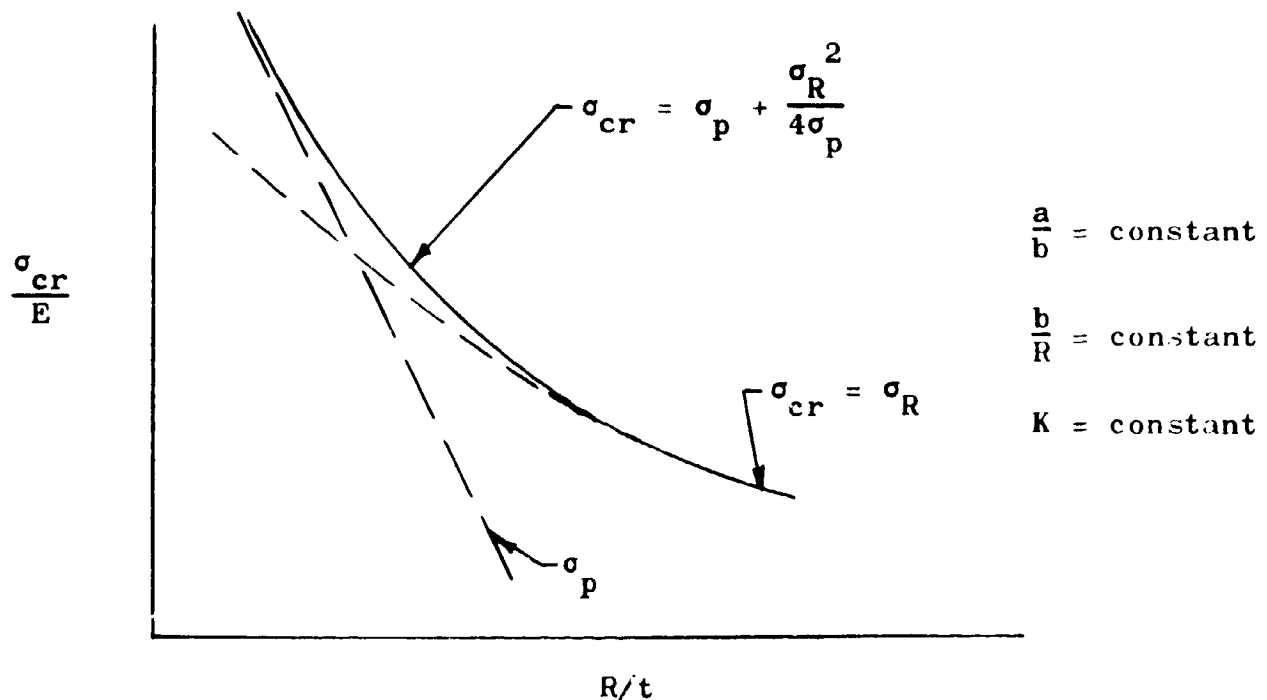


Figure 4 - Nondimensional Logarithmic Plot of Buckling Criteria for Isotropic Skin Panels

Equations (5-1) through (5-12) were programmed for use on a digital computer and an automatic plotter so that families of curves or solutions for particular geometries could be obtained as desired. The computer program is described in Section 18.1 of this document. Detailed design procedures and discussion of the design curves are presented in Section 11. Supplementary curves from OPTIONS 2 and 3 are presented in Appendix A.

### 5.3 Comparisons Against Test Data

Limited comparisons were made of the analyses of Section 5.2 against test data [16, 17]. Included were data for buckling of skin panels from 17 longitudinally stiffened cylinders ( $3.4 < a/b < 17$ ), 46 tests of curved panels having clamped edges ( $2 < a/b < 6$ ), and 14 flat plates having clamped edges ( $2 < a/b < 6$ ). The flat plate data were compared with equation (5-5). The remaining data were compared with results of analyses employing equations (5-1) through (5-4) with (5-5) and each of the following [equations (5-6) through (5-11)]:

- a) OPTION 1 (lower bound  $\sigma_R$ )
- b) OPTION 2 (mean value  $\sigma_R$ )
- c) OPTION 3 (90% probability  $\sigma_R$ )

In every case, it was assumed the loaded edges were simply supported and the unloaded edges were considered both simply supported and clamped. The digital computer program described in Section 18.1 was employed to

obtain calculated buckling stress values. Results and test data are presented and compared in Table I and Figures 5 through 7.

As may be determined from Table I, the flat plate tests covered the range  $0.869 < \sigma_p/\sigma_{test} < 1.29$  with an average value of  $\sigma_p/\sigma_{test} = 1.08$  for the unloaded edges clamped. For comparison, assuming all edges simply supported (although tests were clamped), the analysis showed  $0.500 < \sigma_p/\sigma_{test} < 0.745$  with an average value of  $\sigma_p/\sigma_{test} = 0.619$ .

This considerable scatter in test data for flat plates has not usually been considered a serious problem since their postbuckling strength is known to be significantly higher than the buckling load. However, when such plates are part of a stiffened structure, their change in stiffness due to buckling could cause load redistribution which would affect stability strengths of the composite structure in other modes.

The 46 curved panels gave results which may be summarized from Table I:

OPTION	ANALYSIS EDGE CONDITION		TEST EDGE CONDITION	$\sigma_{cr}/\sigma_{test}$ RANGE	$\sigma_{cr}/\sigma_{test}$ AVERAGE
	UNLOADED EDGES	LOADED EDGES	ALL EDGES		
1	SS	SS	C	0.214-1.29	0.587
	C	SS	C	0.263-1.72	0.715
2	SS	SS	C	0.288-1.70	0.746
	C	SS	C	0.308-1.95	0.906
3	SS	SS	C	0.194-1.21	0.576
	C	SS	C	0.250-1.68	0.707

The 17 longitudinally stiffened cylinders had panel edge conditions actually somewhere between SS and C and gave results for skin panel buckling strengths as follows:

OPTION	ANALYSIS EDGE CONDITION		TEST EDGE CONDITION  ALL EDGES	$\sigma_{cr}/\sigma_{test}$ RANGE	$\sigma_{cr}/\sigma_{test}$ AVERAGE
	UNLOADED EDGES	LOADED EDGES			
1	SS	SS	> SS, < C	0.338-0.700	0.514
	C	SS	> SS, < C	0.431-1.20	0.808
2	SS	SS	> SS, < C	0.451-0.709	0.580
	C	SS	> SS, < C	0.501-1.21	0.846
3	SS	SS	> SS, < C	0.312-0.697	0.505
	C	SS	> SS, < C	0.423-1.20	0.801

The rather large scatter in the test data was expected in the  $\sigma_{cr} = \sigma_R$  range and it should be noted that through the use of either OPTION 1 or 3,  $\sigma_{cr}/\sigma_{test} < 1$  for each specimen where  $\sigma_{cr} = \sigma_R$ . However for  $\sigma_{cr}$  in the transition range (and for flat plates),  $\sigma_{cr}/\sigma_{test}$  as calculated by the Schapitz criterion also shows considerable scatter but in addition can be unconservative with respect to the test data. It should also be noted that the panel tests were likely quite sensitive to actual edge conditions, load introduction techniques, etc. The assumption of simple support along loaded edges tends to introduce underestimation of the test result, which is the observed average effect, although there appears to be a trend toward overprediction of buckling strength in the transition range ( $\sigma_R < 2\sigma_p$ ).

It is expected that OPTION 1 with the assumption of all edges simply supported would give the most realistic values for design purposes but it is also acknowledged that the undesirable scatter shown in Table I and Figures 5 through 7 indicate a more conservative criterion for  $\sigma_p$  or the transition relationship would be desirable.



TABLE I - Buckling of Isotropic Skin Panels

REF.	R in.	t in.	a in.	b in.	Test $\sigma_{cr}$ KSI	E $10^6$ psi	a/b	b/R	R/t	Test $10^3 \sigma_{cr}/E$	Edge Cond. Test	Calculated $\frac{\sigma_{cr}}{\text{Test } \sigma_{cr}}$ OPTION 1 • Range, SS to C	Calculated $\frac{\sigma_{cr}}{\text{Test } \sigma_{cr}}$ OPTION 2 • Range, SS to C	Calculated $\frac{\sigma_{cr}}{\text{Test } \sigma_{cr}}$ OPTION 3 • Range, SS to C
16	23.9	.0249	17.0	2.0	9.6	10.5	8.5	.0838	961	.914	↑	.627-1.08	.532-1.07	.621-1.06
↑	↑	.0244	20.0	↑	9.7	↑	10.0	↑	980	.924	↑	.590-1.01	.596-1.02	.591-1.01
↑	↑	.0246	25.0	↑	9.7	↑	12.5	↑	973	.924	↑	.598-1.03	.608-1.03	.597-1.03
↑	↑	.0248	30.0	↑	10.0	↑	15.0	↑	964	.952	↑	.591-1.02	.600-1.02	.590-1.01
↑	↑	.0248	30.0	↑	10.0	↑	15.0	↑	964	.952	↑	.591-1.02	.600-1.02	.590-1.01
↑	↑	↑	↑	↑	(8.8)**	↑	↑	↑	↑	(.838)**	↑	.672-1.15	.682-1.16	.670-1.15
↑	↑	.0246	34.0	2.0	10.3	↑	17.0	.0838	973	.981	↑	.564-.967	.571-.970	.562-.966
↑	↑	↑	↑	↑	(8.3)**	↑	↑	↑	↑	(.790)**	↑	.700-1.20	.709-1.21	.697-1.20
↑	↑	.0248	17.0	3.125	4.8	↑	5.43	.131	964	.457	↑	.545-.889	.606-.924	.552-.884
↑	↑	.0256	20.0	↑	5.1	↑	6.40	↑	934	.486	↑	.546-.890	.600-.921	.548-.891
↑	↑	.0256	25.0	↑	5.4	↑	8.01	↑	934	.514	↑	.516-.840	.561-.866	.510-.836
↑	↑	↑	↑	↑	(4.3)**	↑	↑	↑	↑	(.409)**	↑	.647-1.03	.704-1.09	.640-1.05
↑	↑	.0240	30.0	↑	5.2	↑	9.61	↑	997	.495	↑	.473-.768	.509-.788	.462-.761
↑	↑	.0217	30.0	3.125	5.4	↑	10.88	.131	968	.514	↑	.481-.782	.516-.801	.471-.777
↑	↑	↑	↑	↑	(4.6)**	↑	↑	↑	↑	(.438)**	↑	.564-.919	.505-.934	.552-.911
↑	↑	.0247	17.0	3.0	4.1	↑	3.4	.21	968	.391	↑	.338-.431	.492-.524	.352-.438
↑	↑	.0248	20.0	↑	4.3	↑	4.0	↑	964	.410	↑	.356-.454	.517-.544	.366-.458
↑	↑	.0244	25.0	↑	4.1	↑	5.0	↑	980	.391	↑	.364-.463	.504-.545	.345-.452
↑	↑	.0237	30.0	↑	3.5	↑	6.0	↑	1010	.333	↑	.406-.514	.544-.594	.372-.496
↑	↑	↑	↑	↑	(3.0)**	↑	↑	↑	↑	(.286)**	↑	.472-.598	.632-.692	.432-.577
↑	↑	.0258	30.0	↑	4.3	↑	6.0	↑	927	.410	↑	.381-.488	.505-.561	.352-.471
↑	↑	↑	↑	↑	(3.6)**	↑	↑	↑	↑	(.343)**	↑	.455-.583	.604-.671	.420-.563
16	23.9	.0247	30.0	5.0	4.4	10.5	6.8	.21	968	.419	↑	.346-.441	.451-.501	.312-.423
17	18.	.067	24	12	17.9	10.5	2	.667	269	1.71	↑	.554	.855	.560
↑	↑	↑	↑	12	14.4	↑	2	.667	↑	1.37	↑	.693	1.07	.700
↑	↑	↑	↑	10	17.1	↑	2.4	.556	↑	1.63	↑	.582	.897	.586
↑	↑	↑	↑	10	17.5	↑	2.4	.556	↑	1.67	↑	.568	.876	.573
↑	↑	↑	↑	8	13.7	↑	3	.225	↑	1.30	↑	.931-1.12	1.25-1.60	1.01-1.46
↑	↑	↑	↑	8	16.7	↑	3	.225	↑	1.59	↑	.761-1.16	1.03-1.51	.826-1.20

\*Range, SS to C, used for unloaded edges. Loaded edges assumed SS.

\*\*Initial buckling observed over small portion of specimen.

TABLE I - Buckling of Isotropic Skin Panels  
(Continued)

REF.	R in.	t in.	a in.	b in.	Test $\sigma_{cr}$ KSI	E $10^6$ psi	a/b	b/R	R/t	Test $10^3 \sigma_{cr}/E$	Edge Cond. Test	Calculated $\frac{\sigma_{cr}}{\text{Test } \sigma_{cr}}$ OPTION 1 *Range, SS to C	Calculated $\frac{\sigma_{cr}}{\text{Test } \sigma_{cr}}$ OPTION 2 *Range, SS to C	Calculated $\frac{\sigma_{cr}}{\text{Test } \sigma_{cr}}$ OPTION 3 *Range, SS to C
17	18	.067	24	6	14.0	10.5	4	.333	269	1.33	↑	.713-.805	1.10	.720-.805
		↑	↑	6	13.7	↑	4	.333	↑	1.31	↑	.725-.813	1.12	.731-.819
		↑	↑	4	16.5	↑	6	.222	↑	1.57	↑	.790-1.20	.991-1.31	.791-1.19
		.067	↑	4	16.2	↑	6	.222	269	1.54	↑	.806-1.22	1.00-1.34	.806-1.22
		.038	↑	12	7.16	↑	2	.667	473	0.681	↑	.620	.876	.573
		↑	↑	12	-	↑	2	.667	↑	-	↑	-	-	-
		↑	↑	12	9.24	↑	2	.667	↑	0.879	↑	.479	.679	.444
		↑	↑	12	9.85	↑	2	.667	↑	0.937	↑	.450	.636	.417
		↑	↑	10	8.29	↑	2.4	.556	↑	0.789	↑	.533	.755	.495
		↑	↑	10	9.29	↑	2.4	.556	↑	0.885	↑	.476	.674	.441
		↑	↑	8	10.9	↑	3	.225	↑	1.04	↑	.440-.609	.628-.717	.469-.625
		↑	↑	6	11.7	↑	4	.333	↑	1.11	↑	.379-.386	.536	.352-.363
		↑	↑	6	12.2	↑	4	.333	↑	1.16	↑	.362-.369	.514	.336-.348
		↑	↑	4	8.47	↑	6	.222	↑	0.806	↑	.575-.801	.744-.899	.551-.788
		.038	↑	4	10.32	↑	6	.222	473	0.985	↑	.470-.656	.609-.735	.451-.645
		.030	↑	12	-	↑	2	.667	600	-	↑	-	-	-
		↑	↑	10	5.55	↑	2.4	.556	↑	0.529	↑	.557	.771	.505
		↑	↑	8	5.46	↑	3	.225	↑	0.521	↑	.591-.781	.862-.944	.626-.801
		↑	↑	6	6.54	↑	4	.333	↑	0.622	↑	.475-.476	.659	.430-.436
		.030	↑	4	2.53	↑	6	.222	600	0.241	↑	1.29-1.72	1.70-1.95	1.21-1.68
		.024	↑	12	4.10	↑	2	.667	750	0.391	↑	.538	.735	.481
		↑	↑	10	4.52	↑	2.4	.556	↑	0.431	↑	.488	.666	.456
		↑	↑	8	4.90	↑	3	.225	↑	0.466	↑	.460-.580	.681-.716	.486-.595
		↑	↑	6	7.19	↑	4	.333	↑	0.685	↑	.307	.419	.274
		.024	↑	4	5.01	↑	6	.222	750	0.477	↑	.451-.576	.602-.665	.415-.556
		.018	↑	12	1.66	↑	2	.667	1000	0.158	↑	.855	1.15	.754
		↑	↑	10	1.84	↑	2.4	.556	↑	0.175	↑	.772	1.04	.691
		↑	↑	8	1.99	↑	3	.225	↑	0.190	↑	.711-.844	1.06-1.08	.753-.870
17	18	.018	24	6	2.78	10.5	4	.333	↑	0.265	↑	.510	.688	.449

TABLE I - Buckling of Isotropic Skin Panels  
(Continued)

Ref.	R	t	a	b	Test $\sigma_{cr}$ KSI	E $10^6$ psi	a/b	b/R	R/t	Test $10^3 \sigma_{cr}/E$	Edge Cond. Test	Calculated $\frac{\sigma_{cr}}{\text{Test } \sigma_{cr}}$ OPTION 1 *Range, SS to C	Calculated $\frac{\sigma_{cr}}{\text{Test } \sigma_{cr}}$ OPTION 2 *Range, SS to C	Calculated $\frac{\sigma_{cr}}{\text{Test } \sigma_{cr}}$ OPTION 3 *Range, SS to C
17	18	.018	24	4	-	10.5	6	.222	1000	-	→	-	-	-
	36	.067	→	12	5.13	→	2	.333	537	0.489	→	.714-.717	1.10	.778
	→	→	→	10	5.35	→	2.4	.278	→	0.510	→	.345-.763	1.05	.745-.804
	→	→	→	8	6.15	→	3	.222	→	0.585	→	.638-.872	.916-1.03	.677-.895
	→	→	→	6	8.81	→	4	.167	→	0.839	→	.616-.975	.725-1.04	.631-.984
	→	.067	→	4	12.5	→	6	.111	537	1.19	→	.884-1.50	.917-1.51	.884-1.50
	→	.038	→	12	2.51	→	2	.333	947	0.239	→	.615	.921	.652
	→	→	→	12	4.05	→	2	.333	→	0.386	→	.381	.570	.404
	→	→	→	10	2.69	→	2.4	.278	→	0.256	→	.576	.861	.610-.617
	→	→	→	8	1.55	→	3	.222	→	0.148	→	1.00-1.22	1.50-1.54	1.06-1.25
	→	→	→	6	4.81	→	4	.167	→	0.458	→	.398-.594	.498-.652	.408-.600
	→	→	→	6	3.98	→	4	.167	→	0.579	→	.480-.717	.602-.789	.494-.726
	→	→	→	4	7.21	→	6	.222	→	0.686	→	.214-.263	.288-.308	.194-.250
17	36	.038	24	4	6.58	10.5	6	.222	947	0.626	→	.235-.288	.316-.338	.213-.274
17	→	.067	24	12.4	1.90	10.5	1.935	0	∞	0.181	→	.586-1.01		
	→	→	→	10.6	2.44	→	2.262	→	→	0.232	→	.625-1.08		
	→	→	→	8.6	3.68	→	2.79	→	→	0.350	→	.634-1.09		
	→	→	→	6.8	5.86	→	3.53	→	→	0.558	→	.635-1.10		
	→	→	→	6.8	5.64	→	3.53	→	→	0.536	→	.660-1.15		
	→	→	→	5	12.3	→	4.8	→	→	1.17	→	.555-.967		
	→	.067	→	5	11.2	→	4.8	→	→	1.07	→	.607-1.06		
	→	.038	→	12	.60	→	2	→	→	0.0571	→	.635-1.10		
	→	→	→	12	.76	→	2	→	→	0.0723	→	.500-.869		
	→	→	→	12	.51	→	2	→	→	0.0486	→	.745-1.29		
	→	→	→	10	.94	→	2.4	→	→	0.0896	→	.584-1.01		
	→	→	→	8	1.64	→	3	→	→	0.156	→	.521-.905		
	→	→	→	6	2.42	→	4	→	→	0.230	→	.631-1.09		
17	→	.038	24	4	4.61	10.5	6	0	∞	0.439	→	.745-1.29		

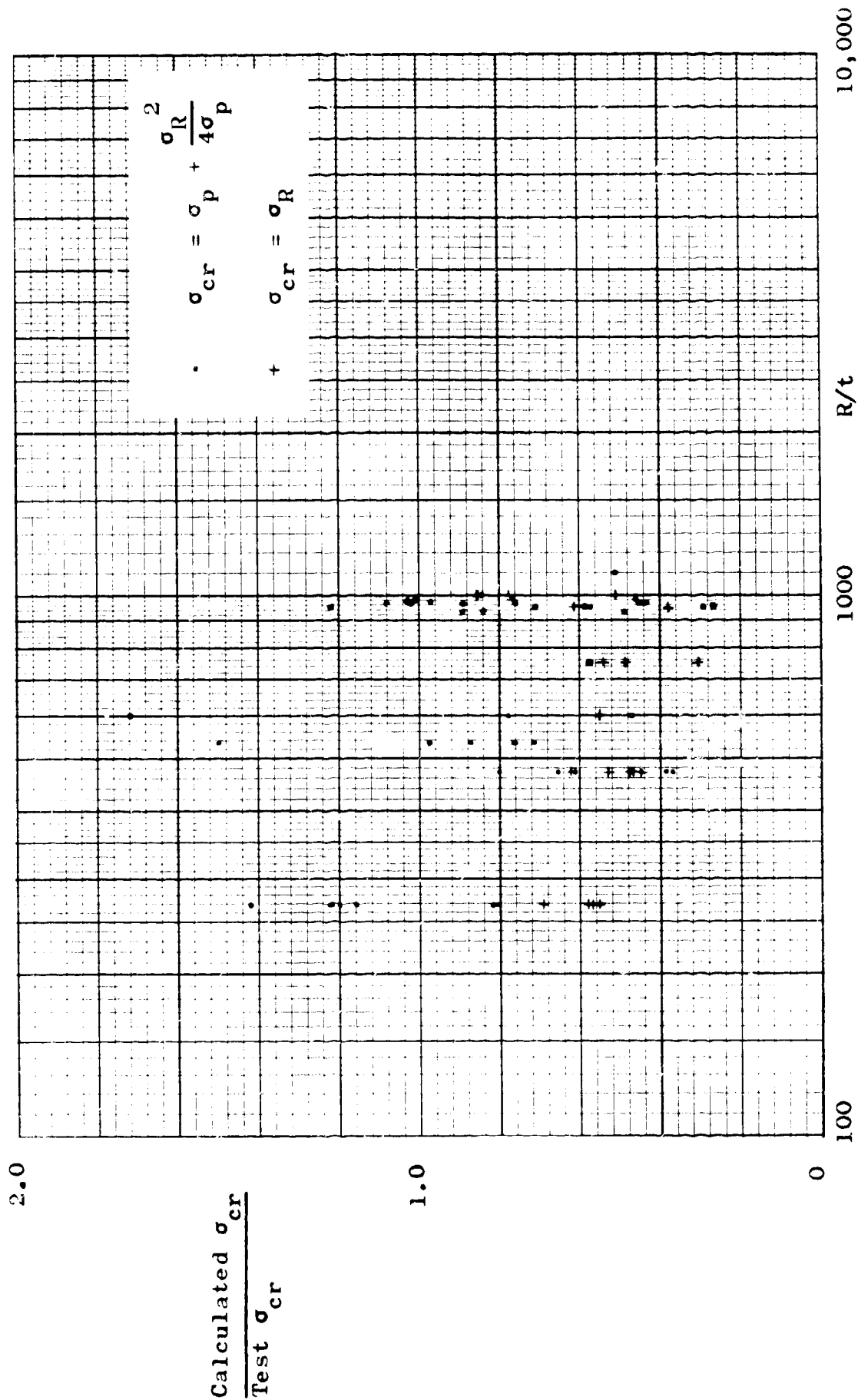


Figure 5 - Buckling of Isotropic Skin Panels  
Calculated vs. Test ( $\sigma_R$  from OPTION 1)

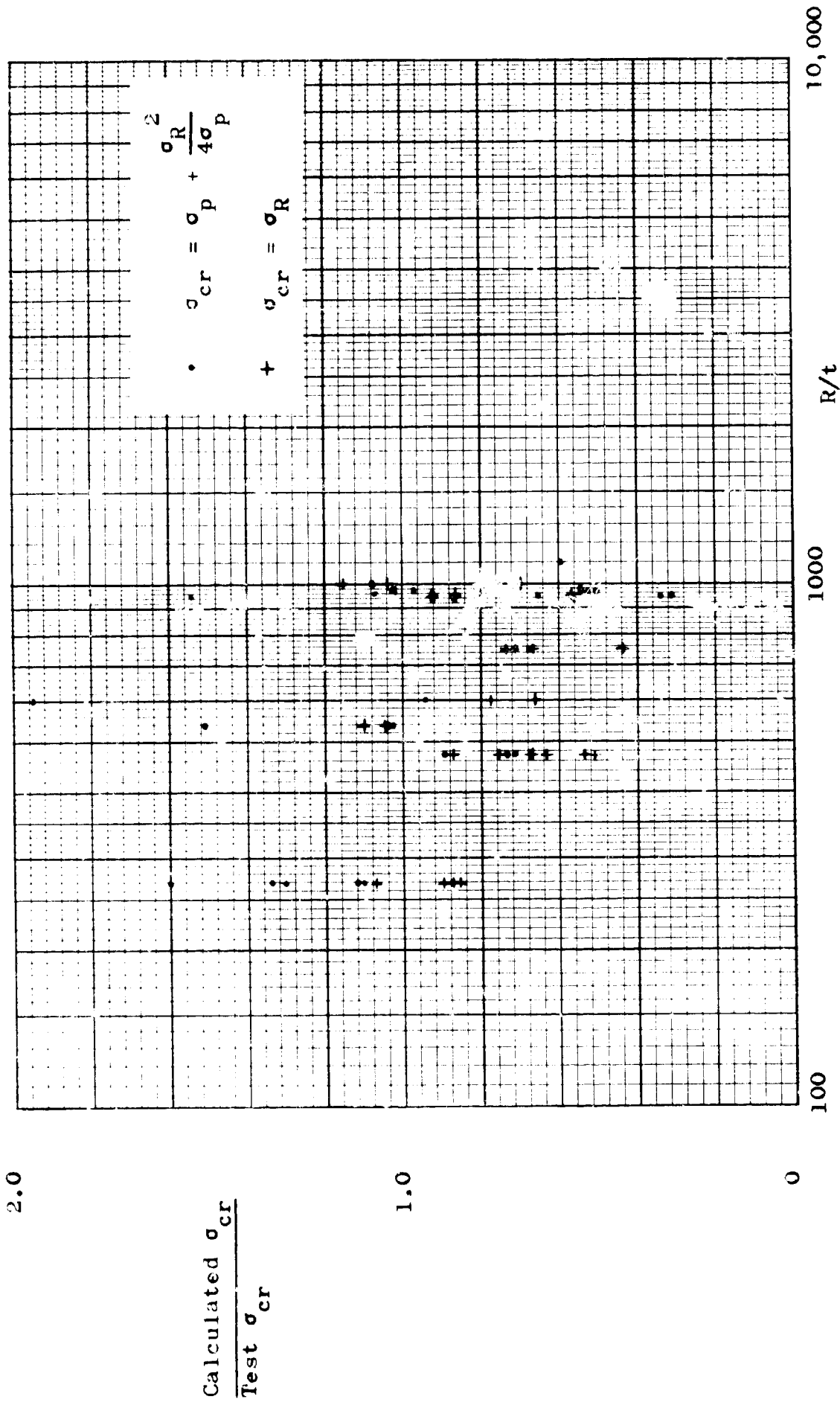


Figure 6 - Buckling of Isotropic Skin Panels -  
Calculated vs. Test ( $\sigma_R$  from OPTION 2)

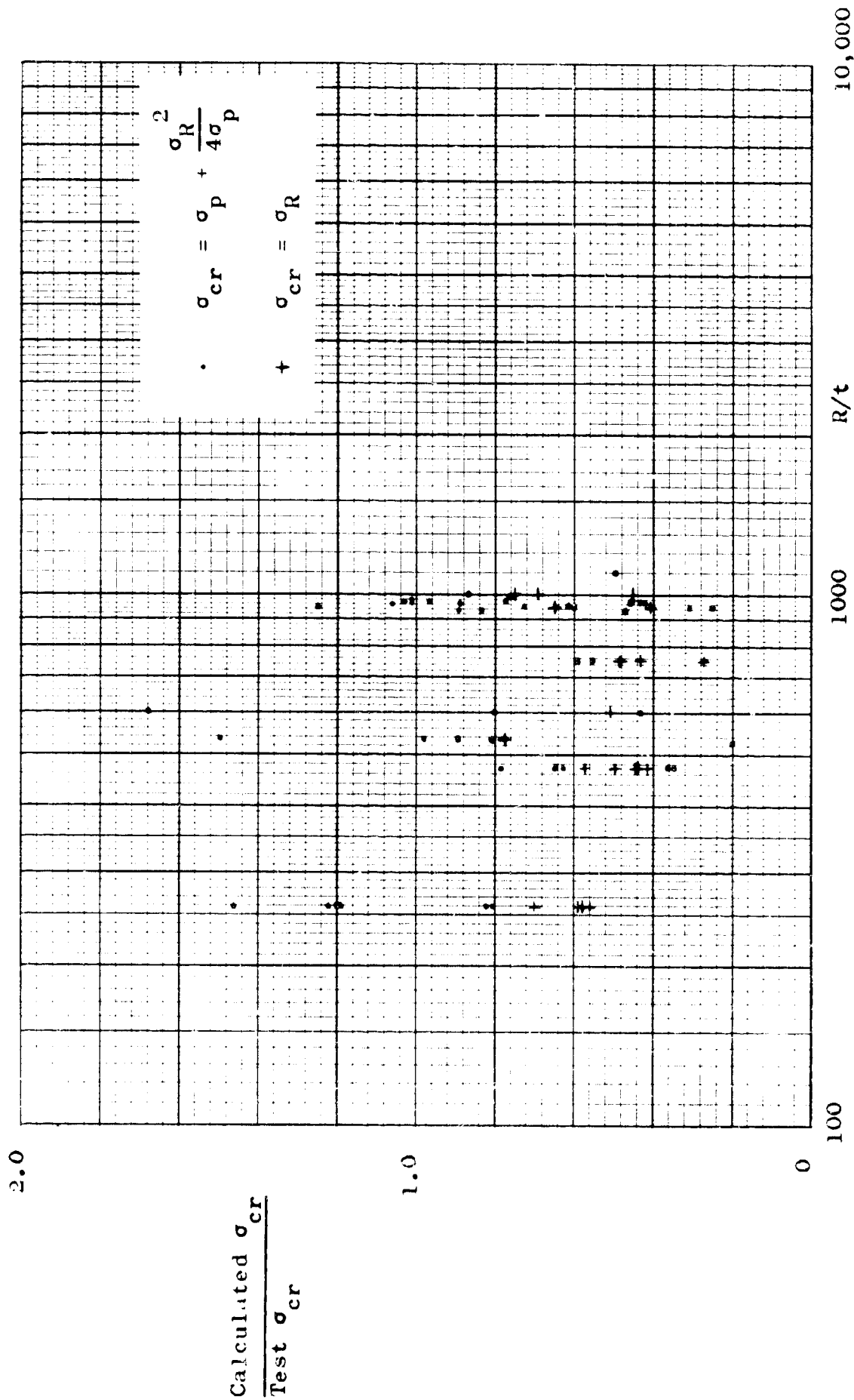


Figure 7 - Buckling of Isotropic Skin Panels -  
Calculated vs. Test ( $\sigma_R$  from OPTION 3)

6.0 COMPRESSIVE BUCKLING OF  
LONGITUDINALLY STIFFENED  
CIRCULAR CYLINDERS

6.1 General

This phase of the study applies both to entire cylinders which incorporate only longitudinal stiffening, and to sections which lie between the circumferential members of cylinders which include both longitudinal and circumferential stiffening. In the latter case, the methods presented furnish a means for prediction of the panel instability mode of buckling. As presented in this report, the procedures deal primarily with configurations for which neither buckling of the isotropic panels nor local buckling of the longitudinal stiffeners is permitted. However, the methods can be extended to situations which do not satisfy these restrictions and brief mention is made in Part II of the means by which this may be accomplished.

6.2 Buckling Criteria

6.2.1 Almroth Extension to Thielemann Solution

In the solution of buckling problems, a number of different approaches may be taken. Two of the most commonly used techniques are the minimum energy method and the bifurcation concept. The former is based upon the theorem of minimum total potential energy which may be stated as follows:

A conservative system is in a configuration of stable equilibrium if, and only if, the value of the total potential energy is a relative minimum.

To apply this theorem, one must formulate the total potential energy of the system, impose the mathematical artifice known as a virtual displacement, and examine the sign of the second-order energy changes (second variation). The second variation must be positive definite (positive regardless of the sign and form of the virtual displacement) for stability to exist.

The bifurcation concept, originally developed by Poincaré [credited in ref. 18] in 1885, constitutes an equilibrium approach to the problem of buckling. Any point at which a single equilibrium path branches into two or more equilibrium paths is known as a bifurcation point. An example of this phenomenon is shown in Figure 8.

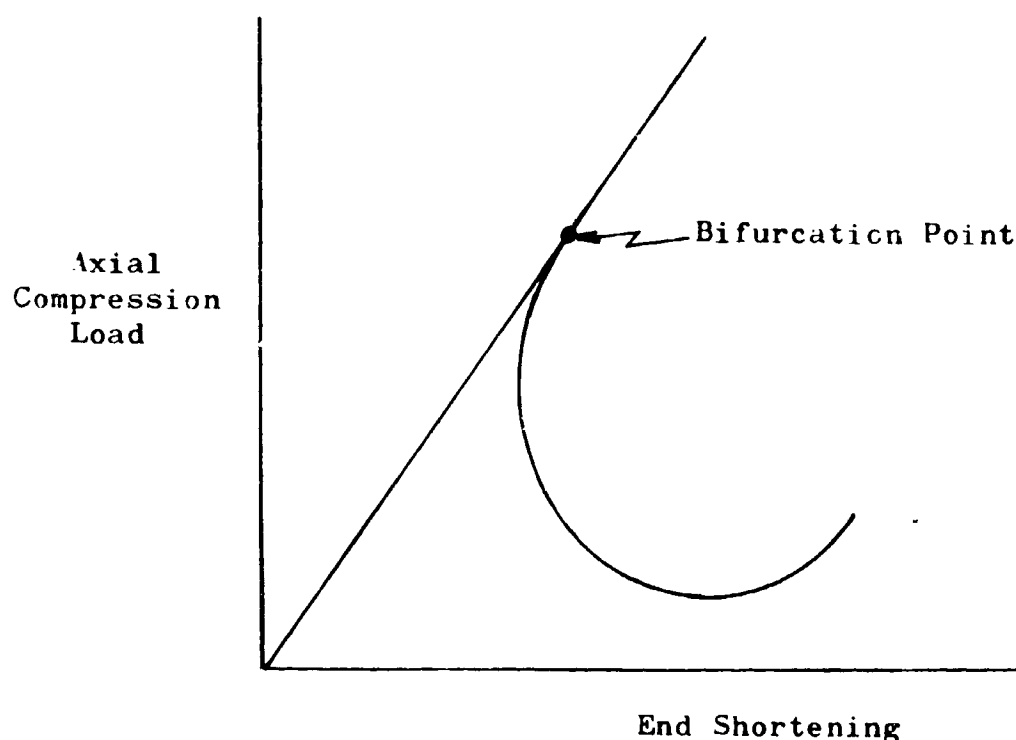


Figure 8 - Equilibrium Paths For a Perfect Isotropic Circular Cylinder Subjected to Axial Compression



This figure depicts the equilibrium paths for a perfect isotropic circular cylinder subjected to axial compression. As a rule, the unbuckled configuration becomes unstable at a bifurcation point, and the bifurcation approach to buckling analysis involves a search for these points. In this search, one must study the character of the equilibrium behavior. As in the Thielemann derivation [19], this study may be conducted with the assistance of energy principles. Such investigations should not be misconstrued as constituting a minimum energy approach, however. In the minimum energy method, a so-called second variation is examined. On the other hand, the bifurcation method involves the study of only the so-called first variation. That is, in this case the system is subjected to a virtual displacement and the first-order change (first variation) in the total potential energy is tested for compliance with the principle of stationary potential energy which may be stated as follows:

A necessary and sufficient condition for the equilibrium of an elastic body is that the first-order change in the total potential energy of the body be equal to zero for any virtual displacement.

Most of the stiffened-cylinder analysis methods presented in this report are outgrowths of the formulations derived by Thielemann [19] in 1959. The particular formulations used here were based on the classical small-deflection theory which locates a bifurcation point

along the initially linear equilibrium path of a perfect monolithic orthotropic circular cylinder subjected to axial compression. The use of small-deflection theory raises some important questions as to the influence of initial imperfections and their interrelationship with the shape of the postbuckling equilibrium path. This matter will be taken up in Section 9, "Initial Imperfections". Using the coordinate system depicted in Figure 9, the Thielemann equations were obtained

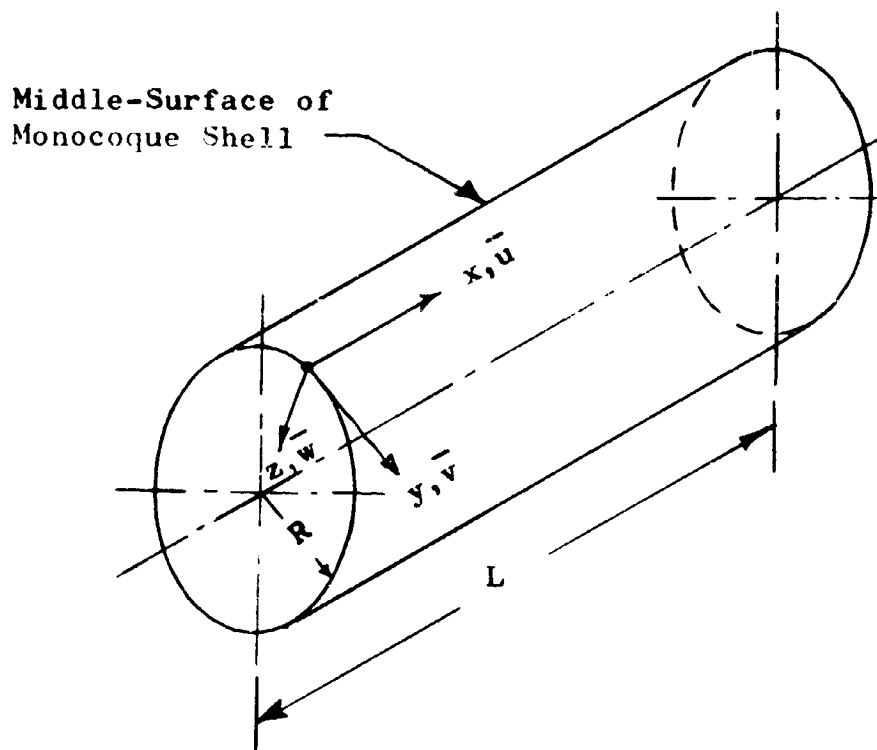


Figure 9 - Thielemann Notation

by first formulating the following expressions for the membrane strain energy  $U_m$ , the flexural strain energy  $U_b$ , and the potential energy  $\Omega$  of the external load:

$$U_m = \frac{1}{2} \int_0^L \int_0^{2\pi R} [A_{11} N_x^2 + 2A_{12} N_x N_y + A_{22} N_y^2 + A_{33} N_{xy}^2] dx dy \quad (6-1)$$

$$U_b = \frac{1}{2} \int_0^L \int_0^{2\pi R} [D_{11} \bar{w}_{,xx}^2 + 2D_{12} \bar{w}_{,xx} \bar{w}_{,yy} + D_{22} \bar{w}_{,yy}^2 + 4D_{33} \bar{w}_{,xy}^2] dx dy \quad (6-2)$$

$$\Omega = - \int_0^{2\pi R} \left( N_x \right)_{x=L} dy \int_0^L \bar{u}_{,x} dx \quad (6-3)$$

The total potential energy of the system is then expressed as follows:

$$V = U_m + U_b + \Omega$$

The principle of stationary potential energy is then utilized to establish the character of the equilibrium for this system.

In Figure 9, the quantities  $x, y, z$  are the coordinates and  $\bar{u}$ ,  $\bar{v}$ ,  $\bar{w}$  represent reference-surface displacements in these respective directions. In equations (6-1) through (6-3), the  $N$ 's represent appropriate stress resultants while the  $A_{ij}$ 's and  $D_{ij}$ 's are the so-called elastic constants. These constants arise through the following

expressions which relate the stress resultants to the deformation of the cylinder:

$$\epsilon_x = A_{11} N_x + A_{12} N_y$$

$$\epsilon_y = A_{21} N_x + A_{22} N_y$$

$$\gamma_{xy} = A_{33} N_{xy}$$

$$M_x = D_{11} \bar{w}_{,xx} + D_{12} \bar{w}_{,yy}$$

$$M_y = D_{21} \bar{w}_{,xx} + D_{22} \bar{w}_{,yy}$$

$$M_{xy} = 2D_{33} \bar{w}_{,xy}$$

(6-4)

Attention is called to the fact that, throughout this report, subscripts which are preceded by commas denote partial differentiation with respect to the subscript variable. For example, the quantity  $\bar{w}_{,xy}$  is identical to  $\frac{\partial^2 \bar{w}}{\partial x \partial y}$ . Thus, in the first of equations (6-4) the absence of commas before the subscripts indicates that these are simply direction identification symbols, whereas in the fourth of equations (6-4) the presence of the commas indicates reference to the partial derivatives  $\frac{\partial^2 \bar{w}}{\partial x^2}$  and  $\frac{\partial^2 \bar{w}}{\partial y^2}$ .

One of the attractive features of the Thielemann equations is their compact and informative structure. This was achieved through the introduction of a dimensionless load parameter  $\bar{N}$  and three dimensionless stiffness parameters which are defined as follows:

$$\bar{N} = \frac{RN_x}{2} \sqrt{\frac{A_{11}}{D_{22}}}$$

$$\eta_s = \frac{\left(A_{12} + \frac{1}{2} A_{33}\right)}{\sqrt{A_{11} A_{22}}}$$

(6-5)

$$\eta_p = \frac{\left(D_{12} + 2D_{33}\right)}{\sqrt{D_{11} D_{22}}}$$

$$\gamma = \frac{D_{11} A_{11}}{D_{22} A_{22}}$$

Using equations (6-1) through (6-5) together with the bifurcation approach to buckling, Thielemann [19] arrived at the following expression from which a classical critical compressive load can be found:

$$\bar{N} = \left[ \frac{1 + 2\eta_p \sqrt{\gamma} \beta^2 + \gamma \beta^4}{1 + 2\eta_s \beta^2 + \beta^4} \right]^{1/2} \quad (6-6)$$

where

$$\beta = \frac{\ell_y}{\ell_x} \left( \frac{A_{22}}{A_{11}} \right)^{1/4} \quad (6-7)$$

$\ell_x$  = Axial half-wavelength of buckle pattern

$\ell_y$  = Circumferential half-wavelength of buckle pattern

This equation simply establishes the magnitudes of longitudinal compressive loads which will maintain the monocoque orthotropic circular cylinder in deflected configurations defined by the half-wavelengths  $\ell_x$  and  $\ell_y$ . For a given combination of stiffness values, an infinite number of load-wavelength combinations can be possible. The critical load is the lowermost load which is just sufficient to hold the shell in the non-cylindrical deflected shape.

It should be kept in mind that equation (6-6) was derived for a monocoque orthotropic circular cylinder. This equation and others likewise developed for monocoque configurations will subsequently be applied to the analysis of discretely stiffened shells. The key to success in these applications lies in the means employed to evaluate the elastic constants (the  $A_{ij}$ 's and  $D_{ij}$ 's). From equations (6-4), it can be seen that these quantities are dependent upon the various structural rigidities of the shell wall. Practical procedures for computing these constants are presented in the procedures of Part II. However, at this time it is profitable to devote some attention to their origins and to examine the formulations which would apply in two very special cases. In the first place, it is helpful to note that for an isotropic cylinder these constants would take on the following forms:

$$\begin{aligned} A_{11} &= A_{22} = \frac{1}{Et} \\ A_{12} &= A_{21} = -\frac{\nu}{Et} \end{aligned} \tag{6-8}$$

$$A_{33} = \frac{1}{Gt}$$

$$D_{11} = D_{22} = \frac{Et^3}{12(1-\nu^2)}$$

(6-8 Cont'd)

$$D_{12} = D_{21} = \frac{\nu Et^3}{12(1-\nu^2)}$$

$$D_{33} = \frac{Gt^3}{12}$$

In general, the buckling analysis procedures and design curves presented in this report are to be considered inapplicable to sandwich structures. However, at this point it is still informative to note that the following formulas could be used to find the elastic constants in the very special case of a sandwich configuration having a core with infinite transverse shear rigidity:

$$A_{11} = A_{22} = \frac{1}{2t_f E}$$

$$A_{12} = A_{21} = -\frac{\nu}{2t_f E}$$

$$A_{33} = \frac{1}{2t_f G}$$

(6-9)

$$D_{11} = D_{22} = \frac{Et_f h^2}{2(1-\nu^2)}$$

$$D_{12} = D_{21} = \frac{\nu E t_f h^2}{2(1-\nu^2)} \quad (6-9 \text{ Cont'd})$$

$$D_{33} = \frac{G t_f h^2}{2}$$

where

$t_f$  = Facing thickness

$h$  = Distance between middle-surfaces of facings.

These equations are applicable when the facings are of the same material and of equal thickness and this thickness is small compared to  $h$ .

From equations (6-4), (6-8), and (6-9), it should be observed that

- (a)  $A_{11}$  constitutes the reciprocal of the longitudinal extensional stiffness per unit length of circumference.
- (b)  $A_{22}$  constitutes the reciprocal of the circumferential extensional stiffness per unit of axial length.
- (c)  $D_{11}$  constitutes the longitudinal flexural stiffness per unit length of circumference.
- (d)  $D_{22}$  constitutes the circumferential flexural stiffness per unit of axial length.
- (e)  $A_{12}$  and  $A_{21}$  each constitute measures of coupling between extensional deformations in the longitudinal and circumferential directions.
- (f)  $D_{12}$  and  $D_{21}$  each constitute measures of coupling between flexural deformations in the longitudinal and circumferential directions.



- (g)  $A_{33}$  constitutes the reciprocal of the in-plane shear stiffness of the shell wall.
- (h)  $D_{33}$  constitutes the twisting stiffness of the shell wall.

The Thielemann solution given above as equation (6-6) was derived for an infinite-length cylinder which is free to accommodate longitudinal half-wavelengths of arbitrary magnitude. Such a solution will ordinarily be adequate for simply supported realistic finite-length cylinders when the calculated longitudinal half-wavelength of the buckle pattern is less than the overall length of the cylinder. However, for short cylinders this conditions frequently will not be satisfied, in which case a finite-length solution is required for acceptable analysis. Such a solution has been obtained by Almroth [20, 21]. The resulting equation is essentially an extended, improved version of the Thielemann formulation. The extension was achieved by enforcing the requirement that the longitudinal half-wavelength of the buckle pattern must be equal to the shell length divided by an integer. To facilitate this development, Almroth defined a new parameter as follows:

$$\alpha = \frac{L^2}{2Rm^2 \pi^2 A_{22} \sqrt{D_{22}/A_{11}}} \quad (6-10)$$

where  $m$  is the number of longitudinal half-waves. The buckling equation which evolved from this work is as follows:

$$\bar{N} = \frac{\alpha \beta^4}{1 + 2\eta_s \beta^2 + \beta^4} + \frac{1 + 2\eta_p \gamma^{1/2} \beta^2 + \gamma \beta^4}{4\alpha \beta^4} \quad (6-11)$$

To establish the critical load from this equation, a minimization process must be employed which establishes the particular value of  $\beta$  for which  $\bar{N}$  (and consequently  $N_x$ ) is a minimum. Almroth [20] notes that for some practical applications,  $\alpha$  will be large and consequently  $\beta$  will be small. For such situations, Almroth further notes that equation (6-11) can be simplified to the following approximation:

$$\text{Critical } \bar{N} = 1 + \frac{\gamma}{4\alpha} \quad (6-12)$$

Substitution of equations (6-5) and (6-10) into (6-12) yields the following result:

$$\text{Critical } N_x = \frac{m^2 \pi^2 D_{11}}{L^2} + \frac{2}{R} \sqrt{\frac{D_{22}}{A_{11}}} \quad (6-13)$$

This equation is identically equivalent to the expression proposed in references 16 and 22 for application to longitudinally stiffened circular cylinders. Clearly, this expression should be used only under rather restrictive conditions. An awareness of this limitation is necessary to appreciate the need for the minimization factor  $\tilde{N}$  to be introduced in Section 6.2.2 below.

Just as in the case of equation (6-6), equations (6-11), (6-12), and (6-13) evolve from monocoque shell theory and their application to discretely stiffened configurations is justified through the means employed for computation of the elastic constants involved.

6.2.2      Stuhlman-DeLuzio-Almroth Solution - Under NASA Contracts NAS 8-5600 and NAS 8-9500, the NASA Marshall Space Flight Center has sponsored a test and study program on the buckling of longitudinally stiffened curved panels and complete cylinders. The longitudinal stiffeners were integral with the basic cylindrical skin on all of these tests. This work was performed by the Lockheed Missiles and Space Company and the results are summarized in references 1, 2, 3, 10, and 23. In order to properly evaluate these experimental results, Stuhlman, et al. [23] found it necessary to develop analysis techniques which account for both end moment and stiffener eccentricity. Making use of the Thielemann parameters, they developed a digital computer program [10] which includes both of these effects as well as the end-restraint to Poisson-ratio hoop growth. This program assumes boundary conditions of simple support and, like the equations of Section 6.2.1, it is based on monocoque shell theory. As before, the application to discretely stiffened cylinders is achieved by properly computing the related elastic constants. The subject program calculates these values internally within the computer. The structure is described to the machine through input geometric dimensions which are applicable only to the particular type of local wall cross section used in the test series cited above. Some generalization could be readily accomplished by modifications which would permit the analyst to input hand-calculated elastic-constant values. It is suggested that this be accomplished to facilitate application to a wide variety of longitudinally stiffened configurations.

GENERAL DYNAMICS  
Convair Division

The proposed generalized version of the Stuhlman, et al. program [10] is recommended for detailed final analysis. However, consistent with the overall philosophy of this report, it is noted that simplified, approximate analysis methods can also be useful, primarily in the early stages of design and analysis. Such methods will now be presented for the longitudinally stiffened configuration. This approach is based on the simplifying assumption that all pre-buckling bending of the shell wall can be neglected. This, of course, rules out consideration both of end moment effects and the influence of restraint to Poisson-ratio hoop growth. Within this framework, Stuhlman, et al. [23] show that their more complicated theory simplifies into the following expression for the non-dimensional load parameter  $\bar{N}$ :

$$\bar{N} = \frac{1 + 2\eta_p \gamma^{1/2} \beta^2 + \gamma \beta^4}{4\alpha \beta^4} + \frac{\alpha \beta^4 \left( 1 - \frac{C_{11}}{2\alpha (A_{22} D_{22})^{1/2} \beta^2} \right)^2}{1 + 2\eta_s \beta^2 + \beta^4} \quad (6-14)$$

This is a monocoque shell equation which, as usual, must be minimized to arrive at the critical  $\bar{N}$  (and consequently critical  $N_x$ ) values. The term  $C_{11}$  is an outgrowth of non-symmetry in the local wall cross section and is taken equal to the distance between the middle surface of the basic cylindrical skin and the centroid of the skin-stringer combination. Equation (6-14) is based on the sign convention whereby  $C_{11}$  is positive in the radially inward direction. Hence this quantity will be positive for internally stiffened configurations and negative

when the stiffeners are on the exterior surface. Although non-zero  $C_{11}$  values were necessarily accounted for in the test data evaluations of Section 6.4, the analysis procedures given in Part II of this report only cover cases for which  $C_{11} = 0$  is a reasonable approximation. However, these procedures could easily be extended to cover non-zero  $C_{11}$  values and it is certainly recommended that this be accomplished. It should be noted at this time that, when  $C_{11} = 0$ , equation (6-14) is identical to the Almroth formulation given in Section 6.2.1 as equation (6-11).

It is pointed out that the design curves presented in Section 12.2 for the buckling of longitudinally stiffened cylinders were developed under the assumption that  $D_{12} = D_{33} = 0$ . From the third of equations (6-5), it can be seen that this is equivalent to assuming that  $\eta_p = 0$ . This same assumption will likewise be made in other of the approximate procedures given in this report. For many practical situations the mechanisms represented by  $\eta_p$  do not play a crucial role in the buckling phenomenon and its neglect will usually lead to a reasonable degree of conservatism. Furthermore,  $\eta_p$  is probably the most difficult to compute of all the Thieleman parameters. In particular, consider the elastic constant  $D_{33}$  which appears in the  $\eta_p$  formulation. The last of equations (6-4) shows  $D_{33}$  to be a measure of the twisting stiffness of the shell wall. The monocoque shell theory used in this report is based on a model for which the twisting rigidities

in the longitudinal and circumferential directions are equal. The rigidities encountered in practical stiffened configurations will usually not comply with this condition. This might suggest the use of an average value in the analysis. However, suspicion is cast upon this practice when one considers the nature of the twisting mechanism in the monocoque wall. That is, the twisting moment  $M_{xy}$  is a stress resultant which arises out of the non-uniform, linear distribution of shear stress depicted in Figure 10. For the infinitesimal element shown, the interaction of twisting moments on faces A and B is influenced by the fact that, for any point along the edge CD, the shearing stresses

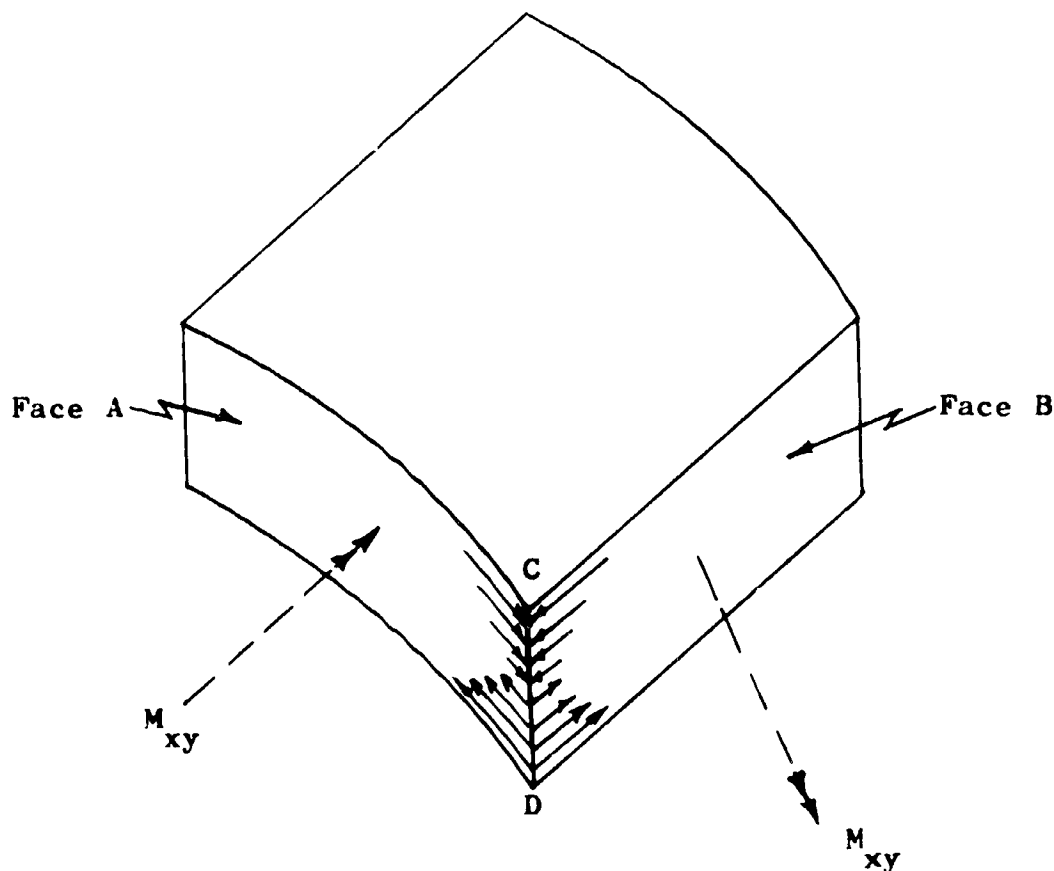


Figure 10 - Interaction of Twisting Moments in  
Wall of Monocoque Cylinder

on the two faces must be equal. The uniformity of the monocoque wall permits this type of interaction to develop over the entire surface. On the other hand, in the case of discretely stiffened structures, intersecting faces such as A and B are not always present. The stiffeners protrude from the basic skin and the mechanism depicted in Figure 10 cannot always develop. In addition, for structures which incorporate both longitudinal and circumferential stiffeners, twisting moments from either type of stiffener will transfer into the other almost entirely in the form of bending. Stringer twisting moments transfer directly into circumferential bending of the rings and ring twisting moments transfer directly into longitudinal bending of the stringers.

In view of the foregoing, justification for neglecting  $\eta_p$  in the buckling analysis does not rest solely in the consequent simplifications. Indeed, there exist some fundamental uncertainties as to what constitutes the best means to mathematically formulate the correspondence between twisting rigidities of the discretely stiffened structure and its monocoque model. Confronted with this uncertainty, it seems best at this time to exercise caution and take no advantage from  $\eta_p$  in the buckling analysis. Even with this omission, the methods presented in this report account for more of the shell wall characteristics than have generally been recognized in procedures of the past.

For any special situation where the analyst might somehow be equipped with means for computing reliable non-zero  $D_{12}$  and  $D_{33}$  values,

the digital computer program of Section 18.3.2 can be applied. Although this program was developed mainly for application to configurations which include both longitudinal and circumferential stiffeners, it can be specialized to applications which involve only longitudinal stiffening. This is accomplished through the input values. It must be kept in mind, however, that this program is restricted to boundary conditions of simple support. As an engineering approximation, it is recommended that one account for fixity influences by investigating only those buckle configurations for which

$$m^2 \geq C_F \quad (6-15)$$

where

$C_F$  = Fixity factor

In addition, since the present Section 18.3.2 program does not account for crippling stress influences, it should not be applied in the slenderness ratio range which is controlled by the Johnson parabola.

With the foregoing as a background, it is now possible to proceed with the development of the equations which were used to plot the design curves of Section 12.2. For this purpose it will be assumed that

$$\eta_p = 0 \quad (6-16)$$

and a quantity  $F$  will be defined as

$$F = \frac{C_{11}}{2\alpha(A_{22}D_{22})^{1/2}} \quad (6-17)$$



so that equation (6-14) may be rewritten in the following form:

$$\bar{N} = \frac{\gamma}{4\alpha} + \left[ \frac{1}{4\alpha\beta^4} + \frac{\alpha(\beta^2 - F)^2}{1 + 2\eta_s\beta^2 + \beta^4} \right] \quad (6-18)$$

It should be recalled that the first of equations (6-5) defined the parameter  $\bar{N}$  as follows:

$$\bar{N} = \frac{RN_x}{2} \sqrt{\frac{A_{11}}{D_{22}}} \quad (6-19)$$

Substitution of this equality into equation (6-18) gives the following:

$$N_x = \frac{2}{R} \sqrt{\frac{D_{22}}{A_{11}}} \left( \frac{\gamma}{4\alpha} \right) + \frac{2}{R} \sqrt{\frac{D_{22}}{A_{11}}} \left[ \frac{1}{4\alpha\beta^4} + \frac{\alpha(\beta^2 - F)^2}{1 + 2\eta_s\beta^2 + \beta^4} \right] \quad (6-20)$$

From equations (6-5) and (6-10), it is known that

$$\gamma = \frac{D_{11}A_{11}}{D_{22}A_{22}} \quad (6-21)$$

and

$$\alpha = \frac{L^2}{2Rm^2\pi^2A_{22}\sqrt{D_{22}/A_{11}}} \quad (6-22)$$

Using equations (6-21) and (6-22), the following equality is easily obtained:

$$\frac{2}{R} \sqrt{\frac{D_{22}}{A_{11}}} \left( \frac{\gamma}{4\alpha} \right) = \frac{m^2\pi^2D_{11}}{L^2} \quad (6-23)$$

It should be recalled that the quantity  $D_{11}$  constitutes the longitudinal flexural stiffness per unit length of circumference. In the case of the longitudinally stiffened cylinder, this value may be computed from one of the following two formulas:

$$D_{11} = EI_x \quad (6-24)$$

or

$$D_{11} = \frac{EI_x}{(1-\nu^2)} \quad (6-25)$$

where

$$I_x = \text{Shell wall local moment of inertia per unit length of circumference taken about the centroidal axis of stringer-skin combination.}$$

The choice between these two formulas depends upon the degree of restraint which the wall geometry affords to anticlastic bending [ref. Glossary] . For most practical discretely stiffened structures, equation (6-24) will be the recommended formulation.

At this point, it is helpful to note that, for longitudinally stiffened cylinders, the elastic constants  $A_{11}$ ,  $A_{22}$ , and  $D_{22}$  can be expressed as follows:

$$\begin{aligned} A_{11} &= \frac{1}{Et_x} \\ A_{22} &= \frac{1}{Et} \\ D_{22} &= \frac{Et^3}{12(1-\nu^2)} \end{aligned} \quad (6-26)$$

where

$t_x$  = Wall thickness for a monocoque circular cylinder of same total cross-sectional area as the actual composite shell wall (including both skin and stringers)

$t$  = Thickness of isotropic skin panel

The  $(1-\nu^2)$  term appears in the expression for  $D_{22}$  since the broad axial extent of the skin panel affords restraint to anticlastic bending in the same manner as that customarily recognized for flat plates.

By direct substitution and simplification, equations (6-26) lead to the following equality:

$$\frac{2}{R} \sqrt{\frac{D_{22}}{A_{11}}} = \frac{Et^2}{R\sqrt{3(1-\nu^2)}} \sqrt{\frac{t_x}{t}} \quad (6-27)$$

Substituting equations (6-23) and (6-27) into equation (6-20) one may then obtain

$$N_x = \frac{m^2 \pi^2 D_{11}}{L^2} + \frac{Et^2}{R\sqrt{3(1-\nu^2)}} \sqrt{\frac{t_x}{t}} \left[ \frac{1}{4\alpha\beta^4} + \frac{\alpha(\beta^2 - F)^2}{1 + 2\eta_s\beta^2 + \beta^4} \right] \quad (6-28)$$

It should be observed that  $m$  (the number of longitudinal half-waves) appears in both the first and the bracketed terms of this equation. Its presence in the latter is due to formulas (6-17) and (6-22) for  $F$  and  $\alpha$  respectively. Hence, for any particular selected  $m$  value, a corresponding critical axial loading  $(N_x)_{cr}$  can be found from the following:

$m=m_i$

$$(N_x)_{cr} = \frac{m_i^2 \pi^2 D_{11}}{L^2} + \frac{Et^2}{R \sqrt{3(1-\nu^2)}} \sqrt{\frac{t_x}{t}} \tilde{N}_{m=m_i} \quad (6-29)$$

where

$$\tilde{N}_{m=m_i} = \left[ \frac{1}{4\alpha\beta^4} + \frac{\alpha(\beta^2 - F)^2}{1 + 2\eta_s \beta^2 + \beta^4} \right] \quad (6-30)$$

Minimum  
for  $m = m_i$

and

$$m_i = \text{Any particular selected value of } m \quad (6-31)$$

The particular  $m_i$  value of interest is that which yields the lowermost axial load intensity. This is, in fact, the critical buckling load for the structure and will henceforth be identified simply as  $(N_x)_{cr}$ . The corresponding stress value will be denoted  $\sigma_{cr}$ .

In order to express equation (6-29) in terms of stress, one may divide through by  $t_x$  to obtain

$$\sigma_{cr} = \frac{m_i^2 \pi^2 E}{\left(\frac{L}{\rho_{11}}\right)^2} + \frac{E}{R \sqrt{3(1-\nu^2)}} \frac{t_x^{3/2}}{t_x^{1/2}} \tilde{N}_{m=m_i} \quad (6-32)$$

where

$$\rho_{11} = \sqrt{\frac{I_x}{t_x}} \quad (6-33)$$

or

$$\rho_{11} = \sqrt{\frac{I_x}{t_x(1-\nu^2)}} \quad (6-34)$$

The formula to be used for  $\rho_{11}$  depends, of course, upon the restraint which the wall affords to anticlastic bending. Henceforth,  $\rho_{11}$  will be referred to as the effective local longitudinal radius of gyration of the shell wall. The word "effective" is included in this identification because of the possible presence of the factor  $(1-\nu^2)$ . Except for this relatively minor influence,  $\rho_{11}$  complies with the usual definition for a radius of gyration.

Equation (6-32) will now be further simplified by introducing the following definition for an effective thickness  $\bar{t}$ :

$$\bar{t} = \frac{t^{3/2}}{t_x^{1/2}} \quad (6-35)$$

Substitution of this equality into equation (6-32) gives the following result:

$$\sigma_{cr} = \frac{m_i^2 \pi^2 E}{\left(\frac{L}{\rho_{11}}\right)^2} + \frac{E}{\sqrt{3(1-\nu^2)}} \left(\frac{R}{\bar{t}}\right) \tilde{N}_{m=m_i} \quad (6-36)$$

From the arrangement of this equation, it is useful to think of the total compressive strength of the cylinder as the sum of several separate components. With this in mind, observe that the first term in equation (6-36) is of the same form as the familiar Euler equation for column-type members. However, it must also be observed that, unlike the case for columns, this term need not be restricted to the condition that  $m_i^2 \leq 4$ .

For the cylinder, the particular  $m_i^2$  value of interest is that which minimizes equation (6-36) in its entirety and, in the case of long cylinders, shell-type influences can result in buckle patterns with  $m_i^2$  considerably in excess of four. The difference between these two situations is an outgrowth of the fact that, for the column, the critical  $m_i^2$  value is dependent solely upon the end conditions. On the other hand, equation (6-36) was developed for the particular case of a cylindrical shell having simply supported boundaries. Hence the critical  $m_i^2$  value of equation (6-36) is a function only of the internal shell stiffnesses. However, since a suitable orthotropic cylindrical shell solution for boundary conditions other than simple support is not available at this time, the methods of this report make use of the  $m_i^2$  influence to provide an engineering approach to the analysis of longitudinally stiffened cylinders having various edge conditions. That is, the nature of the end conditions is expressed in the form of a fixity factor  $C_F$ . This value is taken to be the same as that which the existing boundaries would furnish to ordinary column-type members. Then the search for critical conditions begins with  $m_i^2 = C_F$  and only considers cases where  $m_i^2 \geq C_F$ .

In view of the practice cited above, it is helpful to separate the first term in equation (6-36) into the true wide-column term

$$\frac{C_F \pi^2 E}{\left(\frac{L}{\rho_{11}}\right)^2} \quad (6-37)$$

and a shell-type contribution

$$\frac{(m_i^2 - C_F) \pi^2 E}{\left(\frac{L}{\rho_{11}}\right)^2} \quad (6-38)$$

where

$C_F$  = Fixity factor furnished to column-type members by intermediate rings ( $L=a$ ) or the cylinder boundaries.

In Section 6.3, methods are discussed for the computation of  $C_F$  values in the case of cylinders with intermediate rings. For this case, the ring spacing,  $a$ , is used in place of  $L$  in the equations of this section.

Using expressions (6-37) and (6-38), one may rewrite equation (6-36) in the following equivalent form:

$$\sigma_{cr} = \frac{C_F \pi^2 E}{\left(\frac{L}{\rho_{11}}\right)^2} + \left[ \frac{(m_i^2 - C_F) \pi^2 E}{\left(\frac{L}{\rho_{11}}\right)^2} + \frac{E}{\sqrt{3(1-\nu^2)}} \left(\frac{1}{\frac{R}{t}}\right) \tilde{N}_{m=m_i} \right] \quad (6-39)$$

The first term in this equation will often be referred to simply as the wide-column component. The bracketed sum can therefore be regarded as the total contribution made by shell behavior.

At this point, it should be noted that experimental data for the compressive buckling strength of monocoque cylinders generally fall far below the predictions of classical theory. This phenomenon has been

widely attributed to the combined influences of initial imperfections and the shape of the postbuckling equilibrium path. It has become common practice to account for this behavior by means of an empirical correlation (knock-down) factor. As discussed in Section 9, "Initial Imperfections," the same approach is taken in this report for stiffened configurations. However, the conventional stiffened wall is effectively rather thick and its reduction from theory will usually not be very severe. Based on the ideas presented in Section 9, it was decided that the correlation factor should be introduced only into the shell contribution to the total theoretical strength. Hence, using the symbol  $\Gamma$  to represent the correlation factor, one may modify equation (6-39) as follows:

$$\sigma_{cr}_{m=m_i} = \frac{C_F \pi^2 E}{\left(\frac{L}{\rho_{11}}\right)^2} + \left[ \frac{\Gamma(m_i^2 - C_F) \pi^2 E}{\left(\frac{L}{\rho_{11}}\right)^2} + \frac{E}{\sqrt{3(1-\nu^2)}} \left(\frac{1}{\frac{R}{t}}\right) (\tilde{\Gamma}\tilde{N})_{m=m_i} \right] \quad (6-40)$$

The factors  $\Gamma$  and  $\tilde{N}$  have been grouped together as a convenience despite the fact that  $\Gamma$  is not to be treated as a function of  $m$ .

In order to recognize the influence of the crippling stress for the local wall cross section, the Johnson parabola concept will be applied to the wide-column component of equation (6-40). The following expression results:



$$\sigma_{cr} = \sigma_{cc} - \frac{\sigma_{cc}^2 \left(\frac{L}{\rho_{11}}\right)^2}{4C_F \pi^2 E} + \left[ \frac{\Gamma(m_i^2 - C_F) \pi^2 E}{\left(\frac{L}{\rho_{11}}\right)^2} + \frac{E}{\sqrt{3(1-\nu^2)}} \left(\frac{1}{\frac{R}{t}}\right) (\tilde{\Gamma N})_{m=m_i} \right] \quad (6-41)$$

Then, to facilitate the application of equations (6-40) and (6-41) in the nonlinear range of the stress-strain curve, the tangent modulus is introduced as follows:

$$\sigma_{cr} = \frac{C_F \pi^2 E_{tan}}{\left(\frac{L}{\rho_{11}}\right)^2} + \left[ \frac{\Gamma(m_i^2 - C_F) \pi^2 E_{tan}}{\left(\frac{L}{\rho_{11}}\right)^2} + \frac{E_{tan}}{\sqrt{3(1-\nu^2)}} \left(\frac{1}{\frac{R}{t}}\right) (\tilde{\Gamma N})_{m=m_i} \right] \quad (6-42)$$

and

$$\sigma_{cr} = \sigma_{cc} - \frac{\sigma_{cc}^2 \left(\frac{L}{\rho_{11}}\right)^2}{4C_F \pi^2 E} + \left[ \frac{\Gamma(m_i^2 - C_F) \pi^2 E_{tan}}{\left(\frac{L}{\rho_{11}}\right)^2} + \frac{E_{tan}}{\sqrt{3(1-\nu^2)}} \left(\frac{1}{\frac{R}{t}}\right) (\tilde{\Gamma N})_{m=m_i} \right] \quad (6-43)$$

where

$E_{\text{tan}}$  = Tangent modulus

$E$  = Young's modulus

Equation (6-43) applies only where both of the following conditions are satisfied:

$$\text{a:} \quad \left( \frac{L}{\rho_{11}} \right) < \left( \sqrt{2C_F} \right) (\pi) \left( \sqrt{\frac{E}{\sigma_{cc}}} \right) \quad (6-44)$$

$$\text{b:} \quad \begin{array}{l} \text{Results From} \\ \text{Equation (6-43)} \end{array} < \begin{array}{l} \text{Results From} \\ \text{Equation (6-42)} \end{array}$$

For all other situations, equation (6-42) is the applicable formulation. For the linear portion of the stress-strain curve, condition (a) is a sufficient test for applicability of equation (6-43).

Attention is now called to the fact that most of the longitudinally stiffened circular cylinders of practical interest will fall into the relatively short category for which the critical loading corresponds to  $m_i^2 = C_F$ . In such cases,

$$m_i^2 - C_F = 0 \quad (6-45)$$

and equations (6-42) and (6-43) simplify to the following:

$$\sigma_{cr} = \frac{C_F \pi^2 E_{\text{tan}}}{\left( \frac{L}{\rho_{11}} \right)^2} + \frac{E_{\text{tan}}}{\sqrt{3(1-\nu^2)}} \left( \frac{1}{\frac{R}{t}} \right) (\tilde{\Gamma}N)_m^2 = C_F \quad (6-46)$$

and

$$\sigma_{cr}^2 = \sigma_{cc}^2 - \frac{\sigma_{cc}^2 \left( \frac{L}{\rho_{11}} \right)^2}{4C_F \pi^2 E} + \frac{E_{tan}}{\sqrt{3(1-\nu^2)}} \left( \frac{1}{\frac{R}{t}} \right) (\tilde{N})^2 \quad m^2 = C_F \quad (6-47)$$

These are the expressions which were used to develop the digital computer program of Section 18.2 and the buckling curves of Section 12.2. Hence, in using these tools, one should always perform a check to establish that the actual structure falls into the short-cylinder category. The manner in which this check should be performed is specified in Section 12.1.

In order to establish appropriate tangent modulus values, the digital computer program of Section 18.2 and the buckling curves of Section 12.2 make use of the Ramberg-Osgood [24] representation of the stress-strain curve. In the particular case of bare 7075-T6 aluminum alloy, the following values were used for the Ramberg-Osgood parameters:

$$\begin{aligned} n &= 10 \\ \sigma_{.7} &= 70,000 \text{ psi} \end{aligned} \quad (6-48)$$

The digital computer program of Section 18.2 can accommodate different materials by a simple change in these values and the input Young's modulus.

Note that equation (6-46) is quite similar to the approximate formula proposed by Peterson and Dow in reference 22. The only differences lie in the use of tangent modulus together with the presence of the factors  $\sqrt{1-\nu^2}$  and  $\tilde{N}$  in equation (6-46). Aside from the question of

some relatively minor anticlastic constraint, the assumptions inherent in the Peterson and Dew formulation therefore reduce to the approximation that  $\tilde{N} \approx 1$ . This practice is not followed in the methods of this report. Instead, use is made of  $\tilde{N}$  values which emerge from the minimization process indicated by equation (6-30). As part of the study conducted by Convair under NASA Contract NAS8-11181, a digital computer routine was utilized to accomplish this minimization. From these results, a family of curves like those shown in Figure 11 was developed for the case where  $F = 0$  (no eccentricity). These curves

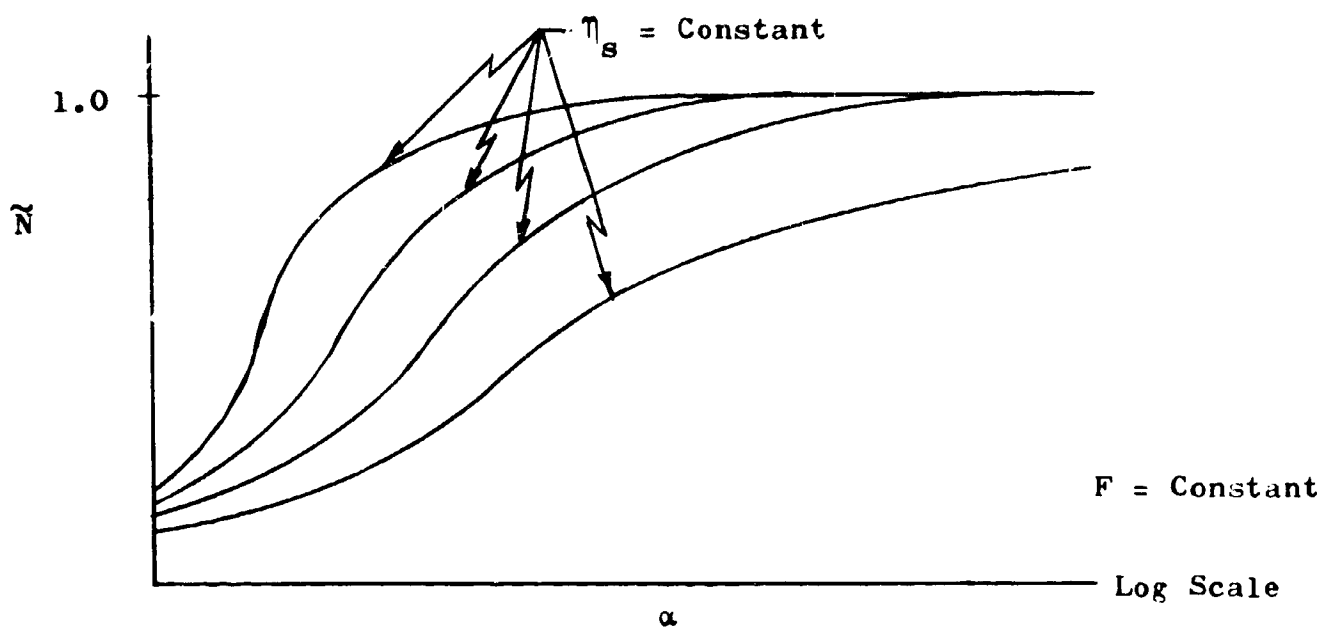


Figure 11 - Semi-Logarithmic Plot of  
 $\tilde{N}$  vs  $\alpha$  With  $\eta_s$  As a Parameter

are given in Section 12. Further work in this area should include the development of additional families for selected non-zero  $F$  values.

In conclusion of this section, attention is directed to the fact that the overall cylinder length  $L$  appears in many of the formulations presented for longitudinally stiffened cylinders. In the absence of general instability, these same equations can be applied to longitudinally stiffened sections which lie between discrete circumferential stiffeners by replacing  $L$  with the frame spacing  $a$ .

### 6.3 Fixity Factor for Longitudinally Stiffened Sections Between Rings

The presentation in the preceding section involved consideration of a fixity factor  $C_F$ . It should be recalled that this value is dependent upon the restraint which intermediate rings ( $L = a$ ) or the cylinder boundaries afford to column-type members. An inspection of equations (6-42) and (6-43) will reveal the role which  $C_F$  plays in the buckling analysis of longitudinally stiffened circular cylinders. Attention will now be devoted to means for selecting numerical values for this factor. In this connection, reference is made to the curves published by Budiansky, et al. [25] for the buckling of infinite length columns supported by equally spaced deflectional and rotational springs. The general form of these curves is shown in Figure 12 where

$C$  = Deflectional spring constant (force per unit deflection)

$K$  = Rotational spring constant (torque per unit rotation).

It was intended that these curves would be used in forming the engineering judgements required in the selection of the subject  $C_F$  values. For this purpose, note that the point A in Figure 12 represents the condition whereby, in the absence of rotational springs, the deflectional springs are sufficiently stiff to enforce undeflected nodal points at each support. This constitutes a condition of simple support. All points along the horizontal portion of the curve  $\frac{Ka}{EI} = 0$  correspond to this

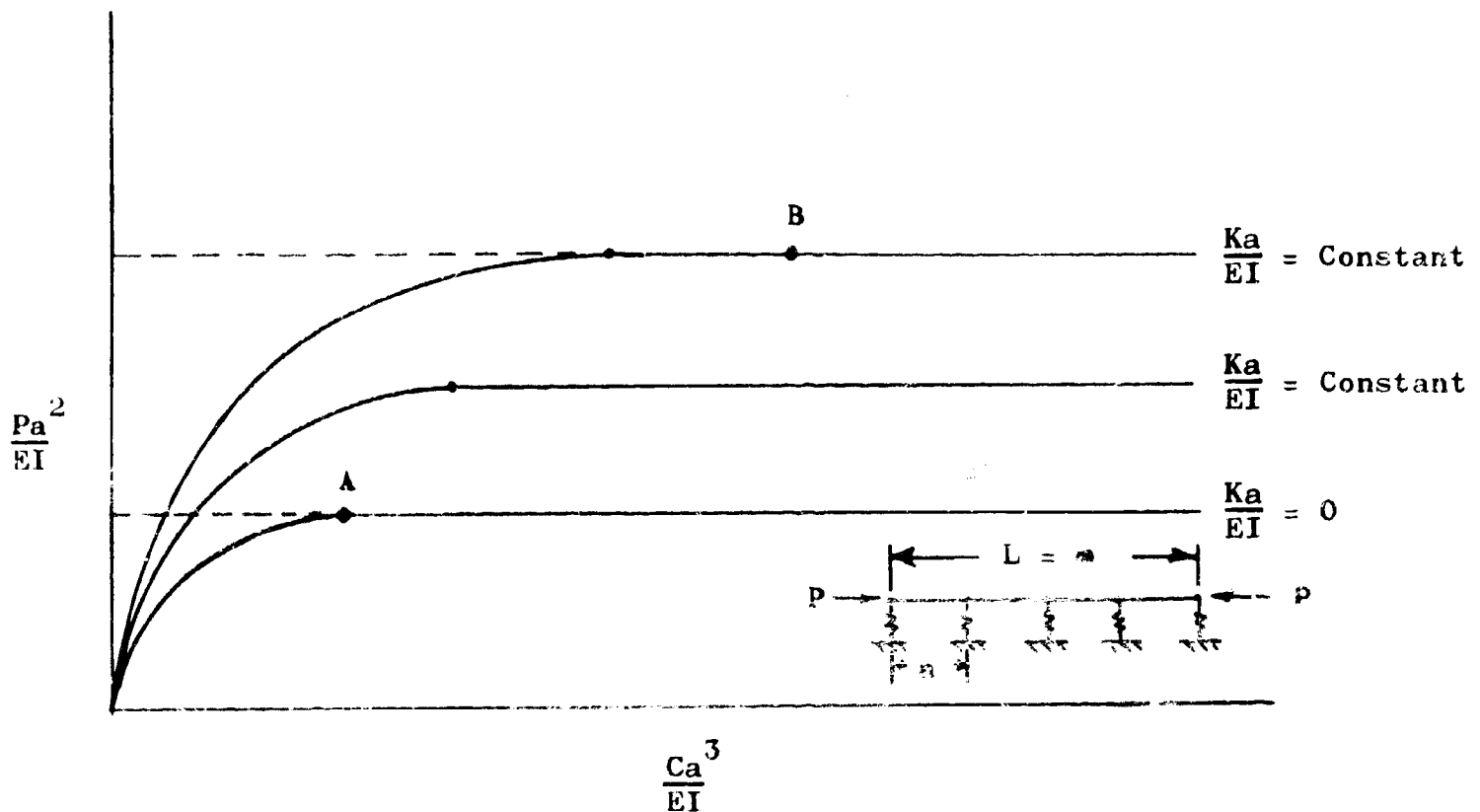


Figure 12 - Buckling Curves for an Infinite Length Column Supported by Equally Spaced Deflectional and Rotational Springs

same condition. In the case of a longitudinally stiffened circular cylinder between rings, appropriate values for the spring constants  $K$  and  $C$  must be obtained through consideration of the behavior of the rings. The resulting values locate a point, such as point B, in Figure 12. The applicable  $C_F$  value can then be found as follows:

$$C_F = \frac{\left(\frac{Pa^2}{EI}\right)_B}{\left(\frac{Pa^2}{EI}\right)_A} \quad (6-49)$$

The primary problem in computing  $C_F$  therefore reduces to the determination of the spring constants  $C$  and  $K$ . To simplify this task, it should be observed that, in the absence of general instability, it can be assumed that all rings are sufficiently rigid to provide undeflecting supports to the column. Consider then the case where the general instability load is considerably higher than the panel instability load. For this case, imagine that the deflectional stiffness of the frames is steadily reduced while their rotational stiffness is held constant. So long as general instability does not take place, the rings will remain undeflected and no change will occur in the buckling load for column-type members that span from ring to ring. Therefore, whenever general instability is prevented, the frames are sufficiently rigid to insure that the related point in Figure 12 lies somewhere along the horizontal portion of the applicable curve. Then the primary problem further reduces to the computation only of a suitable value for the rotational spring constant  $K$ .

In the study conducted under Contract NAS8-11181, two different analytical models were considered for the evaluation of  $K$ . The first of these made use of the Convair digital computer program [26] for



discontinuity analysis. Some modifications were incorporated into the original program to account for the local bending of legs on formed ring sections. Axisymmetric unit external loading was then applied to the rings to determine the desired  $K$  values. The results from these studies indicated that the assumed axisymmetric mode of deformation will usually lead to  $C_F \approx 1.0$  for practical configurations. It was originally intended that this particular approach be used to provide a lower-bound  $C_F$  value which would be of use to the analyst in the application of his engineering judgement. However, in the light of the findings cited here, it would seem that the time and effort involved in the axisymmetric determination cannot be justified and, at present, one should simply consider the lower-bound  $C_F$  to be 1.0. An alternative approach, which was expected to lead to an upper-bound fixity factor was then examined. This method evaluated the spring constant  $K$  by applying a unit torque  $T$  at the mid-point of a straight bar as shown in Figure 13. This bar was assumed to have a total length equal to twice the stringer spacing and its cross section was taken

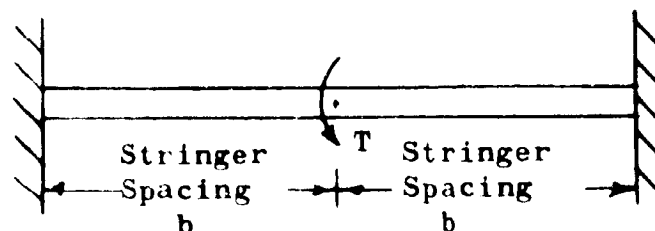


Figure 13 - Alternative Method for  
Evaluating Rotational Spring Constant

identical to that of the rings. It was further assumed that the ends of the bar were fully restrained against rotation. Surprisingly, this approach did not overpredict the test values in the limited number of comparisons made. It would therefore appear that this technique would provide a reasonable estimate of the fixity in at least some practical situations, particularly where the stringers have appreciable spacing and the basic cylindrical skin is relatively thin.

In view of the foregoing, it is concluded that, although a basically sound method has been proposed for the fixity factor determination, considerable uncertainty still remains in connection with the computation of required spring constants. Until further work is accomplished to resolve this uncertainty, it is recommended that the value of  $C_F = 1.0$  be employed for the design of longitudinally stiffened sections which lie between rings. Aircraft design practices have often made use of rule-of-thumb values in excess of unity but these have been used as all-inclusive wide-column corrections which account both for end restraint and the shell contribution to the overall strength. In this report, a more rational assessment is made of the latter component.

## 18.1 Comparisons Against Test Data

### 18.1.1 Longitudinally Stiffened Circular Cylinders - The

methods proposed in this report for the approximate analysis of longitudinally stiffened circular cylinders were evaluated by comparing buckling stress predictions against the test data of references 22, 4, and 8. The results from these investigations are given in Tables II, III, and IV. The predicted buckling stress values were obtained from the digital computer program of Section 18.2. The same program was used to develop the buckling curves shown in Section 12.2. Attention is drawn to the fact that all of the specimens in Tables II and III incorporated appreciable stiffener eccentricities and that these were fully accounted for in the tabulated predictions. Since the procedures of Part II do not account for this influence, suitable extensions to these methods were utilized in the test data evaluations. This involved the retention of non-zero  $F$  values in the minimization process indicated by equation (6-30).

The data listed in Tables II and III show that, as expected, the proposed analytical approach gave conservative predictions. However, for the specimens covered by Table IV, the test data show scatter on either side of the predictions. This circumstance is due to the fact that the inherent conservatism of the proposed methods lies in the neglect of certain stiffnesses which enter into the shell contribution to the

compressive strength. However, all the specimens of Table IV receive virtually no contribution from shell behavior. Their corrugated walls have very little hoop extensional stiffness. This is reflected into the analysis through the  $\left(\frac{\Delta x}{\delta x}\right)$  correction employed in the computation of  $A_{22}$ . The  $\tilde{N}$  value becomes very small and the prediction equation essentially reduces to the familiar Euler column formula. Hence, in these cases, deviations from predicted strengths are due largely to individual geometric variations among the test specimens, maldistribution of applied load, etc.

The following notes have general applicability to Tables II, III, and IV:

- a. A fixity factor of  $C_F = 3.75 (=m_i^2)$  was assumed to be applicable. This value has been widely used for practical configurations with "seeming full fixity". Checks were made to insure that additional numbers of half-waves would not yield lower predictions. That is, the tabulated predictions are less than would be obtained for  $m_j = \sqrt{3.75} + C_i$  where  $C_i$  is any integer.
- b. In order to establish base-line results, the correlation (knock-down) factor  $\Gamma$  was assumed to be unity.

- c. The  $\tilde{N}$  value was computed through the minimization process indicated by equation (6-30). The appropriate non-zero  $F$  value accounting for stringer eccentricity was employed in this determination. The value  $m_i^2 = 3.75$  was used in the computations of both  $\alpha$  and  $F$ .
- d. The quantity  $L$  is the entire overall length of the cylinder.
- e. The test  $\sigma_{cr}$  values were all obtained by dividing the total critical axial load by the total cross-sectional area of the specimen.

TABLE II - Comparison of Calculations vs. Test Data of Ref. 22.

Specimen	Stringer Location	$10^3 \text{ psi}$ $\sigma_{cc}$	$E_1 = E_2 = 3.75$	$\Gamma$	$\left( \frac{E_1}{E_2} = 3.75 \right)$	$\sigma$	$\left( \frac{E_1}{E_2} = 3.75 \right)$	$N$	$\frac{\sigma}{E}$	$\frac{\sigma}{\Gamma}$	Calculated $\sigma_{cr}$ $10^3 \text{ psi}$	Test $\sigma_{cr}$ $10^3 \text{ psi}$	Calculated $\sigma_{cr}$ Test $\sigma_{cr}$
1	Internal	59.2	3.75	1	22.0	1.542	+.215	.1908	823	136.0	22.4	25.0	.90
2	Internal	59.2	3.75	1	12.67	1.542	+.374	.1225	823	103.2	36.0	38.2	.94
3	Internal	59.2	3.75	1	45.0	1.542	+.1050	.306	532	159.0	19.07	23.8	.80
4	Internal	59.2	3.75	1	22.1	1.542	+.214	.1914	538	111.3	33.2	38.0	.87
5	Internal	59.2	3.75	1	88.3	1.542	+.0531	.430	538	224	12.88	17.2	.75
6	Internal	59.2	3.75	1	177.3	1.542	+.0265	.552	538	316	10.48	13.7	.76

## Notes for TABLE II:

- (a) All longitudinal stiffeners were Z-shaped. These were riveted to the basic cylindrical skin.
- (b) No buckling of the isotropic skin panels occurred.
- (c) No local buckling of the longitudinal stiffeners occurred.
- (d) All specimens were made of 7075-T6 aluminum alloy. The following properties were assumed to apply:

Notes for TABLE II, Continued

$E$	$=$	$10.5 \times 10^6$	psi
$G$	$=$	$4 \times 10^6$	psi
$\nu$	$=$	.33	
Ramberg-Osgood $n$	$=$	10	
Ramberg-Osgood $\sigma_{.7}$	$=$	70,000	psi
$\sigma_{cy}$	$=$	67,000	psi

- (e) The crippling stress  $\sigma_{cc}$  was computed by considering all elements of the wall cross section to be flat-plate elements. The crippling stress for each individual element was determined from Figure C1.3.1-13 given in reference 27. The crippling stress for the composite wall was taken as the weighted average of these individual values.
- (f) The section properties  $t_x$ ,  $I_x$ , and  $\rho_{11}$  of the composite wall were assumed to be the same for all specimens. These were computed to be

$$t_x = .0737 \frac{\text{in}^2}{\text{in}}$$

$$I_x = .00258 \frac{\text{in}^4}{\text{in}}$$


$$\rho_{11} = \sqrt{\frac{.00258}{.0737}} = .1868 \text{ in}$$

These values are based on the assumption that all of the skin and stringer material is fully effective. The quantity  $I_x$  is the local running moment of inertia taken about the centroidal axis of the complete stringer-skin combination in the flat configuration obtained by unfolding the shell wall (See instructions in Part II).

TABLE III - Comparison of Calculations vs. Test Data of Ref. 4.

Specimen	Stringer Location	$\sigma_{cc}$ $10^3$ psi	$m_1^2 = C_F$	$I$	$\left(m_1^2 = 3.75\right)$	$\eta$	$\left(m_1^2 = 3.75\right)$	$N$	$\frac{R}{t}$	$\frac{L}{p_{11}}$	Calculated $\sigma_{cr}$ $10^3$ psi	Test $\sigma_{cr}$ $10^3$ psi	Calculated $\sigma_{cr}$ Test $\sigma_{cr}$
1	External	47.5	3.75	1	166.4	1.648	-.0295	1.497	479	368	21.3	30.5	.70
2	Internal	47.5	3.75	1	166.4	1.648	+.0295	.526	495	368	9.69	12.9	.75
3	External	47.5	3.75	1	65.1	1.648	-.0750	1.826	501	230	24.6	34.4	.72
4	Internal	47.5	3.75	1	65.1	1.648	+.0750	.359	488	230	12.07	17.0	.71
5	External	59.2	3.75	1	178.9	1.542	-.0263	1.459	516	316	22.0	23.7	.93

## Notes for TABLE III:

- (a) Specimens 1 through 4 were all integrally stiffened with local wall cross section of the type .
- Specimen 5 had Z-shaped longitudinal stiffeners which were riveted to the basic cylindrical skin.
- (b) No buckling of the isotropic skin panels occurred.
- (c) No local buckling of the longitudinal stiffeners occurred.



Notes for TABLE III, Continued

- (d) Specimens 1 through 4 were made of 2024-T351 aluminum alloy. The following properties were assumed to apply to these specimens:

$$E = 10.5 \times 10^6 \text{ psi}$$

$$G = 4 \times 10^6 \text{ psi}$$

$$\nu = .33$$

$$\text{Ramberg-Osgood } n = 10$$

$$\text{Ramberg-Osgood } \sigma_{.7} = 37,000 \text{ psi}$$

$$\sigma_{cy} = 38,000 \text{ psi}$$

- (e) Specimen 5 was made of 7075-T6 aluminum alloy. The properties listed under note (d) for Table II were assumed to apply to this specimen.
- (f) The crippling stress  $\sigma_{cc}$  was computed by considering all elements of the wall cross section to be flat-plate elements. The crippling stress for each individual element was determined from Figure C 1.3.1-13 of reference 27. The crippling stress for the composite wall was taken as the weighted average of these individual values.

Notes for TABLE III, Continued

(g) The section properties  $t_x$ ,  $I_x$ , and  $\rho_{11}$  of the composite wall were assumed to be the same for specimens 1 through 4. These were computed to be

$$t_x = .0573 \frac{\text{in}^2}{\text{in}}$$

$$I_x = .000612 \frac{\text{in}^4}{\text{in}}$$

$$\rho_{11} = \sqrt{\frac{.000612}{.0573}} = .1033 \text{ in.}$$

These values are based on the assumption that all of the skin and stringer material is fully effective. The quantity  $I_x$  is the local running moment of inertia taken about the centroidal axis of the complete stringer-skin combination in the flat configuration obtained by unfolding the shell wall (See instructions in Part II).

The section properties  $t_x$ ,  $I_x$ , and  $\rho_{11}$  for specimen 5 were taken to be the same as given in note (f) for TABLE II.

TABLE IV - Comparison of Calculations vs. Test Data of Ref. 8.

Specimen	$\sigma_{cc}$ $10^3$ psi	$\sigma_{T/N} = C_F$	L	$\left(\frac{\sigma_T}{\sigma_N} = 3.75\right)$	$\sigma_a$	$\left(\frac{\sigma_T}{\sigma_N} = 3.75\right)$	$\sigma_2$	$\frac{t}{R}$	$\frac{L}{D_{11}}$	Calculated $\sigma_{cr}$ $10^3$ psi	Test $\sigma_{cr}$ $10^3$ psi	Calculated $\sigma_{cr}$ $\frac{\sigma_{cr}}{\sigma_{cr}}$
1	34.0	3.75	1	.00297	.0668	0	.05	1,984	42.0	32.6	27.8	1.17
4	34.0	3.75	1	.00297	.0668	0	.05	1,984	42.0	32.6	32.0	1.02
12	34.0	3.75	1	.00297	.0668	0	.05	1,984	42.0	32.6	34.5	.94
21	34.0	3.75	1	.00297	.0668	0	.05	1,984	42.0	32.6	33.0	.99
2	34.0	3.75	1	.00824	.0668	0	.05	1,984	70.1	30.5	29.5	1.03
19	34.0	3.75	1	.00824	.0668	0	.05	1,984	70.1	30.5	31.0	.98
3	34.0	3.75	1	.0399	.0668	0	.05	1,984	154.1	17.0	15.5	1.10
5	34.0	3.75	1	.0399	.0668	0	.05	1,984	154.1	17.0	14.2	1.20
6	34.0	3.75	1	.0267	.0668	0	.05	1,984	126.1	22.7	18.8	1.21
20	34.0	3.75	1	.0267	.0668	0	.05	1,984	126.1	22.7	19.5	1.16
7	34.0	3.75	1	.00527	.0668	0	.05	1,984	56.0	31.7	34.3	.92
13	34.0	3.75	1	.00527	.0668	0	.05	1,984	56.0	31.7	33.0	.96
32	34.0	3.75	1	.00527	.0668	0	.05	1,984	56.0	31.7	32.8	.97
8	34.0	3.75	1	.01616	.0668	0	.05	1,984	98.1	27.1	23.3	1.16
15	34.0	3.75	1	.01616	.0668	0	.05	1,984	98.1	27.1	25.5	1.06
33	34.0	3.75	1	.01616	.0668	0	.05	1,984	98.1	27.1	25.1	1.08
9	34.0	3.75	1	.0211	.0668	0	.05	1,984	112.1	25.0	20.9	1.20
17	34.0	3.75	1	.0211	.0668	0	.05	1,984	112.1	25.0	23.4	1.07
18	34.0	3.75	1	.0211	.0668	0	.05	1,984	112.1	25.0	23.6	1.06
10	34.0	3.75	1	.01187	.0668	0	.05	1,984	84.1	29.0	26.0	1.12
16	34.0	3.75	1	.01187	.0668	0	.05	1,984	84.1	29.0	28.5	1.02
11	34.0	3.75	1	.001317	.0668	0	.05	1,984	28.0	33.3	31.9	1.04
14	34.0	3.75	1	.0741	.0668	0	.05	1,984	210	9.23	8.57	1.08
22	34.0	3.75	1	.00915	.0668	0	.05	1,148	56.0	31.8	33.4	.94
23	34.0	3.75	1	.00728	.0668	0	.05	1,433	56.0	31.8	34.0	.94

TABLE IV - Comparison of Calculations vs. Test Data of Ref. 8 (Cont'd)

Specimen	$\sigma_{cc}$ $10^3$ psi	$\sigma_{F1}^2 = C_{F1}$	$T$	$\left( \sigma_{F1}^2 = 3.75 \right)$	$\sigma_s$	$\left( \sigma_{F1}^2 = 3.75 \right)$	$N$	$\frac{t}{R}$	$\frac{t}{R}$	Calculated $\sigma_{cr}$ $10^3$ psi	Test $\sigma_{cr}$ $10^3$ psi	Calculated $\sigma_{cr}$ Test $\sigma_{cr}$
24	34.0	3.75	1	.00608	.0668	0	.05	1,721	56.0	31.7	32.0	.99
25	34.0	3.75	1	.0279	.0668	0	.05	1,148	98.1	27.3	28.2	.97
26	34.0	3.75	1	.0223	.0668	0	.05	1,433	98.1	27.2	27.8	.98
27	34.0	3.75	1	.01861	.0668	0	.05	1,721	98.1	27.1	26.7	1.01
28	34.0	3.75	1	.0515	.0668	0	.05	1,148	133.1	21.5	20.1	1.07
29	34.0	3.75	1	.0380	.0668	0	.05	1,721	140.1	20.0	17.0	1.18
30	34.0	3.75	1	.0412	.0668	0	.05	1,433	133.1	21.4	21.3	1.00
31	34.0	3.75	1	.0330	.0668	0	.05	1,984	140.1	20.0	15.7	1.27
34	28.0	3.75	1	.00244	.0807	0	.05	1,755	33.6	27.5	27.6	1.00
35	28.0	3.75	1	.00244	.0807	0	.05	1,755	33.6	27.5	26.3	1.05
36	28.0	3.75	1	.00549	.0807	0	.05	1,755	50.5	26.8	26.8	1.00
37	28.0	3.75	1	.00749	.0807	0	.05	1,755	58.9	26.4	27.6	.96
38	28.0	3.75	1	.00979	.0807	0	.05	1,755	67.3	25.9	27.3	.95
39	28.0	3.75	1	.0185	.0807	0	.05	1,755	92.5	23.9	26.7	.90
40	28.0	3.75	1	.0299	.0807	0	.05	1,755	117.7	21.4	22.9	.93
41	28.0	3.75	1	.0391	.0807	0	.05	1,755	134.6	19.3	17.9	1.08
42	28.0	3.75	1	.0495	.0807	0	.05	1,755	151.4	17.0	16.1	1.06
43	28.0	3.75	1	.0675	.0807	0	.05	1,755	176.6	13.0	12.6	1.03
44	28.0	3.75	1	.0955	.0807	0	.05	1,755	210	9.25	9.90	.93
45	28.0	3.75	1	.1376	.0807	0	.138	1,755	252	6.82	8.67	.79

Notes for TABLE IV:

- (a) Each of these specimens consisted of corrugated walls which were joined to heavy end rings by casting Woods' Metal into annular grooves that held the corrugation in place. No intermediate rings were used. The following two types of local wall cross section were tested:

Specimens 1-33Specimens 34-45

For specimens 1 through 33, the cross section is essentially composed of intersecting flats while for specimens 34 through 45, the corrugation is essentially of sine-wave form.

- (b) No eccentricities were present. Hence, for all specimens,  $F = 0$ .
- (c) All specimens reported here were made of 5086-H34 aluminum alloy. The following properties were assumed to apply:

$$E = 10.8 \times 10^6 \text{ (From test data given in ref. 8)}$$

$$G = 3.9 \times 10^6$$

$$\nu = .35$$

$$\text{Ramberg-Osgood } n = 43.8 \text{ (Calculated from stress-strain curve given in ref. 8)}$$

$$\text{Ramberg-Osgood } \sigma_{.7} = 34,200 \text{ (Obtained from stress-strain curve given in ref. 8)}$$

$$\sigma_{cy} = 34,400 \text{ (From test data given in ref. 8)}$$

Notes for TABLE IV, Continued

- (d) In order that like geometries might be grouped together, the specimens are not listed in numerical sequence. This manner of presentation permits one to observe the degree of scatter that exists among the test data obtained from nominally identical specimens.
- (e) The crippling stress values were selected on the basis of the test data reported for specimens having lengths of 3 inches or less. As shown in reference 8, these specimens failed in the crippling mode. The selected values were then substantiated by calculations. For this purpose, both types of corrugations were assumed to be composed solely of flat elements. The sine-wave configuration was approximated by a saw-tooth pattern. Crippling stresses for individual flat elements were determined from Figure C 1.3.1-13 of reference 27. The crippling stress for an entire corrugation was taken as the weighted average of these individual values.

The calculated values showed good agreement with those selected from the test data. The latter were used in the analysis.

- (f) The section properties  $t_x$ ,  $I_x$ , and  $\rho_{11}$  were taken as follows:

$$\text{Specimens 1-33} \\ t_x = .01262 \frac{\text{in}}{\text{in}}^2$$

$$I_x = .0000642 \frac{\text{in}}{\text{in}}^4$$

$$\rho_{11} = \sqrt{\frac{.0000642}{.01262}} = .0713 \text{ in.}$$

$$\text{Specimens 34-45} \\ t_x = .01168 \frac{\text{in}}{\text{in}}^2$$

$$I_x = .0000412 \frac{\text{in}}{\text{in}}^4$$

$$\rho_{11} = \sqrt{\frac{.0000412}{.01168}} = .0594 \text{ in.}$$

Notes for TABLE IV, Continued

These values are based on the assumption that all of the corrugation material is fully effective.


- (g) For both of the corrugations used here, whenever  $\alpha < .1$ , the  $\tilde{N}$  value will lie between 0 and 0.1. To reduce the scope of computational effort, it was assumed that, in all such cases,  $\tilde{N} = 0.05$ . The maximum error that could be introduced into  $\sigma_{cr}$  by this practice is  $\pm 300$  psi.
- (h) The computations for  $\alpha$  and  $\eta_s$  involve the elastic constant  $A_{22}$ . It is noted in Part II that the accordion-like hoop flexibility of corrugations requires the use of a correction factor  $\frac{\Delta x}{\delta x}$  in the calculation of  $A_{22}$ . The following values were obtained here:

Specimens 1-33

$$\left( \frac{\Delta x}{\delta x} \right) = 1,513$$

Specimens 34-45

$$\left( \frac{\Delta x}{\delta x} \right) = 817$$

To compute the latter correction factor, the sine-wave configuration was approximated by a series of flat elements of the form 

Notes for TABLE IV, Continued

- (i) The skin thickness  $t$  enters into the  $\bar{t}$  formulation through the elastic constant  $D_{22}$ . It is pointed out in Part II that, as a result of this origin, the nature of corrugated walls requires that the actual  $t$  value be multiplied by a correction factor  $\left(\frac{\delta\theta}{\Delta\theta}\right)^{1/3}$  before computing  $\bar{t}$ . For the specimens covered here, this correction factor was found to be as follows:

$$\frac{\text{Specimens 1-33}}{\left(\frac{\delta\theta}{\Delta\theta}\right)^{1/3}} = .844$$

$$\frac{\text{Specimens 74-45}}{\left(\frac{\delta\theta}{\Delta\theta}\right)^{1/3}} = .893$$



During the preparation of this final report, the NASA Marshall Space Flight Center conducted a buckling test on a full-scale Saturn V S-IC intertank cylinder which consisted of a 7075-T6 aluminum alloy corrugated wall supported by rings. The critical load achieved in this test was 14,300,000 pounds. Dividing this load by the total cross sectional area, it is found that

$$\text{Test } \sigma_{cr} = \frac{14,300,000}{317} = 45,100 \text{ psi} \quad (6-50)$$

This served as an additional data point for an evaluation of the analysis procedures presented in Part II. For this purpose, a predicted critical stress was obtained using the digital computer program of Section 18.2. The buckling curves of Section 12.2 do not extend to  $(\bar{N})$  values low enough for this particular structure. A value of

$$\text{Calculated } \sigma_{cr} = 45,045 \text{ psi} \quad (6-51)$$

was obtained from the digital computer. Hence,

$$\frac{\text{Calculated } \sigma_{cr}}{\text{Test } \sigma_{cr}} = 1.00 \quad (6-52)$$

The following input values were used for the machine solution:

	$E$	$= 9.6 \times 10^6 \text{ psi}$	(Furnished by NASA)
	$\sigma_{cy}$	$= 66,000 \text{ psi}$	(Furnished by NASA)
Ramberg-Osgood	$\sigma_{.7}$	$= 70,000 \text{ psi}$	
Ramberg-Osgood	$n$	$= 10$	
	$\nu$	$= .35$	

$$\begin{aligned}
 \sigma_{cc} &= 56,700 \text{ psi (Furnished by NASA)} \\
 C_F &= 1.0 \\
 \text{Correction Factor } \left( \tilde{\Gamma N} \right) &= .01445 \text{ (Assuming } \Gamma = 1.0) \\
 R/\bar{t} &= 1,479 \\
 \frac{L}{\rho_{11}} &= 37.0
 \end{aligned}$$

#### 6.4.2 Longitudinally Stiffened Circular Cylinders With Frames,

##### Panel Instability Mode - In order to investigate the

applicability of the procedures discussed in Section 6.3 for the influence of ring stiffnesses on the panel instability mode of failure in longitudinally stiffened cylinders, comparisons were made with limited available data. Buckling stress predictions were obtained using the axisymmetric method discussed in Section 6.3 for two specimens from reference 28 and one from reference 29. The two 49-inch diameter specimens of reference 28 had corrugated skin with I-section rings and failed in the panel instability mode. The corrugated skin and short ring spacing ( $a/R \approx 1/4$ ) combined to make the shell contribution to the buckling strength [refer to equation (6-47)] negligible so that the buckling strength for these specimens was essentially their wide column strength. To assess the fixity felt by the corrugations at the frames the axisymmetric rotational and radial stiffnesses of the frame were determined using a General Dynamics Convair digital computer program as discussed in Section 6.3. These stiffnesses were then employed in conjunction with

the curves of reference 25 to obtain the fixity factor  $C_F$ . For both cylinders, this fixity factor was very nearly that for simple support because of the axisymmetric rotational flexibility of the ring. Essential agreement with test results was obtained.

The specimen selected from reference 29 was reported to have failed in the panel instability mode. This 77-inch diameter cylinder was tested in pure bending and was stiffened by Z-section stringers and hat-section frames ( $a/R = .47$ ). The skin panels buckled early and thus necessitated effective width considerations as presented in Section 7.3. The cylinder wall stiffness factors determined in that analysis were employed in this stability calculation.

An axisymmetric analysis for ring stiffnesses simply considering the ring as a compact section and neglecting bending of elements still resulted in a fixity factor of only 1.02. However, since this frame is a closed section with the skin giving high torsional rigidity and because the stringers are spaced such that they can behave more or less independently, this torsional stiffness has significant effect on the fixity felt by the stringers. As an approximate approach, the torsional stiffness of the frame was determined by applying a unit torque at the center of a straight bar whose ends were fixed against rotation and whose cross section was identical to that of the ring. The length selected was twice the stringer spacing. This torsional stiffness was then used in the analysis of reference 25 giving the

fixity factor  $C_F = 1.2$ . It was noted that an effective length of one stringer spacing corresponds to adjacent stringers buckling alternately inward and outward. This gives the fixity factor  $C_F = 1.5$ . For data comparison purposes, the value of  $C_F = 1.2$  was used.

The results of calculations for these three specimens and comparisons with test values are shown in Table V.

TABLE V - Comparison of Fixity Factor Analyses With Panel

Instability Data of Refs. 28 and 29.

(1)	(2)	(3)	(4)	(5)	(6)	(7)	(8)	(9)	(10)	(11)	(12)
Reference	Specimen No.	Analysis Technique (Ref. Notes and Section 6.3)	$\frac{C_b}{C_a} \frac{EI}{I^3}$	$\frac{K_b}{EI}$	$C_T = \frac{M_1}{M_2}$	$\sigma_{cc}$	$\frac{C_{P1}^2}{E} \left( \frac{L}{P_{11}} \right)^2 \text{ or } \sigma_{cc} - \frac{4C_{P1}^2}{E} \left( \frac{P_{11}}{L} \right)^2$ (Wide-Column Strength)	$\frac{E}{1} \frac{(N)^2}{(R/t)} \sqrt{\frac{3(1-\nu^2)}{2}} (C_F)^2$ (Shell Contribution)	Calculated $\sigma_{cr} = (8) + (9)$ (Ref. equations 6-46, 47)	Test $\sigma_{cr}$	Calculated $\sigma_{cr} = \frac{(10)}{(11)} = \frac{(10)}{(11)}$
						KSI	KSI	KSI	KSI	KSI	KSI
28	7	1, 2	53.7	.027	1.01	66	51.6	---	51.6	50.7	1.02
28	8	1, 2	59.8	.030	1.01	62	49.3	---	49.3	49.9	.99
29	II-4	1, 3	322.8	.133	1.02	71	11.4	7.0	18.4	25.	.74
29	II-4	4	----	.892	1.2	71	.4	7.2	20.6	25.	.82

## Notes for TABLE V

- a) 1: Axisymmetric analyses employed in determination of C and K.
- 2: Digital computer program [26] employed which includes effects of bending flexibility of ring elements.
- 3: Analyzed as compact section only. Bending flexibility of ring elements neglected.

Notes for TABLE V (Continued)

- 4: K determined by applying a unit torque at middle of straight bar whose length is twice the stringer spacing, cross section is that of the ring, and ends are fixed.
- b) For specimens 7 and 8, equation (9-9) gives  $t_{eff} = 0.4$  so that  $R/t_{eff} = 61$  which implies  $\Gamma = 1.0$  from 50% probability curve of reference 20.
- c) For specimen II-4, equation (9-9) gives  $t_{eff} = 0.5$  so that  $R/t_{eff} = 77$  which implies  $\Gamma = 1.0$  from 50% probability curve of reference 20.
- d) Calculation of shell contribution for specimen II-4 includes effects of stringer eccentricity in N evaluation.

7.0 GENERAL INSTABILITY OF ORTHOTROPICALLY  
STIFFENED CIRCULAR CYLINDRICAL  
SHELLS UNDER AXIAL COMPRESSION

7.1            General

Designing for the prevention of general instability in stiffened cylinders usually centers around the choice of a suitable criterion to establish dimensions for the circumferential stiffeners. In the past, a number of empirical formulas have been proposed for this purpose. One of the earliest of these was proposed by the Guggenheim Aeronautical Laboratory, California Institute of Technology (GALCIT), as an outgrowth of their tests on small-scale cylinders [30]. Shortly thereafter the Polytechnic Institute of Brooklyn Aeronautical Laboratory (PIBAL) proposed a different criterion based on their own test results from similar specimens [31]. Shanley [7] then drew upon both the GALCIT and PIBAL data to generate the following empirical formula for the minimum frame stiffness required to prevent general instability in stiffened cylinders subjected to pure bending:

$$EI_r = \frac{C_f MD^2}{a} \quad (7-1)$$

where

E = Young's modulus

$I_r$  = Centroidal moment of inertia for frame

$C_f$  = Experimentally determined constant

M = Overall bending moment

D = Cylinder diameter

a = Frame spacing

Although derived specifically for the case of pure bending, this formula has been widely used for cases of axial compression by considering the peak running load intensity to be the controlling factor. Still another criterion was suggested by Becker [32] in 1958. This approach employs certain geometrical features of the inward-bulge along with an estimate of the elastic restraints afforded by the frames. However, the Shanley formula still stands as the most widely known of the various criteria proposed to date. In general, all of these approaches represent oversimplifications of the problem in that they do not grant recognition to all the important variables involved. Engineers have long been wary of these criteria and have hedged their frame designs through the use of generous safety factors and extensive proof-testing.

In recent years, a number of orthotropic shell formulations have attracted increasing attention in connection with this problem. The most prominent of these are the following:

- (a) The formulation derived by Thielemann [19] and subsequently extended by Almroth [21] .
- (b) Stein and Mayers' [33] formulation originally developed for the compressive buckling of sandwich cylinders.
- (c) The set of equations given by Flügge [34] for cylindrical shells which incorporate longitudinal and circumferential stiffeners.



For the primary application to be discussed here, the Thielemann solution was selected in view of its simple form and the clarity with which it identifies the important physical variables.

## 7.2 Buckling Criteria

7.2.1 Thielemann Solution - The basic Thielemann formulation to be considered here is as follows:

$$\bar{N} = \left[ \frac{1 + 2\eta_p \sqrt{\gamma} \beta^2 + \gamma \beta^4}{1 + 2\eta_s \beta^2 + \beta^4} \right]^{1/2} \quad (7-2)$$

where

$$\beta = \frac{\ell_y}{\ell_x} \left( \frac{A_{22}}{A_{11}} \right)^{1/4} \quad (7-3)$$

$\ell_x$  = Axial half-wavelength of buckle pattern.

$\ell_y$  = Circumferential half-wavelength of buckle pattern.

The theoretical background for this equation has already been discussed in Section 6.2.1. As noted there, in order to establish the critical buckling load  $(N_x)_{cr}$ , equation (7-2) must be minimized. To achieve this, the curve of  $\bar{N}$  versus  $\beta^2$  is examined to locate points of zero slope. These points, together with two additional limiting possibilities, are then studied to determine which corresponds to the lowermost  $\bar{N}$  (and consequently  $N_x$ ) value. The zero-slope locations are found from the relationship

$$\frac{dY}{dX} = 0 \quad (7-4)$$

where

$$\begin{aligned} Y &= \bar{N}^2 \\ X &= \beta^2 \end{aligned} \quad (7-5)$$

By performing this operation, the following result is obtained:

$$\left[ \eta_s \gamma - \eta_p \sqrt{\gamma} \right] X^2 + \left[ \gamma - 1 \right] X + \left[ \eta_p \sqrt{\gamma} - \eta_s \right] = 0 \quad (7-6)$$

Since this equation is of the form

$$aX^2 + bX + c = 0 \quad (7-7)$$

its roots are easily found by direct application of the quadratic formula. This yields the following:

$$X = \frac{[1-\gamma] \pm \sqrt{[\gamma-1]^2 - 4\eta_p \eta_s \gamma^{3/2} + 4\eta_p^2 \gamma + 4\eta_s^2 \gamma - 4\eta_p \eta_s \gamma^{1/2}}}{2 [\eta_s \gamma - \eta_p \gamma^{1/2}]} \quad (7-8)$$

From the second of equations (7-5), it is seen that negative X values require that  $\beta$  be imaginary. The physical significance of the terms involved in equation (7-3) show this circumstance to be incompatible with the realities of the problem. Hence, negative X values are to be discarded.

Similarly, no imaginary roots to equation (7-6) should be retained.

Hence, the solution proceeds by retaining only positive, real X values which are then substituted into equation (7-2) to find the corresponding  $\bar{N}$  (and consequently  $N_x$ ) values. At most, these constitute two load values for which there can exist buckled equilibrium configurations.

These configurations are described by the corresponding  $l_x$  and  $l_y$  values. Two additional possibilities must also be considered. The first of these involves the axisymmetric (bellows) mode of buckling. Equation (7-2) can be specialized to this case by allowing  $\beta$  to approach infinity. This gives

$$\bar{N}_{\beta \rightarrow \infty} = \sqrt{\gamma} \quad (7-9)$$

The only remaining possibility arises as  $\beta$  approaches zero, in which case equation (7-2) gives

$$\bar{N}_{\beta \rightarrow 0} = 1 \quad (7-10)$$

The critical  $\bar{N}$  (and consequently  $N_x$ ) value is selected as the lowermost value from among  $\bar{N}_{\beta \rightarrow 0}$ ,  $\bar{N}_{\beta \rightarrow \infty}$  and the  $\bar{N}$  corresponding to positive, real  $X$ . In the interest of completeness, it might be noted here that the relationship between  $\bar{N}$  and  $N_x$  is given by the first of equations (6-5), which can be transposed into the following form:

$$N_x = \frac{2}{R} \left( \frac{D_{22}}{A_{11}} \right)^{\frac{1}{2}} \bar{N} \quad (7-11)$$

The foregoing procedure can be employed to develop families of curves of the type shown in Figure 14. Separate families may be plotted for particular selected  $\eta_p$  values. Such curves are given by Almroth in reference 20. It can be established that all points along the curve MQ involve the axisymmetric buckling mode ( $\beta \rightarrow \infty$ ). Hence, the equation for this curve is simply  $\bar{N} = \sqrt{\gamma}$ . On the other hand,

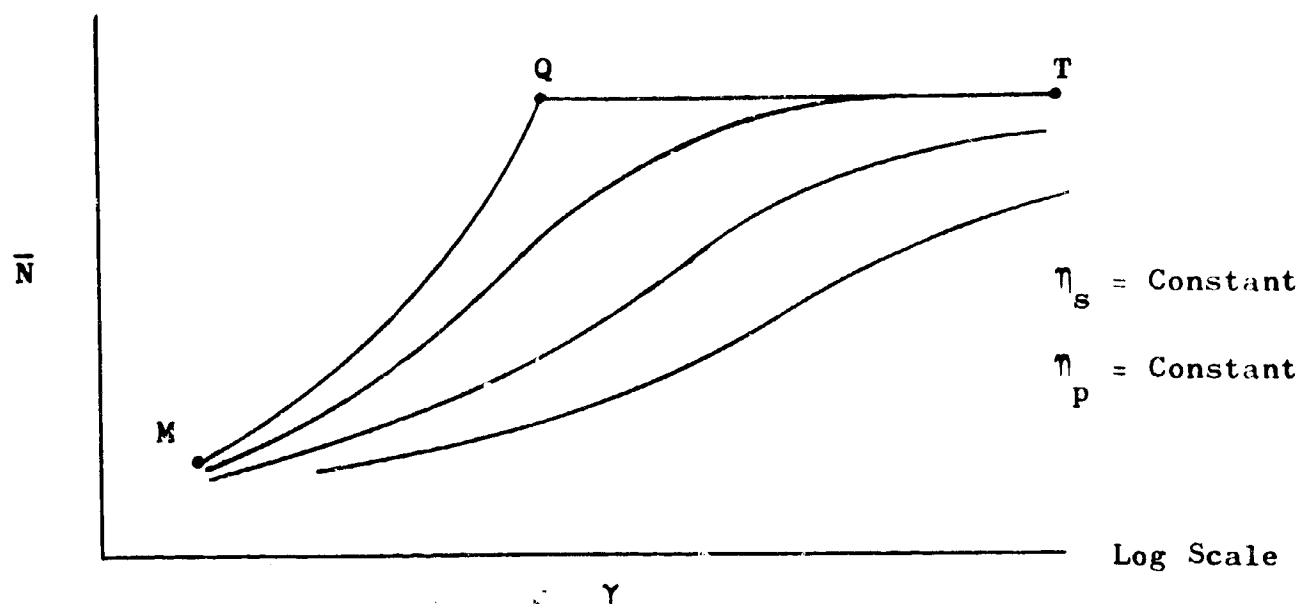


Figure 14 - Semi-Logarithmic Plot of  $\bar{N}$  vs  $\gamma$

all points along the boundary QT involve the mode which is characterized by an infinite axial half-wavelength ( $\beta \rightarrow 0$ ). All points below these two boundaries involve the so-called checkerboard mode.

In Part II of this report, both approximate and detailed analysis techniques are presented for the general instability of stiffened circular cylinders. The approximate method includes the use of a series of design curves. This approach is based upon a modified version of equation (7-2). The modification incorporated constitutes an attempt to at least partially account for the effects of finite stringer spacings through a correction factor  $C_R$ . The role which this factor plays is a consequence of the axisymmetric behavior recognized above for those points which lie on curve MQ in Figure 14. The fact that the axisymmetric mode is associated with the condition  $\beta \rightarrow \infty$  led to the conclusion that, for this case,

$$\bar{N} = \sqrt{\gamma} = \sqrt{\frac{D_{11} A_{11}}{D_{22} A_{22}}} \quad (7-12)$$

The constant  $A_{22}$  enters into this equation in the same way as the hoop extensional flexibility enters into the widely-known analogy between a beam on an elastic foundation and the axisymmetric deformation of monocoque cylinders. This analogy is discussed in reference 35. When the monocoque behavior is compared to that of cylinders with discrete longitudinal stiffening, it becomes clear that the  $A_{22}$  value in equation (7-12) should reflect the difference in flexibility between the discretely loaded ring of Figure 15a and its uniformly loaded counterpart shown in Figure 15b. The  $C_R$  correction factor, which has been

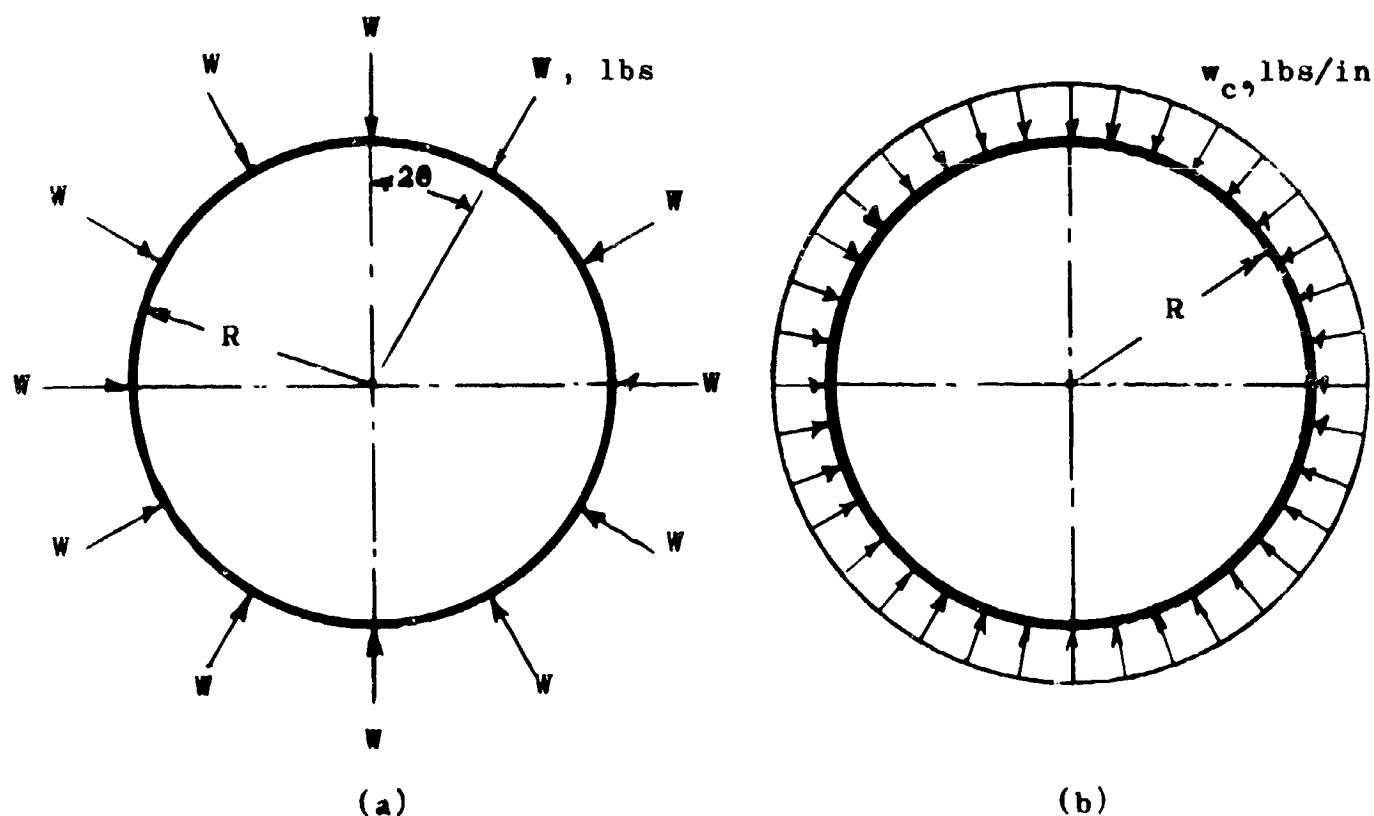


Figure 15 - Alternative Ring Loading Conditions

employed for this purpose, is simply a ratio of these two flexibilities. To arrive at an appropriate expression for  $C_R$ , the following formula [36] was used for the discretely loaded case:

$$\Delta_R = \frac{WR^3}{2EI_r} \left[ \frac{1}{\sin^2 \theta} \left( \frac{\theta}{2} + \frac{\sin \theta \cos \theta}{2} \right) - \frac{1}{\theta} \right] \quad (7-13)$$

where

$\Delta_R$  = Radial deflection

$\theta$  = Half-angle between discrete load points, radians.

The radial deflection for the uniformly loaded case is denoted  $\delta_R$  and the following formula for this quantity is easily derived:

$$\delta_R = \frac{w_c R^2}{A_r E} \quad (7-14)$$

To establish a basis for comparison between these two situations, the following relationship between  $W$  and  $w_c$  was employed:

$$W = \frac{2\pi R}{N_s} w_c \quad (7-15)$$

where

$N_s$  = Number of discrete load points for the case of Figure 15a  
(Number of stringers)

The factor  $C_R$  is then defined as follows:

$$C_R = \frac{\delta_R}{\Delta_R + \delta_R} = \frac{1}{\frac{\Delta_R}{\delta_R} + 1} \quad (7-16)$$

By substituting equations (7-13), (7-14), and (7-15) into equation (7-16), the following result is obtained:

$$C_R = \frac{1}{1 + \left( \frac{\pi K}{N_s} \right) \left( R^2 A_r / I_r \right)} \quad (7-17)$$

where

$$K = \left[ \frac{1}{\sin^2 \theta} \left( \frac{\theta}{2} + \frac{\sin \theta \cos \theta}{2} \right) - \frac{1}{\theta} \right] \quad (7-18)$$

and

$$\theta = \frac{\pi}{N_s} \quad (7-19)$$

Equation (7-17) can be used to develop a family of curves of the form shown in Figure 16. Such curves were generated within the study covered by this report and are given in Part II. It is pointed out that the form

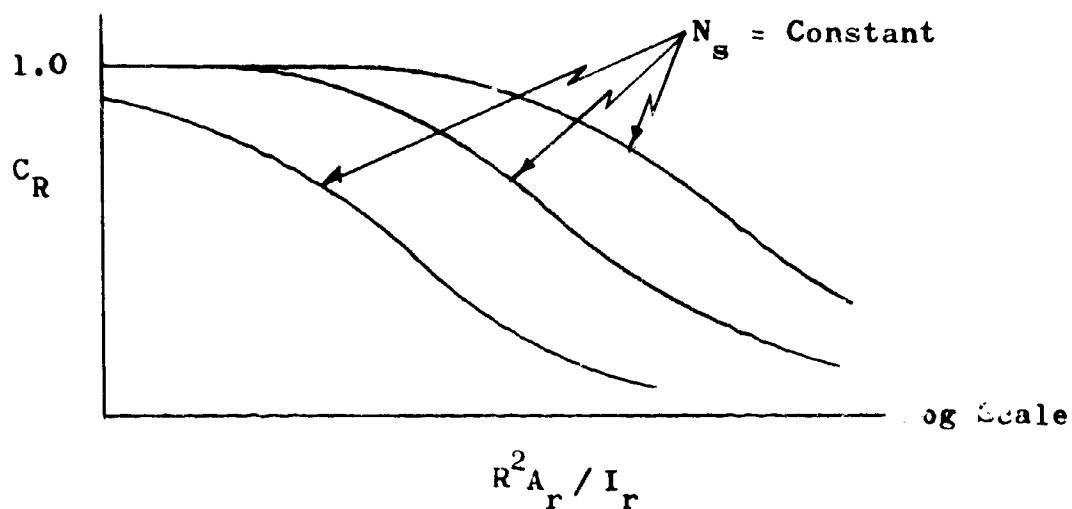


Figure 16 - Semi-Logarithmic Plot  
of  $C_R$  Correction Factor

of equation (7-18) leads to the usual numerical difficulties that one encounters when handling small differences between relatively large numbers. Therefore the  $C_R$  curves given in Part II of this report were plotted from digital computer results obtained to double-precision accuracy.

For most realistic stiffened configurations, the stringer spacings and frame dimensions will be such that the related  $C_R$  value is essentially unity. However, significantly lower values can result when the frames are of shallow depth, as in the case of the GALCIT [30] specimens. In addition, the  $C_R$  value can be separately employed to assist in the interpretation of results from the Langley solution [5] discussed in Section 7.2.2 below. Its use for such purposes will be further clarified in Part II.

To incorporate the  $C_R$  factor into equation (7-2), it should be observed that only the last term in the numerator of (7-2) retains any significance as  $\beta \rightarrow \infty$  (the axisymmetric mode). By considering this to be a boundary-type condition for the equation, the  $C_R$  ratio is applied only to that particular term. Thus, the modified expression becomes

$$\bar{N} = \left[ \frac{1 + 2\eta_p \sqrt{\gamma} \beta^2 + C_R \gamma \beta^4}{1 + 2\eta_s \beta^2 + \beta^4} \right]^{1/2} \quad (7-20)$$



where

$$\beta = \frac{\ell_y}{\ell_x} \left( \frac{A_{22}}{A_{11}} \right)^{1/4} \quad (7-21)$$

Some degree of clarity can be added to this formulation by noting that, when Young's modulus is the same in both the longitudinal and circumferential directions, the parameter

$$\gamma = \frac{D_{11} A_{11}}{D_{22} A_{22}} \quad (7-22)$$

can be expressed as

$$\gamma = \frac{\rho_{11}^2}{\rho_{22}^2} \quad (7-23)$$

where

$\rho_{11}$  = Effective longitudinal radius of gyration of shell wall.

$\rho_{22}$  = Effective circumferential radius of gyration of shell wall.

The proper means for computing  $\rho_{11}$  and  $\rho_{22}$  are presented in Part II.

Equation (7-23) can now be substituted into equation (7-20) to obtain

$$\bar{N} = \left[ \frac{1 + 2\eta_p \left( \frac{\rho_{11}}{\rho_{22}} \right) \beta^2 + \left( \frac{\sqrt{C_R} \rho_{11}}{\rho_{22}} \right)^2 \beta^4}{1 + 2\eta_s \beta^2 + \beta^4} \right]^{1/2} \quad (7-24)$$

To facilitate the presentation of plots most suitable to the stipulations of NASA Contract NAS8-11181, equation (7-24) is rewritten in the following equivalent form:

$$\bar{N} = \left[ \frac{1 + 2\eta_p \left( \frac{D/\rho_{22}}{a/\rho_{11}} \frac{a}{D} \right) \beta^2 + \left\{ \frac{(\sqrt{C_R} D/\rho_{22})^2}{(a/\rho_{11})^2} \left( \frac{a}{D} \right)^2 \right\} \beta^4}{1 + 2\eta_s \beta^2 + \beta^4} \right]^{1/2} \quad (7-25)$$

where

$D$  = Cylinder diameter.

$a$  = Spacing between circumferential stiffeners.

Proceeding in a manner similar to that described earlier for equation (7-2), equation (7-25) was minimized with respect to  $\beta^2$  by means of a digital computer program. The Stromberg Carlson 4020 plotting machine was used in conjunction with this program to obtain families of curves of the type shown in Figure 17. In order to hold the curves in Part II

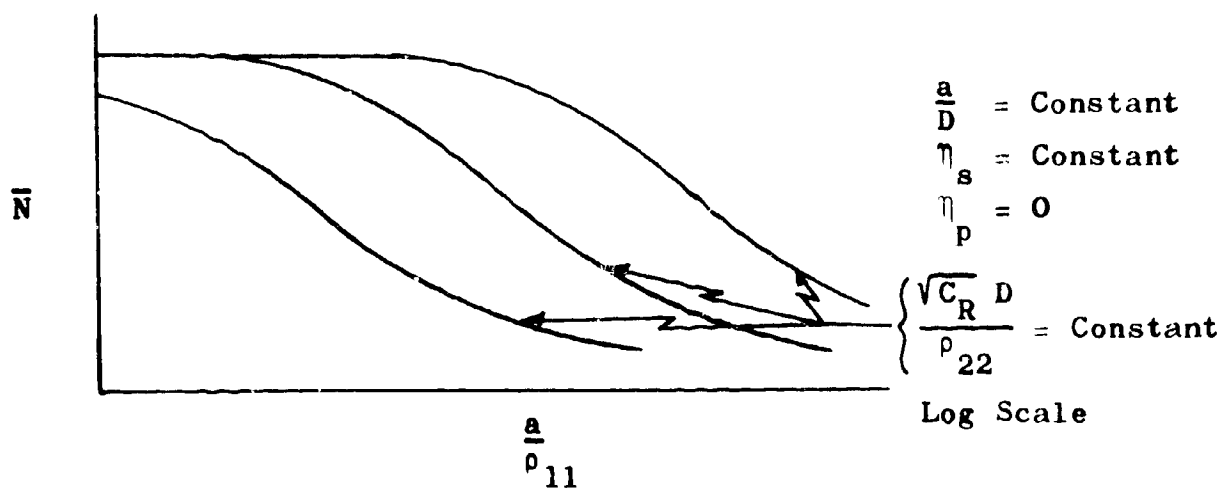


Figure 17 - Semi-Logarithmic Plot of Compressive Loading Coefficient For The General Instability of Stiffened Circular Cylinders

to a reasonable number, it was assumed that

$$\eta_p = D_{12} = D_{33} = 0 \quad (7-26)$$

Since this assumption will often result in a moderate degree of conservatism, it is a most useful approximation. The digital computer program is presented in Section 18.3.1 to facilitate the plotting of addition design curves or the determination of point solutions, as the need arises. It is pointed out, however, that the minimization procedure currently built into the program requires that the input  $\eta_p$  value always be zero.

7.2.2 Langley Solution - THE NOMENCLATURE USED IN THIS SECTION IS PRIMARILY THAT OF REFERENCE 5. THIS SECTION CONTAINS ITS OWN LISTINGS OF THESE SYMBOLS. HENCE, THE NOMENCLATURE PROVIDED IN "LIST OF SYMBOLS" DOES NOT APPLY HERE.

The analysis methods discussed in Section 7.2.1 are consistent with the primary intended spirit of this report in that they provide working tools for the purposes of preliminary sizing, rough checking, and the study of trends. Even though approximate, these tools still constitute improvements over most of the techniques currently in use for the prediction of general instability in stiffened circular cylinders. Nevertheless, attention will now be focused upon the inherent shortcomings of the approximate approach and means will be indicated through which more detailed analysis can be accomplished.

In the first place, it should be recalled that the general instability curves presented in this report are only for the special case of  $\eta_p = 0$ , where  $\eta_p$  is defined by the third of equations (6-5). It is noted that the assumption of  $\eta_p = 0$  is equivalent to neglecting the two stiffnesses  $D_{12}$  and  $D_{33}$  defined by equations (6-4). Hence, this simplification should introduce some conservatism into the analysis. However, since the analyst might sometimes be equipped with reliable means for the computation of these elastic constants, it would be desirable to remove the  $\eta_p = 0$  requirement inherent in the digital computer program of Section 18.3.1. This could be readily accomplished and it is recommended that such a task be included in future studies.

The most serious limitation of the approximate methods given in the preceding section lies in their neglect of eccentricities which can be a major factor in the buckling process. Their influences must be carefully evaluated before the analyst can grant final acceptance to a particular design. Therefore, in this report it was considered necessary to include appropriate means for conducting a general instability analysis which accounts for eccentricities of longitudinal and/or circumferential stiffeners. Such a tool is given in Section 18.3.2 in the form of a digital computer program which solves the basic buckling equation

developed by the NASA Langley Research Center in reference 5. Where desired, this program can likewise account for finite-length effects by requiring that only integral numbers of half-waves be considered. In addition, the program can be used to study some interaction phenomena which arise out of simultaneous application of axial compression and pressure differentials (either positive or negative). However, it must be emphasized here that the Langley solution does not account for any of the discontinuity-type deformations which result from pressure differentials. These effects can be very important. In addition, the present solution cannot handle cases involving the application of external shear loading in the surface of the shell. However, it appears that the theory could be readily extended to cover such situations.

In addition to its obvious application to cylinders which incorporate both longitudinal and circumferential stiffening, the subject digital computer program can also be applied to cylinders which are stiffened only in the longitudinal direction. Specialization to this case is achieved through the input values. Therefore, until such time as the Stahman-Bellucci-Almroth program [10] might be generalized for broader application, it is recommended that the programmed Langley solution be used for the detailed analysis of longitudinally stiffened cylinders, particularly for the detailed analysis of configurations which incorporate both longitudinal and circumferential stiffeners.

The Langley solution was developed in reference 5 by Block, Card, and Mikulas by first formulating expressions for the changes in strain energy due to the buckling displacements. This change in strain energy for the basic cylindrical skin is found from the following:

$$\pi_c = \frac{1}{2} \int_0^{2\pi R} \int_0^a \left( N_x \epsilon_x + N_{xy} \gamma_{xy} + N_y \epsilon_y - M_x w_{,xx} + 2M_{xy} w_{,xy} - M_y w_{,yy} \right) dx dy \quad (7-27)$$

where

- $N_x, N_{xy}, N_y,$   
 $M_x, M_{xy}, M_y$  = Stress resultants of basic cylindrical skin.  
 $\epsilon_x, \epsilon_y, \gamma_{xy}$  = Strains at middle surface of basic cylindrical skin.  
 $\pi_c$  = Change (due to buckling displacements) in strain energy of basic cylindrical skin.  
 $x$  = Longitudinal direction.  
 $y$  = Circumferential direction.  
 $R$  = Cylinder radius.  
 $a$  = Overall length of cylinder.

The manner in which Block, et al. formulate the stress resultants facilitates analysis where the basic cylindrical skins themselves have orthotropic properties. Proceeding then to the longitudinal stiffening elements, their change in strain energy is found from the following:

$$\pi_s = \frac{1}{2} \int_0^{2\pi R} \int_0^a \left( \int_{A_s} \frac{E_s \epsilon_{x_s}^2}{d} dA_s + \frac{G_s J_s}{d} w_{,xy}^2 \right) dx dy \quad (7-28)$$

where

- $\pi_s$  = Change (due to buckling displacements) in strain energy of longitudinal stiffener.
- $A_s$  = Cross-sectional area of longitudinal stiffener (no cylindrical skin included).
- $\epsilon_{x_s}$  = Longitudinal strain of longitudinal stiffener.
- $d$  = Stringer spacing.
- $G_s$  = Shear modulus of longitudinal stiffener.
- $J_s$  = Torsional constant of longitudinal stiffener.
- $w$  = Radial displacement.

The change in strain energy of the circumferential stiffeners is found from

$$\pi_r = \frac{1}{2} \int_0^{2\pi R} \int_0^a \left( \int_{A_r} \frac{E_r \epsilon_{y_r}^2}{\ell} dA_r + \frac{G_r J_r}{\ell} w_{,xy}^2 \right) dx dy \quad (7-29)$$

where

- $\ell$  = Ring spacing.
- $r$  = Subscript denoting ring (circumferential stiffener not including any cylindrical skin).

The change in the potential energy of the external loading is obtained from the following:

$$\pi_L = - \frac{1}{2} \int_0^{2\pi R} \int_0^a \left( \bar{N}_x w_{,x}^2 + \bar{N}_y w_{,y}^2 \right) dx dy \quad (7-30)$$

where

$\pi_L$  = Change (due to buckling displacements) in potential energy of external loading.

$\bar{N}_x$  = Stress resultant (positive in compression) obtained by considering the basic cylindrical skin and the longitudinal stiffeners to be loaded with a uniform normal stress in the longitudinal direction.

$\bar{N}_y$  = Stress resultant (positive in compression) obtained by considering the basic cylindrical skin and the circumferential stiffeners to be loaded with a uniform normal stress in the circumferential direction.

The change (due to buckling displacements) in the total potential energy of the system can then be expressed as follows:

$$\pi = \pi_c + \pi_s + \pi_r + \pi_L \quad (7-31)$$

The next step is to employ the principle of stationary potential energy to arrive at a set of equilibrium equations in terms of the buckling displacements  $u$ ,  $v$ , and  $w$  which are measured in the coordinate directions using the middle-surface of the basic cylindrical skin as the reference surface. Block, et al. then obtained a solution to these equations by assuming boundary conditions of simple support ( $w = M_x = N_x = v = 0$ ) and the following set of displacement functions:



$$\begin{aligned}
 u &= u \cos \frac{m\pi x}{a} \cos \frac{n\pi y}{R} \\
 v &= v \sin \frac{m\pi x}{a} \sin \frac{n\pi y}{R} \\
 w &= w \sin \frac{m\pi x}{a} \cos \frac{n\pi y}{R}
 \end{aligned}
 \tag{7-32}$$

where

$m$  = Number of longitudinal half-waves in buckle pattern.

$n$  = Number of full waves in the buckle pattern in the circumferential direction.

It is emphasized that the conditions  $w = M_x = N_x = v = 0$  relate only to incremental quantities that arise through the buckling deformations.

By substituting equations (7-32) into the equilibrium equations, it was observed that the existence of non-trivial buckling displacements requires that a certain determinant vanish. This condition reduces to the following stability equation:

$$\begin{aligned}
 \left(\frac{m\pi}{a}\right)^2 \bar{N}_x + \left(\frac{n}{R}\right)^2 \bar{N}_y &= A_{33} + \left(\frac{A_{12}A_{23} - A_{13}A_{22}}{A_{11}A_{22} - A_{12}^2}\right) A_{13} \\
 &+ \left(\frac{A_{12}A_{13} - A_{11}A_{23}}{A_{11}A_{22} - A_{12}^2}\right) A_{23}
 \end{aligned}
 \tag{7-33}$$

where the  $A_{ij}$ 's are functions of the material properties, the geometry of the cylinder, and the shape of the buckle pattern. These functions are given in Section 18.3.2 and will not be reproduced here. NOTE THAT THE  $A_{ij}$ 's OF EQUATION (7-33) ARE NOT THE ELASTIC CONSTANTS DEFINED BY EQUATIONS (6-1) - (6-4).

Equation (7-33) is the fundamental buckling criterion that emerges from the Langley derivation. It should be observed that this equation does nothing more than establish  $\bar{N}_x$  and  $\bar{N}_y$  values which are capable of maintaining the cylinder in deformed configurations corresponding to particular numbers of half-waves in the longitudinal and circumferential directions. Calling upon the bifurcation concept discussed in Section 6.2.1, it follows that the critical buckling load can be established by exploring the possible deformed equilibrium configurations for a minimum-load condition. The digital computer program of Section 18.3.2 operates in precisely this manner. Through the input, the analyst prescribes the ranges and increments of  $m$  and  $n$  to be investigated. The machine computes the  $\bar{N}_x$  or  $\bar{N}_y$  values corresponding to each of these configurations and prints out the lowermost load encountered. This program was developed under NASA Contract NAS8-11181 primarily to assist in the evaluation of test data and, since these data provided a basis for selecting the  $m$  and  $n$  to be explored, the current program is quite adequate for such applications. Lacking this prior knowledge of the buckle pattern, the user will find the program to be less satisfactory. Hence, future work in this area should include further development of this program. In particular, automatic means should be incorporated to establish the minimum-load condition without any need for the analyst to prescribe the wave patterns to be screened. This procedure should recognize the possibility for multiple relative minima to emerge from equation (7-33) if a study reveals that such situations might be encountered.

Although the Langley solution can be considered suitable to final analysis, it is not intended that the reader interpret this to mean that this is a perfectly rigorous tool. At best, it represents a state-of-the-art capability in a rapidly changing technology. For one thing, it should be noted that this solution is based on monocoque shell theory and its application to discretely stiffened cylinders is achieved by the conventional smearing-out technique. For this purpose, the elastic properties of the discrete stiffeners are averaged over the entire shell surface to obtain an "equivalent" monocoque analysis model. In addition, the Langley solution in its present form only treats boundary conditions of classical simple support. Furthermore, it is based on the assumption that the pre-buckling displacements are perfectly cylindrical. That is, no pre-buckling bending of the shell wall is considered. Consequently, neither end moment effects nor influences due to localized restraint to Poisson-ratio hoop growth can be treated.

### 7.3 Comparisons Against Test Data

The methods proposed in this report for the approximate analysis of general instability in cylinders with both longitudinal and circumferential stiffening were evaluated by comparing calculated critical stresses against the test data of reference 29. The results from this investigation are given in Tables VI, VII, and VIII. The predictions were based on the critical compressive loading coefficient  $\bar{N}$  obtained from the digital computer program of Section 18.3.1. This is the same program that was used to plot the general instability design curves given in Section 13.2. However, attention is drawn to the fact that all of the subject specimens incorporated appreciable stiffener eccentricities and, to assess their influences, it proved necessary to also employ the digital computer program of Section 18.3.2.

In all cases, the stringers were Z-shaped while hat-shaped frames were used. The stringers were external and spot-welded to the basic cylindrical skin whereas the frames were internal and riveted. The stringer cross-sectional dimensions were such that they did not experience any local buckling. The entire construction was of 7075-T6 aluminum alloy for which the following properties were assumed:

$$\begin{aligned} E &= 10.5 \times 10^6 \text{ psi} \\ G &= 4.0 \times 10^6 \text{ psi} \end{aligned}$$

In order to establish base-line results, the correlation (knock-down) factor  $\Gamma$  was assumed to be unity.

All of the specimens were tested to failure under pure bending moment. Consistent with the conclusions of Section 8.0, the theoretical critical running load under pure bending was considered to be the same as that for uniform axial compression. Since each specimen experienced early buckling of the isotropic skin panels, it was required that effective skin widths and reduced in-plane skin shear stiffnesses be used in the analyses. These values are, of course, dependent upon the postbuckling capabilities of the isotropic skins. In particular, the effective skin widths were based on equations (A2) and (A3) of reference 16 while the in-plane shear rigidities of the buckled skin panels were obtained using reference 37. In order to introduce these phenomena into the analyses, it was necessary to employ the following trial-and-error iterative procedure:

1. Assume a value for the critical general instability stress.
2. Based on the value assumed in Step (1), compute effective skin widths and the in-plane shear stiffness of the isotropic skin panels.
3. Calculate the critical stress for general instability.
4. Compare the result from Step (3) against the value assumed in Step (1). If adequate agreement is obtained, no further iterations are required. However, when this is not the case, one must assume a new value for the critical general instability stress and repeat the computational cycle.

For the analyses presented here, the first iterations were performed using the digital computer program of Section 18.3.1. Hence, at this point, no consideration was given to eccentricities. The initial assumed stress values were taken to agree with the test data. The results from these computations are given in Table VI. The second iterations were performed in exactly the same manner except that the output stresses from the first iterations were selected as the new initially assumed values. Once again, no consideration was given to eccentricities. The results from these computations are given in Table VII. Note that close agreement was obtained between the assumed critical stress and the computed values. Hence, no further iterations were made.

Since eccentricity influences were not considered for any of the calculated critical stresses in Tables VI and VII, these results cannot in themselves provide a valid basis for evaluation of the basic analysis method. Therefore, it was necessary that further analysis be undertaken to determine the degree by which the eccentricities would alter the predictions. This was accomplished by using the digital computer program of Section 18.3.2 to obtain the results presented in Table VIII. As shown there, for each specimen, two separate runs were made with this program. The first run used the same input stiffnesses as were used in the second-iteration calculation. In addition, once again, eccentricities were not considered. The results obtained from this run are listed in column ③ of Table VIII. Note that, as expected, these values correspond very closely

TABLE VI - Comparison of First-Iteration Calculations  
vs. Test Data of Ref. 29 (Eccentricities  
not considered in calculations)

(1)	(2)	(3)	(4)	(5)	(6)	(7)	(8)	(9)	(10)	(11)	(12)	(13)	(14)
Specimen	Assumed $\sigma_{cr}$ 10 <sup>3</sup> psi	$\sigma_{11}$	$C_R$	$\sqrt{\frac{C_R}{D}} \frac{p}{p_{22}}$	$p_{11}$	$\eta_s$	$\eta_p$	$\frac{N}{N_p}$ (Digital Computer Output)	$\sqrt{\frac{D_{22}}{A_{11}}}$	$(N_x)_{cr} = (9) \times (10)$	Calculated $\sigma_{cr}$ 10 <sup>3</sup> psi	Test Data Test $\sigma_{cr}$ 10 <sup>3</sup> psi Failure Mode	Calculated $\sigma_{cr}$ Test $\sigma_{cr}$
I-1	44.0	.0777	1.0	373	29.1	1.879	0	.588	1,765	1,038	44.2	44.0 GI	1.005
I-2	42.0	.1166	1.0	372	43.6	1.508	0	.630	1,443	909	38.2	42.0 GI	.910
I-3	36.0	.1554	1.0	373	58.1	1.283	0	.661	1,259	832	34.4	36.0 GI	.956
II-1	40.0	.0777	.98	667	29.1	1.742	0	.768	718	551	37.1	40.0 GI	.928
II-2	38.0	.1166	.98	667	43.6	1.425	0	.809	587	475	31.8	38.0 GI	.837
II-3	35.0	.1554	.98	667	58.3	1.197	0	.841	513	431	28.6	35.0 GI	.817
II-4	25.0	.233	.98	672	87.5	.927	0	.885	428	379	23.9	25.0 PI	.956

TABLE VII - Comparison of Second-Iteration Calculations  
vs. Test Data of Ref. 29 (Eccentricities  
not considered in calculations)

(1)	(2)	(3)	(4)	(5)	(6)	(7)	(8)	(9)	(10)	(11)	(12)	(13)		(14)
Specimen	Assumed $\sigma_{cr}$ $10^3$ psi	$D/\delta$	$C_R$	$\sqrt{\frac{C_R D}{p_{22}}}$	$\sigma_{11}^c$	$\sigma_a$	$\sigma_p$	$N$ (Digital Com- puter Output)	$R/\sigma$ $\sqrt{\frac{D_{22}}{A_{11}}}$	$(N_x)_{cr} = \frac{(9)}{(10)}$	Calculated $\sigma_{cr}$ $10^3$ psi	Test $\sigma_{cr}$ $10^3$ psi	Failure Mode	Calculated $\sigma_{cr}$ Test $\sigma_{cr}$
I-1	44.2	.0777	1.0	373	29.0	1.874	0	.589	1,761	1,038	44.2	44.0	GI	1.005
I-2	38.2	.1166	1.0	372	43.7	1.489	0	.632	1,451	919	38.4	42.0	GI	.914
I-3	34.4	.1554	1.0	374	58.2	1.292	0	.660	1,262	833	34.3	36.0	GI	.953
II-1	37.1	.0777	.98	667	29.1	1.711	0	.772	721	557	37.2	40.0	GI	.929
II-2	31.8	.1166	.98	668	43.7	1.385	0	.815	595	485	31.7	38.0	GI	.834
II-3	28.6	.1554	.98	671	58.3	1.168	0	.847	519	439	28.2	35.0	GI	.806
II-4	23.9	.233	.98	674	87.4	.930	0	.885	429	379	23.7	25.0	PI	.948



to the second-iteration results. The small differences can be attributed to the fact that, when using the program of Section 18.3.2, consideration was only given to buckle patterns having integral numbers of axial half-waves and circumferential full-waves. On the other hand, the program of Section 18.3.1 is based on an infinite-length cylinder solution for which no such restrictions are imposed. This point was explored to some degree by running the Section 18.3.2 program for specimen I-1 allowing for non-integral numbers of the respective half and full-waves. This gave the result  $(N_x)_{cr} = 1,038$  which provided agreement to four significant figures with the second-iteration value shown in Table VII.

For the second runs with the Section 18.3.2 program, the input values were selected as prescribed in that section including the appropriate eccentricities. Once again the effective widths and in-plane skin panel shear stiffnesses were taken from the second-iteration data. The results obtained from this run are listed in column (4) of Table VIII. Comparison of the results in columns (3) and (4) of this table provided an eccentricity factor as shown. This factor was then applied to the second-iteration results to obtain the final (Calculated  $\sigma_{cr}$ /Test  $\sigma_{cr}$ ) ratios.

In Tables VI, VII, and VIII, the test failure modes for the various specimens are identified as follows:

GI = General Instability (see Glossary)

PI = Panel Instability (see Glossary)

TABLE VIII - Final Comparison of Calculations vs. Test  
Data of Ref. 29 (Eccentricities included  
in calculations)

(1)	(2)	(3)	(4)	(5)	(6)	(7)	(8)	(9)
Specimen	$(N)_{cr}$ From Table VII	$(N)_{cr}$ Using Program of Section 18.3.2 (No Eccentricities)	$(N)_{cr}$ Using Program of Section 18.3.2 (With Eccentricities)	Eccentricity Correction Factor = $\frac{(4)}{(3)}$	Calculated $\sigma_{cr}$ of Table VII $10^3$ psi	Final Calculated $\sigma_{cr}$ = $\frac{(5) \times (6)}{(7)}$ $10^3$ psi	Test $\sigma_{cr}$ $10^3$ psi Failure Mode	Final Calculated $\sigma_{cr}$ Test $\sigma_{cr}$ = $\frac{(7)}{(8)}$
I-1	1,038	1,050	1,119	1.066	44.2	47.1	44.0	1.070
I-2	919	923	989	1.072	38.4	41.2	42.0	.981
I-3	833	844	904	1.071	34.3	36.7	36.0	1.019
II-1	557	563	682	1.211	37.2	45.0	40.0	1.125
II-2	485	490	587	1.198	31.7	38.0	38.0	1.000
II-3	439	442	519	1.174	28.2	33.1	35.0	.946
II-4	379	386	450	1.166	23.7	27.6	25.0	1.104

All the calculated  $\sigma_{cr}$  values are based on the general instability mode of failure. Hence, for specimen II-4, the comparison ratio (Calculated  $\sigma_{cr}$ /Test  $\sigma_{cr}$ ) is somewhat higher than the value which would have been attained if panel instability had been prevented.

## 8.0 INTERACTION BEHAVIOR

### 8.1 General

For cylinder loading conditions involving axial compression combined with other applied loadings such as pure bending, shear, or external pressure, it has been convenient to represent nondimensionally the results of isotropic cylinder theory on charts by the well known so-called interaction curves. For example, Figure 18 shows how the relationship between two types of loadings may be represented graphically.

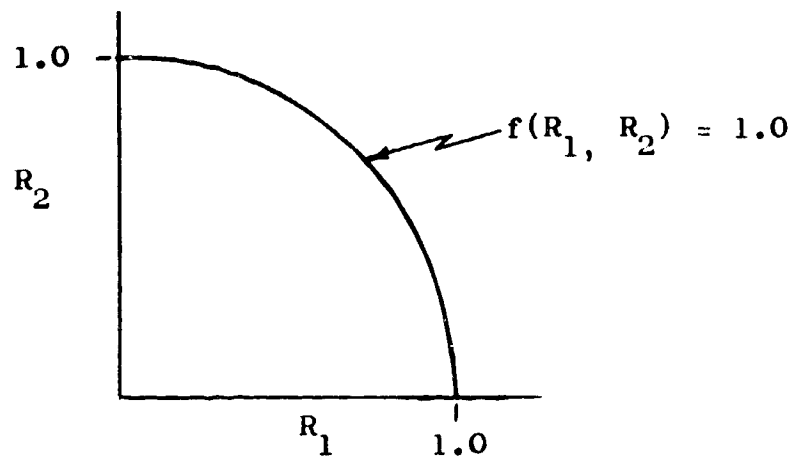


Figure 18 - Example Interaction Curve

$R_1$  is the ratio of an applied load or stress to the critical value for that type of loading acting alone and  $R_2$  is similarly defined for the second type of loading. Curves of the type shown in Figure 18 are convenient to use in design analysis since any calculated point within the area bounded by the curve indicates that stability exists for the

particular loading combination. Further, an indication of the margin of safety is given by the ratio of distances from the point to the curve and the origin. Calculations to obtain the point  $(R_1, R_2)$  involve only the evaluation of the critical values for each type of loading acting alone and dividing these into the applied loads.

For isotropic cylindrical shells, it has been the practice to represent the interaction relationship for two combined loadings by means of a single curve of the type shown in Figure 18. The findings of this study show that this is generally not true for stiffened cylindrical shells and that each particular stiffened shell geometry may have a unique interaction curve or belong to one of a family of such curves which is required to describe a desired range of geometry parameters.

A detailed analysis of existing theory to establish possible parametric representation of families for interaction curves was beyond the scope of this study. However, interaction of axial compression with the cases of external pressure and internal pressure was investigated neglecting eccentricities of stiffening elements from the skin for three arbitrary stiffened cylinder configurations: one circumferentially stiff, a typical frame/stringer geometry, and one longitudinally stiff. The latter two geometries were also investigated including eccentricities. The digital computer program discussed in Section 18.3.2 employed the analysis of reference 5 and was used to perform these numerical interaction computations. No actual analyses or numerical computations

were performed for the cases of combined axial compression with pure bending or shear although recommendations based on available information are presented in this section regarding the treatment of these loading combinations.

## 8.2 Axial Compression and Pure Bending

Interaction relationships for the case of combined axial compression and pure bending require determination of critical values for each loading acting independently. The critical loading for uniform axial compression may be determined by the methods discussed in Sections 6 and 7; however, there is current disagreement regarding the critical loading for the case of pure bending of orthotropic cylinders. For example, the results of reference 38 indicate that the buckling stresses for orthotropic cylinders under bending or axial compression loading are equal while reference 39 shows for a particular corrugated cylinder with internal rings that the buckling stress due to pure bending is approximately 1.23 times the buckling stress for uniform axial compression.

A related situation existed for isotropic cylinders and is worthy of note. An analysis of non-uniform axial compression presented in references 40 and 34 indicated that for an assumed buckle wave form, the critical stress for buckling due to bending alone was 1.3 times the stress for pure compression. The calculation was cited by Timoshenko [41] without a qualifying statement as to the assumed buckle wave length.

Because test data seemed to substantiate the existence of such an increase, the 1.3 factor was used for decades as a general rule. Only recently did the small deflection analysis of reference 42 reveal that the ratio of bending and compressive stresses can vary widely with longitudinal wave lengths and that minimization with respect to wave length gives the maximum critical bending stress equal, for all practical purposes, to the critical compressive stress.

The apparent increase of bending strength over compressive strength indicated by isotropic test data may be explained by consideration of the sensitivity of such cylinders to localized geometrical defects. These defects are a dominant factor used to explain the severe reduction of isotropic compressive data from classical theory. Since, under bending, only a small portion of the cylinder circumference experiences stresses which initiate the buckling process, there is a statistical influence from the probability of occurrence of defects or weak spots in that portion of the cylinder wall. For uniform axial compression, every element of the wall is equally stressed so that the random occurrence of defects would be more deleterious. The boundary conditions may have similar relative influences on the two cases. Furthermore, carefully conducted experiments [ 43 ] on the stability of unstiffened thin-walled cylindrical shells indicate that under nonuniformly distributed axial loading, buckling will occur when the maximum stress reaches the critical load for uniform compression.

The practical case of orthotropic cylindrical shells having discrete stiffeners eccentric from the skin has not been sufficiently analyzed for pure bending to permit definite conclusions regarding the comparison of critical bending and axial loadings. The analysis of reference 38 neglects eccentricities but concludes, as in the case of isotropic cylinders, that the critical axial and bending stresses are essentially the same for orthotropic cylinders. The analysis further concluded that the appropriate interaction relationship was linear:

$$R_c + R_b = 1.0 \quad (8-1)$$

where  $R_c$  and  $R_b$  are ratios of applied stress to buckling stress for axial compression and pure bending respectively.

Reference 38 also reports test data obtained on longitudinally, circumferentially and grid stiffened cylinders, each having outside stiffening elements whose eccentricity from the skin would not be expected to be very important. Correlation of the data of that reference was shown to be within approximately 90-98% of the pure bending theory proposed there. Time was not available to compare these tests with the analyses of Sections 6 and 7 of this report as the data were obtained too late in the study. Two combined loading tests were also conducted and reported in reference 38. These test results are shown in Figure 19 as are some of the pure bending results and axial compression data of reference 38 from which the figure was obtained.



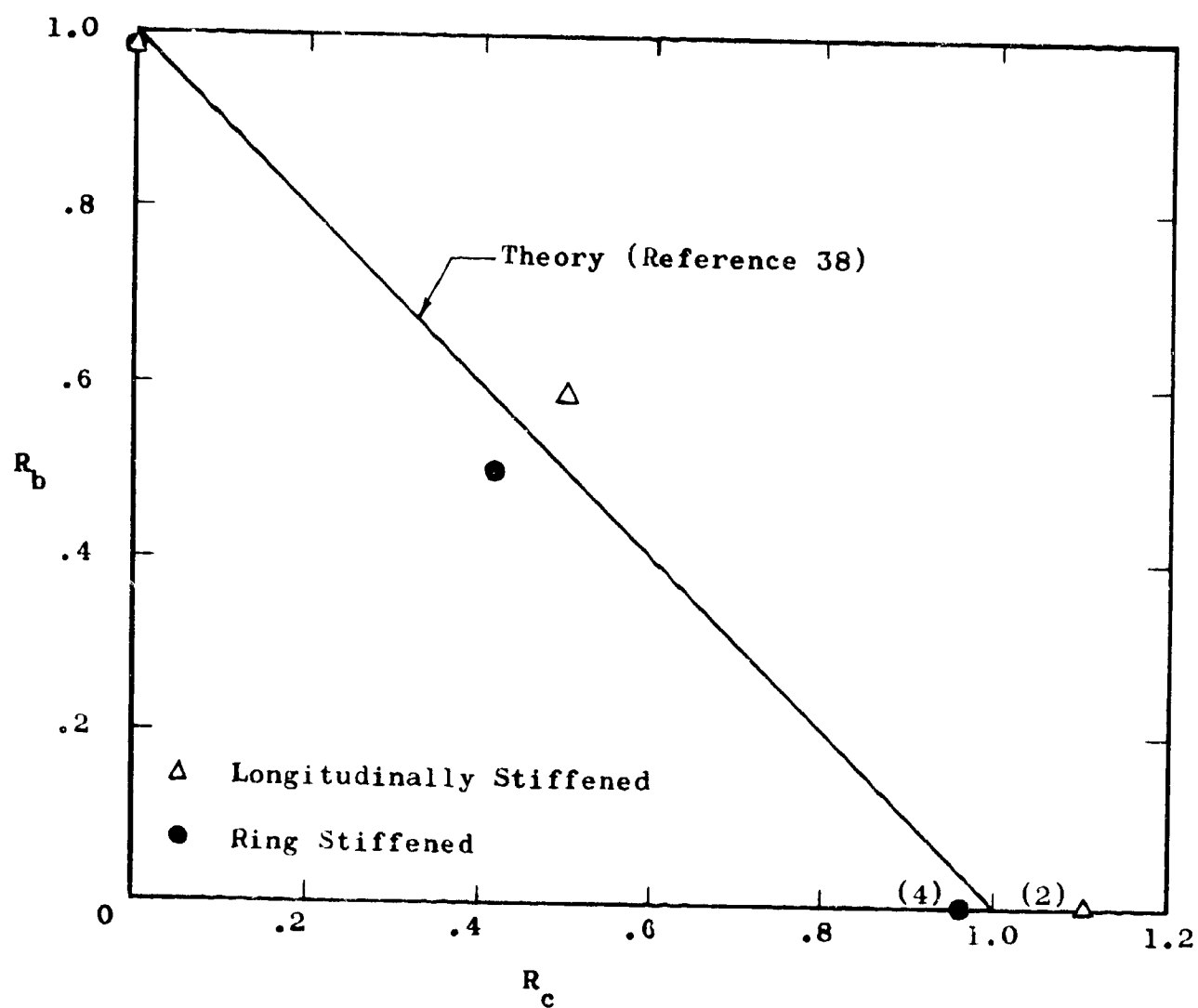


Figure 19 - Combined Axial and Bending Loading  
Interaction Curve for Orthotropic  
Cylinders (from reference 38)

Although reference 39 indicates significant theoretical increase in bending strength over axial compression for a particular corrugated cylinder with internal rings, it is recommended that the conclusions of reference 38 be adopted for design practice until further investigation of the case of bending of stiffened cylindrical shells is accomplished and substantiated by careful tests of realistic specimens. Therefore, until more conclusive results are obtained, it is recommended that for pure bending, the critical running load or maximum stress be considered theoretically the same as that for uniform axial compression presented in Sections 6 and 7 of this report. It is further concluded that the linear interaction relationship of equation (8-1) should be used presently for design. Because it is unknown what effects boundary conditions, mode of failure (panel instability, general instability), prebuckling of skin panels, etc. have on the interaction relation, further theoretical and testing efforts are indicated.

### 8.3 Axial Compression and External Pressure

Interaction behavior for stiffened cylinders under combined axial compression and external radial pressure was investigated using the theory of reference 5. The effects of prebuckling deformations due to wall differential pressure and discreteness of stiffening elements were completely neglected in the analysis. These discontinuity-type bending deformations are likely important for all but very closely spaced stiffening geometries where monocoque behavior may be approached.

The formulation of the theory of reference 5 and the form of the resulting stability relationship make it ideally suited for application to the case of axial compression and wall differential pressures. As may be seen in equation (7-33) of Section 7.2.2, the stability relationship is expressed in terms of applied running loadings,  $\bar{N}_x$  and  $\bar{N}_y$ , and various stiffness parameters  $A_{ij}$  involving material and geometric properties. Effects of eccentricities of the stiffening elements are included.

The digital computer program described in Section 18.3.2 was used to apply this stability relationship to three arbitrary examples of stiffened cylinder geometries which may be described in terms of the parameters defined in Section 18.3.2 as:

Example 1: (Typical Frame/Stringer Stiffened Configuration)

$R$	=	Cylinder Radius = 38.6 in.		
$a$	=	Overall Length = 72 in.		
$d$	=	Stringer Spacing = 2.48 in.		
$l$	=	Ring Spacing = 6.00 in.		
$E_x$	=	$1.5 \times 10^6$ lbs/in.	$E_y$	= $2 \times 10^6$ lbs/in.
$D_x$	=	250 lb-in.	$D_y$	= 300 lb-in.
$G_{xy}$	=	$2 \times 10^5$ psi	$D_{xy}$	= 200 lb-in.
$\mu_x'$	=	0.25	$\mu_y'$	= 0.35
$\mu_x$	=	0.30	$\mu_y$	= 0.40
$E_s$	=	$30 \times 10^6$ psi	$E_r$	= $25 \times 10^6$ psi.

$$G_s = 12 \times 10^6 \text{ psi.}$$

$$A_s = 0.020 \text{ sq. in.}$$

$$I_{os} = 0.005 \text{ in.}^4$$

$$J_s = 0.004 \text{ in.}^4$$

$$\bar{z}_s = 0$$

$$G_r = 10 \times 10^6 \text{ psi.}$$

$$A_r = 0.040 \text{ sq. in.}$$

$$I_{or} = 0.010 \text{ in.}^4$$

$$J_r = 0.006 \text{ in.}^4$$

$$\bar{z}_r = 0$$

Example 2: (Circumferentially Stiff Configuration)

Same as Example 1 except that:

$$l = \text{Ring Spacing} = 0.5 \text{ in.}$$

Example 3: (Longitudinally Stiff Configuration)

Same as Example 1 except that:

$$l = \text{Ring Spacing} = 72 \text{ in.}$$

Examples 1 through 3 neglected the effects of stiffener eccentricities and therefore apply for the case of stiffener centroids located at the skin midsurface. The following examples were also investigated including stiffener eccentricities.

Example 4: (Stiffening elements outside)

Same as Example 1 except that

$$\bar{z}_s = 0.50 \text{ in. and } \bar{z}_r = 0.75 \text{ in.}$$

Example 5: (Stiffening elements outside)

Same as Example 3 except that

$$\bar{z}_s = 0.50 \text{ in. and } \bar{z}_r = 0.75 \text{ in.}$$

Various critical combinations of axial compression ( $\bar{N}_x$ ) and external radial compression ( $\bar{N}_y$ ) were determined for each of the preceding examples so that interaction curves could be plotted. The results are tabulated in Table IX and plotted in Figure 20 where example numbers corresponding to Table IX are shown in parentheses. As may be seen in Figure 20, widely differing interaction relationships exist for combined axial compression and external radial pressure. Not only basic geometry affects the curves, but the inclusion of eccentricity can have a significant influence. It is likewise probable that boundary conditions, prebuckling deformations, and other influences affect the shape of the appropriate interaction curve for a given stiffened cylinder. In view of the unknowns involved, it is recommended that until more complete analyses become available, the following simple linear interaction relation be used for design:

$$R_x + R_y = 1.0 \quad (8-2)$$

The quantity  $R_x$  is the ratio of applied axial loading to the critical value of axial loading if acting alone and  $R_y$  is the ratio of applied circumferential loading to the critical value of circumferential loading if acting alone.

TABLE IX

Calculated Data for Interaction  
Example Configurations - Axial  
Compression and External Radial Pressure

EXAMPLE	$\bar{N}_y$	$\bar{N}_x$	m	n	$\frac{\bar{N}_y}{\bar{N}_{y_0}}$	$\frac{\bar{N}_x}{\bar{N}_{x_0}}$
1	0	7868	4	7	0	1
	309	7452	3	7	.25	.947
	567	5901	1	5	.459	.75
	619	5450	1	5	.50	.693
	791	3934	1	5	.639	.50
	928	2725	1	5	.75	.346
	1014	1967	1	5	.820	.25
	1237	0	1	5	1	0
2	0	15157	5	5	0	1
	1761	14536	5	5	.25	.959
	3521	13915	5	5	.50	.918
	4983	11368	1	3	.708	.75
	5282	9931	1	4	.75	.655
	5699	7579	1	4	.809	.50
	6371	3789	1	4	.905	.25
	7042	0	1	4	1	0
3	0	4089	1	6	0	1
	62	3282	1	7	.25	.803
	74	3066	1	7	.301	.75
	124	2215	1	7	.50	.542
	185	1148	1	7	.75	.281
	193	1022	1	7	.780	.25
	219	560	1	7	.888	.137
	247	0	1	8	1	0

TABLE IX  
(Continued)

Calculated Data for  
Interaction Example Configurations -  
Axial Compression and External  
Radial Pressure

EXAMPLE	$\bar{N}_y$	$\bar{N}_x$	m	n	$\frac{\bar{N}_y}{\bar{N}_{y_0}}$	$\frac{\bar{N}_x}{\bar{N}_{x_0}}$
4	0	8347	3	7	0	1
	266	7396	1	5	.25	.886
	395	6260	1	5	.371	.75
	533	5049	1	5	.50	.605
	632	4174	1	5	.593	.50
	799	2701	1	5	.75	.324
	868	2086	1	5	.816	.25
	1065	0	1	6	1	0
5	0	4301	1	6	0	1
	62	3405	1	7	.25	.792
	125	2326	1	7	.50	.541
	187	1247	1	7	.75	.290
	225	564	1	8	.90	.131
	250	0	1	8	1	0

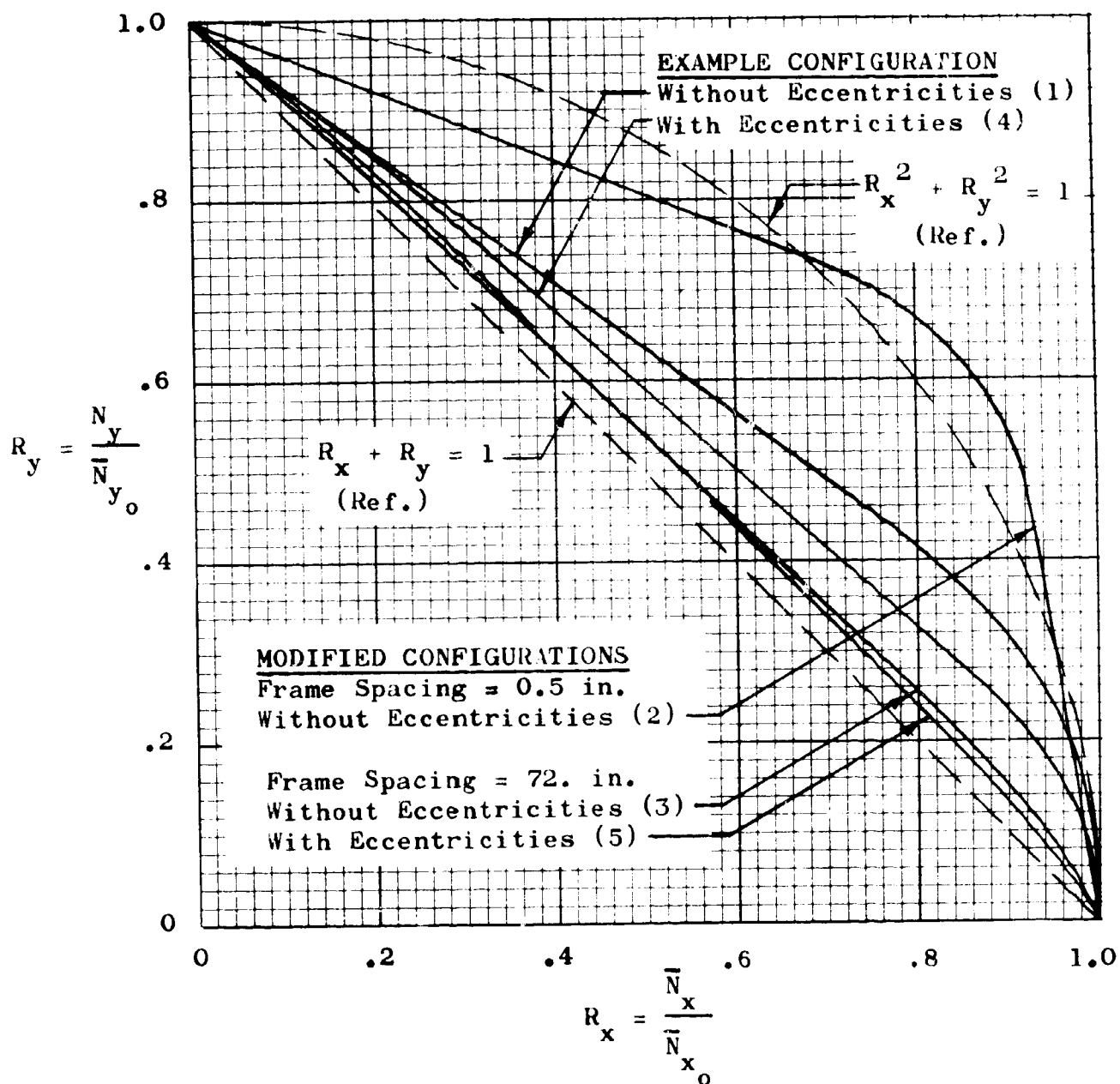


Figure 20 - Stability Interaction Results for  
 Combined Axial Compression and  
 External Radial Pressure



#### 8.4 Axial Compression and Internal Pressure

The procedures followed in Section 8.3 for external pressure were also applied to the case of internal pressure and axial compression. The theory of reference 5 was employed using the digital computer program of Section 18.3.2 of this report. This required that the prebuckling deformations caused by wall differential pressure and discreteness of stiffening elements be neglected.

The five example configurations listed in Section 8.3 were also used for the axial loading and internal pressure investigation. The results are shown in Table X and Figure 21 where the example numbers are shown in parentheses. The circumferential tensile loading due to internal pressure is shown nondimensionally in terms of the circumferential critical compressive loading. It can be seen that stiffening configuration and eccentricities play significant roles in the interaction and that each configuration has a unique curve or belongs to one of a family of curves. The identification of appropriate parameters to represent this interaction in families of curves was not attempted in this study so that the recommended procedure for analysis is to employ the computer program of Section 18.3.2 to obtain the indicated critical loading. The program may be used to find either the critical value of  $\bar{N}_y$  to support a given  $\bar{N}_x$  or a maximum  $\bar{N}_x$  for a given  $\bar{N}_y$ . The results from such an analysis must be used with caution because of the neglect of the pressure induced prebuckling deformations. However, the analysis supplies the best available estimate for combined axial compression and internal pressure and should give reasonable elastic estimates for many practical configurations. No known test data are available for comparison purposes which suggests a fertile area for future effort.

TABLE X

Calculated Data for Interaction  
Example Configurations - Axial  
Compression and Internal Radial Pressure

EXAMPLE	$\bar{N}_y$	$\bar{N}_x$	m	n	$\frac{\bar{N}_y}{\bar{N}_{y_0}}$	$\frac{\bar{N}_x}{\bar{N}_{x_0}}$
1	1237	0	1	5	1	0
	0	7868	4	7	0	1
	-309	8202	4	7	-.25	1.042
	-618	8535	4	7	-.50	1.085
	-1237	9189	4	6	-1	1.168
	-2474	10,071	5	7	-2	1.280
	-4948	11,339	5	6	-4	1.441
	-12369	13,809	6	5	-10	1.755
2	7042	0	1	4	1	0
	0	15,157	5	5	0	1
	-1761	15,665	6	5	-.25	1.034
	-3521	16,096	6	5	-.50	1.062
	-7042	16,958	6	5	-1	1.119
	-14085	18,245	7	4	-2	1.204
	-28170	19,866	7	4	-4	1.511
	-70424	22,989	9	3	-10	1.517
3	247	0	1	8	1	0
	0	4089	1	6	0	1
	-62	4569	2	8	-.25	1.118
	-124	4917	2	8	-.50	1.203
	-247	5427	3	8	-1	1.327
	-494	6046	3	8	-2	1.479
	-988	7033	4	8	-4	1.720
	-2470	8868	4	7	-10	2.196

TABLE X  
(Continued)

Calculated Data for Interaction  
Example Configurations - Axial  
Compression and Internal Radial Pressure

EXAMPLE	$\bar{N}_y$	$\bar{N}_x$	m	n	$\frac{\bar{N}_y}{\bar{N}_{y_0}}$	$\frac{\bar{N}_x}{\bar{N}_{x_0}}$
4	1065	0	1	6	1	0
	0	8347	3	7	0	1
	- 266	8661	4	7	-.25	1.038
	- 533	8948	4	7	-.50	1.072
	-1065	9523	4	7	-1	1.141
	-2131	10,265	5	7	-2	1.230
	-4262	11,303	6	6	-4	1.354
	-10654	13,117	7	5	-10	1.571
5	250	0	1	8	1	0
	0	4301	1	6	0	1
	- 62	4938	2	8	-.25	1.148
	- 125	5290	2	8	-.50	1.230
	- 250	5848	3	8	-1	1.360
	- 500	6474	3	8	-2	1.505
	- 1000	7360	4	8	-4	1.711
	- 2499	8947	5	7	-10	2.080

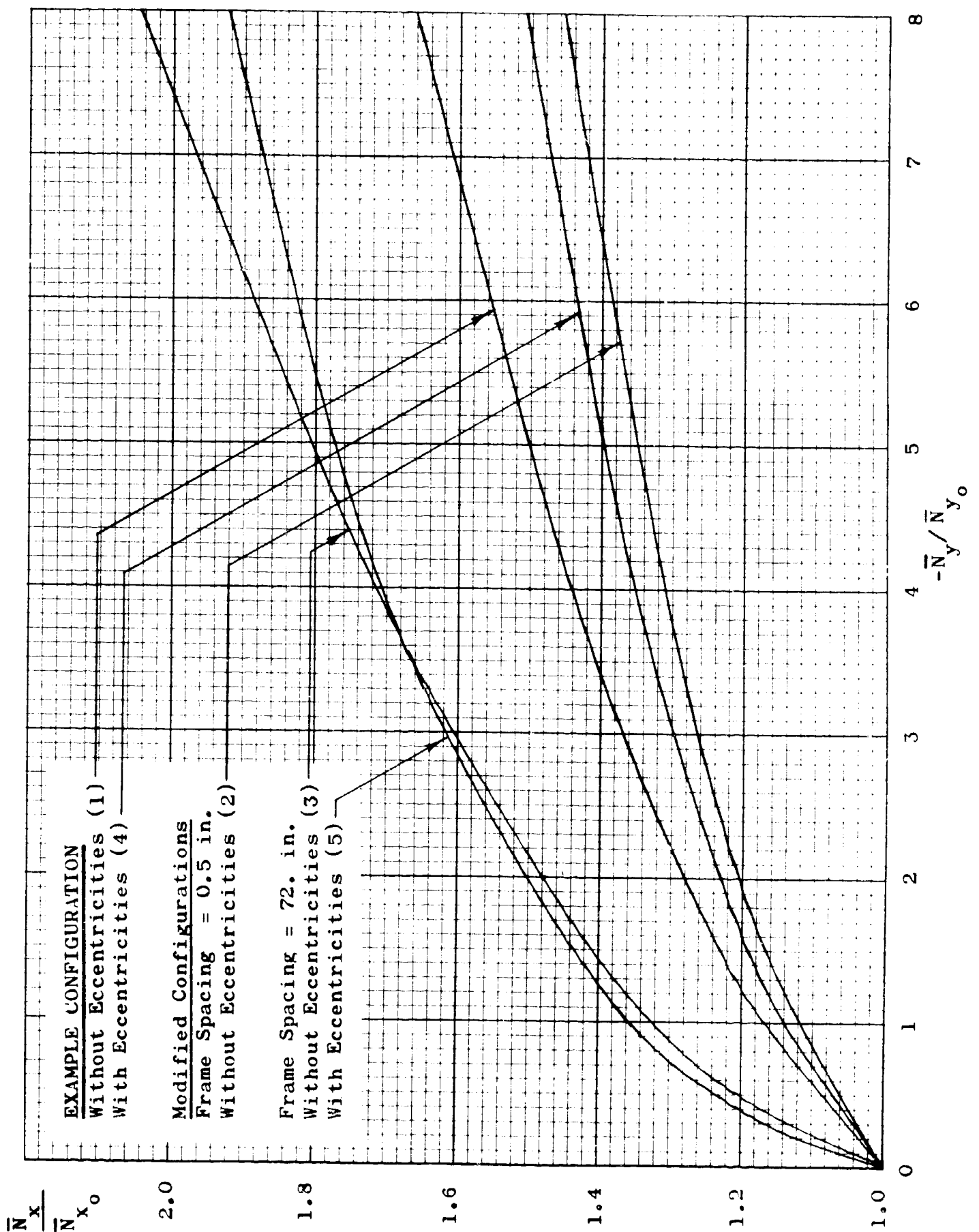


Figure 21 - Stability Interaction Results for  
Combined Axial Compression and  
Internal Radial Pressure

## 8.5 Axial Compression and Shear

The case of combined axial compression and shear is not covered by any of the theoretical approaches of this report since in-plane shear loadings are not included in the analyses. It would be expected that, as in the combined loading cases discussed in the previous paragraphs, geometry of stiffening, eccentricities, etc. would again influence the interaction relationship so that individual interaction curves or families of curves would be necessary to be accurate. No known theory or test results are available which are directly applicable to the case of axial compression and shear stability interaction for stiffened cylinders. The most applicable information appears in reference 44 which presents test data on interaction between pure bending and torsion on frame/stringer stiffened cylinders. Although the loading combination tested was pure bending with torsion rather than the desired combination of axial compression and shear, maximum applied stresses due to each loading are combined in both cases as contrasted, for example, to pure bending and transverse shear where maximum stresses occur in widely differing locations on the specimen. The results of tests from reference 44 are shown in Figure 22 which was taken from that reference. These results indicate interaction relations of the form

$$(\sigma/\sigma_0)^2 + (\tau/\tau_0)^2 = 1 \quad (8-3)$$

or

$$\sigma/\sigma_0 + (\tau/\tau_0)^2 = 1 \quad (8-4)$$

where

$\sigma$  = applied axial compressive stress

$\sigma_0$  = critical value of  $\sigma$  if acting alone

$\tau$  = applied shearing stress (torsion)

$\tau_0$  = critical value of  $\tau$  if acting alone

As may be seen in Figure 22, the data follow the trend of equations (8-3) or (8-4) depending upon stiffener spacing for the particular basic geometry tested. This further substantiates the influence of stiffening geometry on interaction relationships and implies that these two interaction relations can be unconservative for other geometries. Until adequate theory and/or tests become available for the case of stiffened cylinders under axial compression and shear, it is therefore recommended that the linear interaction relation be used for preliminary evaluations:

$$\frac{\sigma}{\sigma_0} + \frac{\tau}{\tau_0} = 1 \quad (8-5)$$

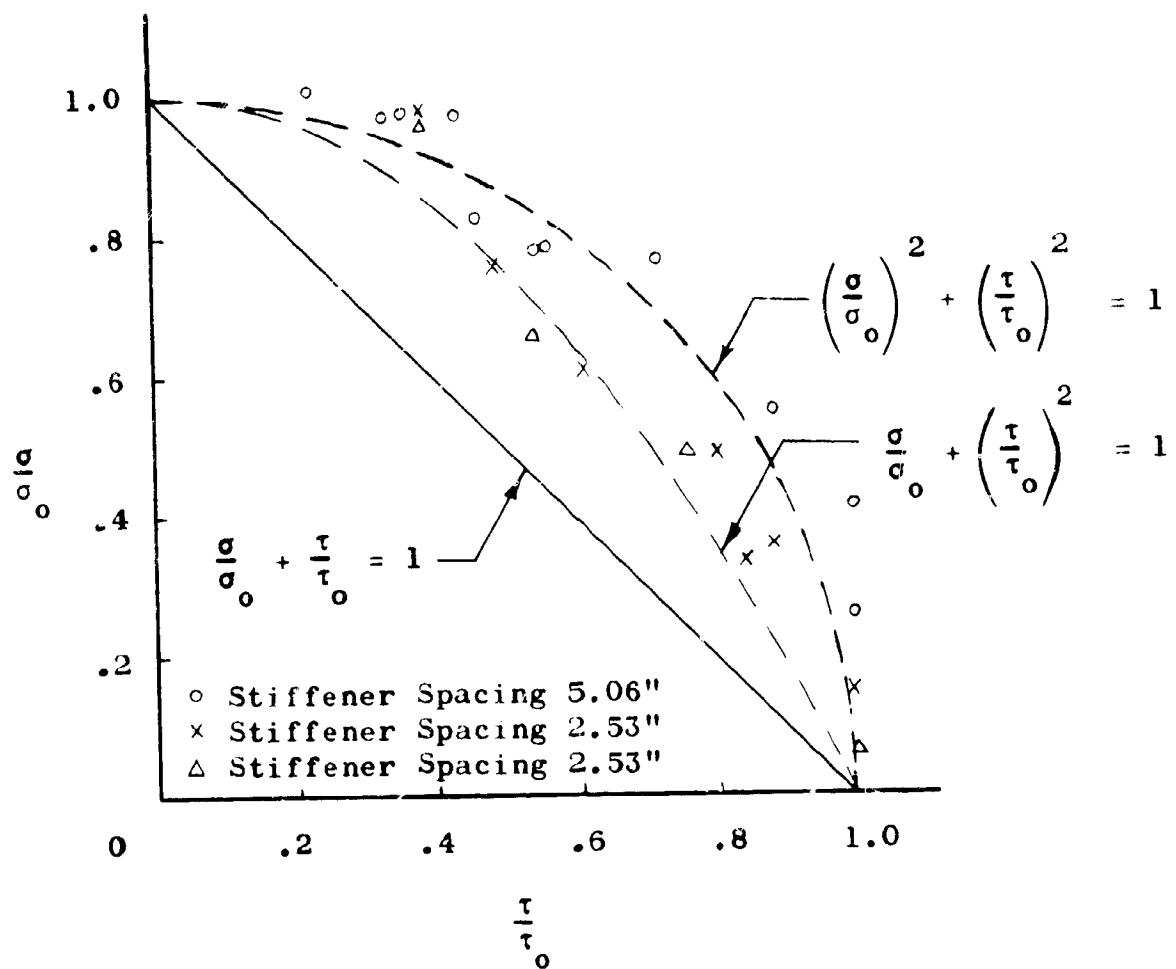


**Figure 22 - Interaction of Pure Bending  
and Torsion for Stiffened Cylinders**  
(data from reference 44)

## 9.0 INITIAL IMPERFECTIONS

For isotropic cylinders under axial compression, the wide disparity between classical theory and test results has frequently been blamed solely on initial imperfections and the shape of the postbuckling equilibrium path. However, recent theoretical and experimental investigations have identified that a significant portion of the difference can be attributed to test boundary conditions that differ from those assumed in the classical analysis. The current design practice for isotropic cylinders is to lump together both of these influences along with other known or unknown factors through the use of an empirical correlation (knock-down) factor. This factor is denoted here by the symbol  $\Gamma$ . Hence, the design buckling load for an isotropic cylinder may be established as follows:

$$\left(N_x\right)_{cr} = \Gamma \left(N_x\right)_{CL} \quad (9-1)$$

The factor  $\Gamma$  is generally recognized to be a function of the ratio  $R/t$ . Various sources have proposed different relationships in this regard. The differences here usually arise out of chosen statistical criteria or out of the particular test data selected as the empirical basis. For the purposes of this report, attention is called to reference 13 which develops a lower-bound criterion that can be presented in the manner of Figure 23. Note that the equation for the curve



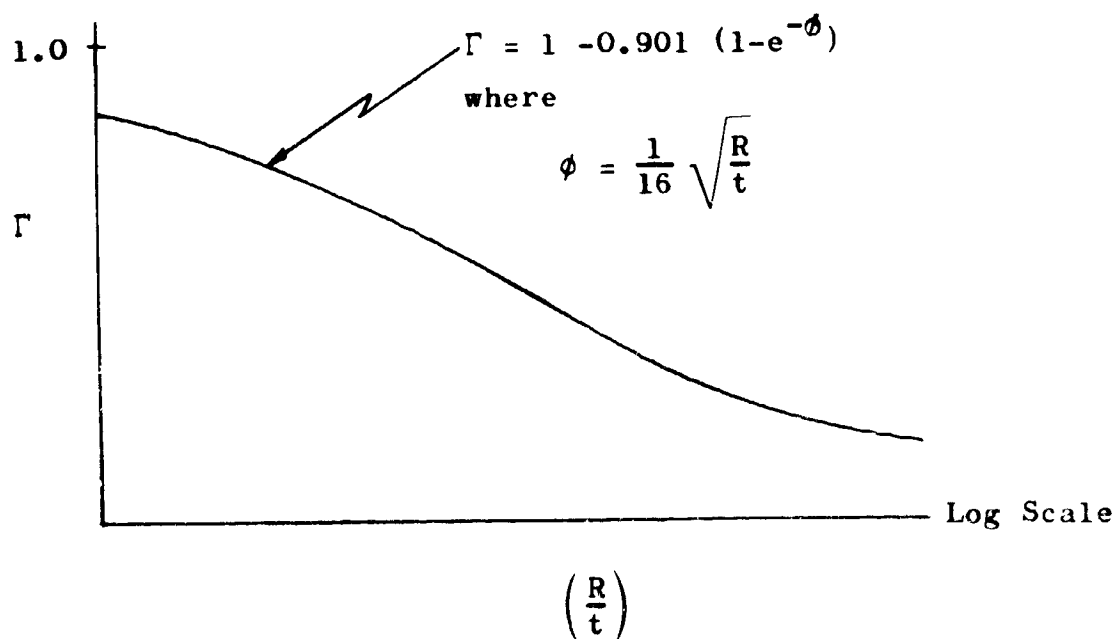


Figure 23 - Semi-Logarithmic Plot of  $\Gamma$  vs  $R/t$  For Unstiffened Isotropic Cylinders Under Axial Compression

in this figure may be written as follows:

$$\Gamma = 1 - 0.901 (1 - e^{-\phi}) \quad (9-2)$$

where

$$\phi = \frac{1}{16} \sqrt{\frac{R}{t}} \quad (9-3)$$

This same criterion was employed in the OPTION 1 analysis for the buckling of isotropic skin panels (See Section 5.0). Although written in slightly different form, equations (5-6) and (5-7) can be easily transformed into equations (9-1) through (9-3). Also note that this same criterion is recommended in reference 11.

For stiffened cylindrical shells, the limited available test data tends to indicate that the predictions from classical small-deflection theory are more nearly approached than in the case of thin-walled isotropic cylinders. This undoubtedly is the result of the stiffened configurations being effectively "thick". Therefore, the currently popular viewpoint is to consider small-deflection theory as directly applicable to many practical stiffened shells. Nevertheless, to account for uncertainties and to guard against reckless extrapolation into extreme parameter ranges, it is suggested here that a correlation (knock-down) factor be retained in the analysis of stiffened cylinders. This should result in reasonably conservative compressive strength estimates which can be confidently employed in the design of actual hardware. One of the major obstacles to a refined development of stiffened-cylinder correlation factors is the lack of sufficient test data for a thorough empirical determination. In the face of this deficiency, it becomes necessary to employ the isotropic data in conjunction with an effective thickness concept. For example, the curve of Figure 23 might be applied to stiffened cylinders if the ratio  $R/t$  is replaced by an appropriate  $R/t_{\text{eff}}$  ratio. The crux of the problem then reduces to the choice of a suitable criterion for the establishment of  $t_{\text{eff}}$ . Toward this end, note that, for the monocoque shell, the local radius of gyration of the shell wall can be expressed as follows:

$$\rho = \sqrt{\frac{I}{A}} = \sqrt{\frac{t^3}{12}} \div t = \frac{t}{\sqrt{12}} \quad (9-4)$$

This gives the following relationship:

$$t = \sqrt{12} \rho \quad (9-5)$$

It should be recognized that equation (9-5) gives the monocoque wall thickness that will provide a given local radius of gyration value. Most of the effective thickness concepts used for relating monocoque cylinder behavior to stiffened-shell mechanisms are based on this simple relationship. That is, it is assumed that equal sensitivity to initial imperfections, etc., results from equivalence of the local radii of gyration. However, this equivalence is rather difficult to establish for stiffened cylinders since the local  $\rho$  value usually is not the same in the longitudinal and circumferential directions. This requires the use of some type of averaging technique. The two most prominent techniques for this purpose are by Peterson in reference 45 and by Almroth in reference 20. It is noted that the former method is specified in the criterion of reference 11.

The effective thickness selected by Peterson bases the desired equivalence on the geometric mean of the longitudinal and circumferential radii of gyration for the stiffened cylinder. Converting into the notation of the present report, this leads to the expression

$$t_{\text{eff}} = \sqrt{12} \left[ \sqrt{D_{11} A_{11}} \sqrt{D_{22} A_{22}} \right]^{1/2} \quad (9-6)$$

or

$$t_{\text{eff}} = \left[ \left( \begin{smallmatrix} 1 & 4 & 4 \end{smallmatrix} \right) \left( \begin{smallmatrix} D_{11} & A_{11} \end{smallmatrix} \right) \left( \begin{smallmatrix} D_{22} & A_{22} \end{smallmatrix} \right) \right]^{1/4} \quad (9-7)$$

Section 15.0 specifies the proper means for computing the elastic constants  $A_{ij}$  and  $D_{ij}$  to be used in this equation. In the interest of clarity at this time, it is pointed out that the  $D_{ij}$  computations should not include the anticlastic correction  $(1-\nu^2)$ .

The effective thickness selected by Almroth [20] bases the desired equivalence on a stiffened shell radius of gyration which considers the arithmetic mean of the longitudinal and circumferential flexural stiffnesses. This leads to the expression

$$t_{\text{eff}} = \sqrt{12} \sqrt{\left( \frac{D_{11} + D_{22}}{2} \right) A_{11}} \quad (9-8)$$

$$t_{\text{eff}} = \sqrt{6 \left( D_{11} + D_{22} \right) A_{11}} \quad (9-9)$$

where once again the  $D_{ij}$  computations should not include the  $(1-\nu^2)$  correction. Equations (9-7) and (9-9) both reduce to  $t_{\text{eff}} = t$  in the special case of an isotropic monocoque cylinder. In addition, for stiffened cylinders having  $D_{11} = D_{22}$  and  $A_{11} = A_{22}$ , equations (9-7) and (9-9) will give identical results. For all other geometries, the two approaches will yield differing effective thicknesses.

The choice between the above two methods must be somewhat arbitrary in view of the lack of rigor in both. Therefore, primarily in the interest of conforming with the criterion of reference 11 it was decided to employ equation (9-7) in the procedures of Part II.

Once having used the appropriate  $R/t_{\text{eff}}$  ratio to find a numerical value for  $\Gamma$ , it then becomes necessary to decide upon the means by which this correction should be injected into the stiffened cylinder analysis. To shed some light on this question, reference is made to a presentation by Almroth [20]. Assuming that the shape of the postbuckling equilibrium path is of primary importance to this issue, Almroth suggests that this shape be reflected in the way  $\Gamma$  is introduced. In particular, the postbuckling curve is used to establish a correctable fraction of the total theoretical compressive strength. This concept is illustrated in the non-dimensional load-displacement curves shown in Figures 24 and 25. As implied by these figures, the postbuckling behavior of unstiffened and stiffened cylinders may greatly differ.

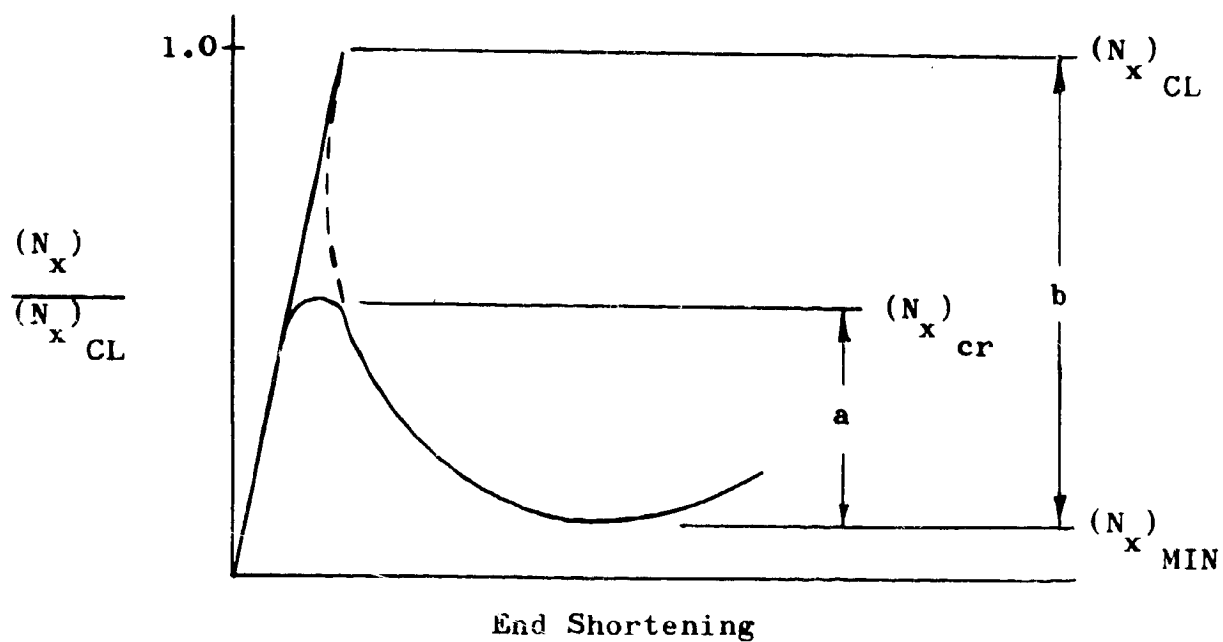


Figure 24 - Load-Displacement Curve For Example Monocoque Cylinder

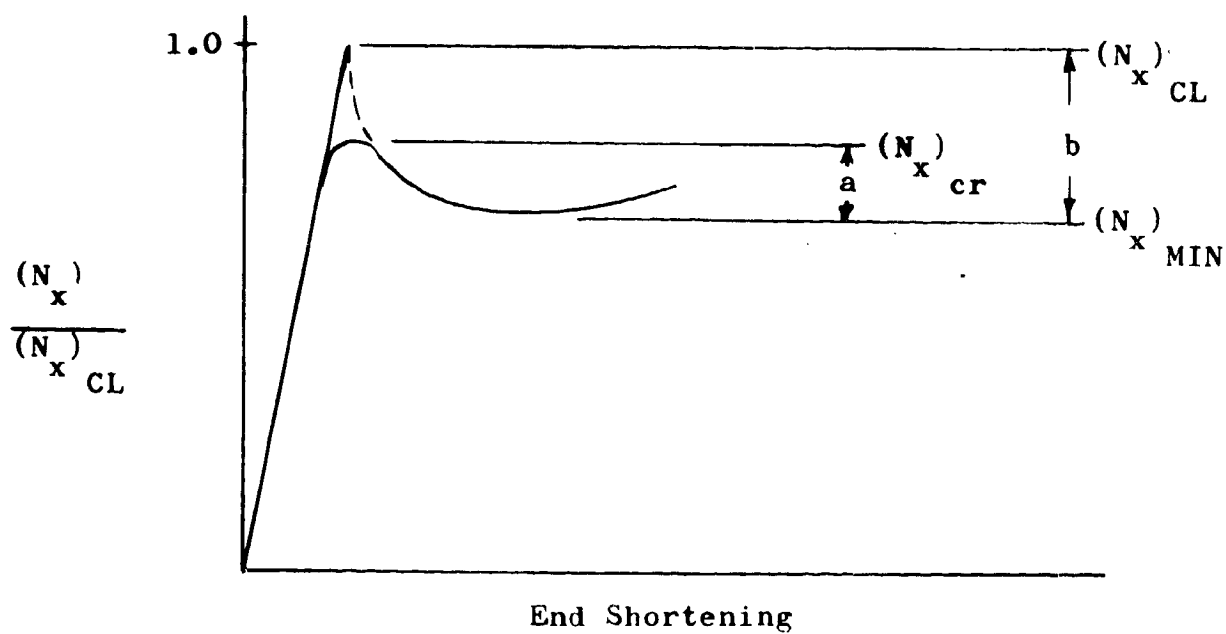


Figure 25 - Load-Displacement Curve For Example Orthotropic Cylinder

Almroth's proposal is that all cylinders which have the same  $\left(R/t_{\text{eff}}\right)$  values might be assumed to have identical values for the ratio

$$\frac{\left(N_x\right)_{\text{cr}} - \left(N_x\right)_{\text{MIN}}}{\left(N_x\right)_{\text{CL}} - \left(N_x\right)_{\text{MIN}}} = \frac{a}{b} \quad (9-10)$$

Assuming the minimum postbuckling strength for isotropic cylinders to be zero, this approach yields the following expression for the stiffened cylinders:

$$\left(N_x\right)_{\text{cr}} = \left(N_x\right)_{\text{MIN}} + \Gamma \left[ \left(N_x\right)_{\text{CL}} - \left(N_x\right)_{\text{MIN}} \right] \quad (9-11)$$

All of the  $N$ 's in this equation refer to the stiffened configuration. The formula presented by Almroth in reference 20 is slightly more complicated because of his assumption that the minimum postbuckling load for isotropic cylinders is  $.12 \left(N_x\right)_{\text{CL}}$ . This choice was based on an earlier Almroth paper [46]. However, Hoff, et al. [47] have subsequently contended that an increase in the number of terms used in the trigonometric series for the radial displacements significantly lowers the isotropic cylinder  $\left(N_x\right)_{\text{MIN}}$  value below that presented by Almroth. Hoff, et al. [47] interpret their own results to imply "that the minimal value of the compressive load, under which a large-displacement equilibrium is possible, is zero".

To properly apply equation (9-11), one must perform a post-buckling analysis of the stiffened cylinder to establish the applicable  $(N_x)_{\text{MIN}}$  value. However, this is considered to be beyond the scope and degree of complexity intended for the methods of this report. Therefore, as an engineering approximation, it will be assumed that  $(N_x)_{\text{MIN}}$  for a stiffened cylinder is the wide-column strength  $(N_x)_{\text{wc}}$  chosen as follows: Whenever the applicable slenderness ratio satisfies

$$\left(\frac{L}{\rho_{11}}\right) \geq \left(\sqrt{2C_F}\right)(\pi)\left(\sqrt{\frac{E}{\sigma_{cc}}}\right) \quad (9-12)$$

use

$$(N_x)_{\text{wc}} = \left[ \frac{C_F \pi^2 E t_{\text{an}}}{\left(\frac{L}{\rho_{11}}\right)^2} \right] (t_x) \quad (9-13)$$

Whenever the applicable slenderness ratio satisfies

$$\left(\frac{L}{\rho_{11}}\right) < \left(\sqrt{2C_F}\right)(\pi)\left(\sqrt{\frac{E}{\sigma_{cc}}}\right) \quad (9-14)$$

use

$$(N_x)_{\text{wc}} = \left[ \sigma_{cc} - \frac{\sigma_{cc}^2 \left(\frac{L}{\rho_{11}}\right)^2}{4C_F \pi^2 E} \right] (t_x) \quad (9-15)$$

These equations are applied to the wide column obtained by unfolding the composite circular wall into a flat configuration, retaining equivalent boundary constraint. Equation (9-11) may then be rewritten as follows:

$$(N_x)_{\text{cr}} = (N_x)_{\text{wc}} + \left[ (N_x)_{\text{CL}} - (N_x)_{\text{wc}} \right] \quad (9-16)$$



For the analysis of general instability (see Glossary), the entire overall length  $L$  is used in equations (9-12) through (9-15) regardless of the ring spacing  $a$ . In such cases, the  $(N_x)_{wc}$  value will usually be small and its influence in equation (9-16) will not be very significant. However, for cylinders which are stiffened only in the longitudinal direction, the situation will usually be quite different. Although these structures still employ the overall length  $L$  in the wide-column computation, the  $(N_x)_{wc}$  component will usually comprise a major part of the total compressive strength. The remaining possibility of interest to this report is the situation encountered in the analysis of panel instability (see Glossary) in cylinders that incorporate both longitudinal and circumferential stiffening. In this case, one is concerned with the behavior of longitudinally stiffened sections that lie between rings and the wide-column component is calculated by inserting  $L = a$  into equations (9-12) through (9-15). Here again, the usual result is that  $(N_x)_{wc}$  comprises a major portion of the total resistance to instability.

The concept expressed in the form of equation (9-16) furnished the basis for the final equations of Section 6.2.2. As noted there, this approach is consistent with the method originally proposed by Peterson and Dow [22] for the analysis of longitudinally stiffened cylinders.

In conclusion, it is noted that the foregoing discussion has been confined to pure axial loading, and that equations (9-2) and (9-3) apply

only to this case. For pure bending, different equations should be used to evaluate the correlation (knock-down) factor  $\Gamma$ . These are as follows:

$$\Gamma = 1 - 0.731 (1 - e^{-\phi}) \quad (9-17)$$

where

$$\phi = \frac{1}{16} \sqrt{\frac{R}{t}} \quad (9-18)$$

This formulation recognizes a reduced probability for the peak bending stress to coincide with the location of an imperfection.

SECTIONS 10.0 THROUGH 19.0 ARE PRESENTED  
IN VOLUME II. FOR CONVENIENCE, SECTION  
19.0, REFERENCES, IS ALSO PRESENTED IN  
VOLUME I.

19.0 REFERENCES

1. DeLuzio, A. and Lunsford, L. R., "Theoretical and Experimental Analysis of Orthotropic-Shell Stability," Contract NAS 8-9500, Lockheed Missiles and Space Company Report LMSC- A701014, 11 September 1964.
2. Anonymous, "Structural Panel Stability Development Program, Final Report, Phase I," Contract NAS 8-9500, Lockheed Missiles and Space Company Report LMSC-A746888, 30 April 1965.
3. Anonymous, "Structural Panel Stability Development Program," Contract NAS 8-9500, Lockheed Missiles and Space Company Report LMSC-A770422, 30 October 1965.
4. Card, M. F., "Preliminary Results of Compression Tests on Cylinders with Eccentric Longitudinal Stiffeners," NASA TMX-1004, September 1964.
5. Block, D. L., Card, M.F. and Mikulas, M. M., Jr., "Buckling of Eccentrically Stiffened Orthotropic Cylinders," NASA TN D-2960, August 1965.
6. Schapitz, E., Festigkeitslehre für den Leichtbau, 2 Aufl., VDI-Verlag GmbH Düsseldorf, 1963.
7. Shanley, F. R., "Simplified Analysis of General Instability of Stiffened Shells in Pure Bending," Journal of the Aeronautical Sciences, October 1949.
8. Cheatham, J. F., "Buckling Characteristics of Corrugated Cylinders," Part II - Summary, Watertown Arsenal Technical Report No. WAL TR 715/3-Pt. 2, July 1960.
9. Zahn, J. J. and Kuenzi, E. W., "Classical Buckling of Cylinders of Sandwich Construction in Axial Compression - Orthotropic Cores," Forest Products Laboratory Report FPL-018, November 1963.
10. Stuhlman, C. E., "Computer Program for Integrally Stiffened Cylinders Under Axial Compression," Contract NAS 8-9500, Lockheed Missiles and Space Company Report LMSC- A740914, Rev. 1, 23 October 1965.
11. Anonymous, "Buckling of Thin-Walled Circular Cylinders," NASA Space Vehicle Design Criteria, NASA SP-8007, September 1965.

12. Timoshenko, S. P. and Gere, J. M., Theory of Elastic Stability, McGraw-Hill Book Company, Inc., New York, 1961.
13. Seide, P., Weingarten, V. I., and Morgan, E. J., "Final Report on the Development of Design Criteria for Elastic Stability of Thin Shell Structures," STL-TR-60-0000-19425, 31 December 1960.
14. Schumacher, J. G., "Development of Design Curves for the Stability of Thin Pressurized and Unpressurized Circular Cylinders," General Dynamics Convair Report No. AZS-27-275, Revision B, 22 July 1960.
15. Gerard, G. and Becker, H., "Handbook of Structural Stability, Part I - Buckling of Flat Plates," NACA TN 3781, July 1957.
16. Peterson, J. P., Whitely, R. O., and Deaton, J. W., "Structural Behavior and Compressive Strength of Circular Cylinders with Longitudinal Stiffening," TN D-1251, May 1962.
17. Cox, H. L. and Clenshaw, W. J., "Compression Tests on Curved Plates of Thin Sheet Duralumin," British A.R.C. Technical Report R. & M. No. 1894, November 1941.
18. Langhaar, H. L., "General Theory of Buckling," Applied Mechanics Reviews, Vol. 11, No. 11, November 1958, p. 585.
19. Thielemann, W. F., "New Developments in the Nonlinear Theories of the Buckling of Thin Cylindrical Shells," Proceedings of the Durand Centennial Conference, Held at Stanford University, 5-8 August 1959, Pergamon Press, New York, 1960.
20. Almroth, B. O., "Buckling of Orthotropic Cylinders Under Axial Compression," Lockheed Missiles and Space Company Report LMSC-6-90-63-65, June 1963.
21. Almroth, B. O., "Postbuckling Behavior of Orthotropic Cylinders Under Axial Compression," AIAA Journal, Vol. 2, No. 10, October 1964, pp 1795-1799.
22. Peterson, J. P. and Dow, M. B., "Compression Tests on Circular Cylinders Stiffened Longitudinally by Closely Spaced Z-Section Stringers," NASA Memo 2-12-59L, March 1959.

GENERAL DYNAMICS  
Convair Division

23. DeLuzio, A. J., Stuhlman, C. E., and Almroth, B.O., "Influence of Stiffener Eccentricity and End Moment on the Stability of Cylinders in Compression," Paper Presented at AIAA 6th Structures and Materials Conference, Palm Springs, Calif., April 5-7, 1965.
24. Ramberg, W. and Osgood, W. R., "Description of Stress-Strain Curves by Three Parameters," NACA TN 902, July 1943.
25. Budiansky, B., Seide, P., and Weinberger, R. A., "The Buckling of a Column on Equally Spaced Deflectional and Rotational Springs", NACA TN 1519, March 1948.
26. Smith, G. W., "Analysis of Multiple Discontinuities in Shells of Revolution Including Coupled Effects of Meridional Load", General Dynamics Convair Report Number GD/A 63-0044, 31 July 1963.
27. Anon., NASA (MSFC) Structures Manual, Page 17, Section C1, 25 May 1961.
28. Balog, E. M., "Subscale Intertank Structural Test Program", Boeing Document No. T5-6029, Vol's. 1 and 2, 12 August 1965.
29. Card, M. F., "Bending Tests of Large-Diameter Stiffened Cylinders Susceptible to General Instability", NASA TN D-2200, April 1964.
30. Dunn, L. G., "Some Investigations of the General Instability of Stiffened Metal Cylinders", NACA Technical Note No. 1198, November 1947.
31. Hoff, N. J., Boley, B. A., and Nardo, S. V., "The Inward Bulge Type Buckling of Monocoque Cylinders", NACA Technical Note No. 1499, September 1948.
32. Becker, H., "Handbook of Structural Stability, Part VI - Strength of Stiffened Curved Plates and Shells", NACA Technical Note 3786, July 1958.
33. Stein, M. and Mayers, J., "Compressive Buckling of Simply Supported Curved Plates and Cylinders of Sandwich Construction", NACA Technical Note 2601, January 1952.
34. Flügge, W., Stresses in Shells, Springer-Verlag, Berlin, 1962.

35. Hetenyi, M., Beams on Elastic Foundation , University of Michigan Press, Ann Arbor, 1955.
36. Roark, R. J., Formulas for Stress and Strain , Third Edition, McGraw-Hill Book Company, Inc., New York, 1954.
37. Boley, B. A., "The Shearing Rigidity of Buckled Sheet Panels", Journal of the Aeronautical Sciences, June 1950.
38. Lakshmikantham, C., Gerard, G., and Milligan, R., "General Instability of Orthotropically Stiffened Cylinders , Part II, Bending and Combined Compression and Bending", Air Force Flight Dynamics Laboratory Technical Report AFFDL TR 65 161, Part II.
39. Hedgepeth, J. M. and Hall, D. B., "Stability of Stiffened Cylinders", AIAA Journal, Vol. 3, No. 12, December 1965.
40. Flügge, W., "Die Stabilität der Kreiszyinderschale", Ingenieur-Archiv, Vol. 3, 1932, pp. 463-506.
41. Timoshenko, S., Theory of Elastic Stability , McGraw-Hill Book Company, Inc., New York, N. Y., 1932, pp 463-467.
42. Seide, P. and Weingarten, V. I., "On the Buckling of Circular Cylindrical Shells Under Pure Bending", Trans. of the ASME, Journal of Applied Mechanics, March 1961.
43. Horton, W. H. and Cox, J. W., "The Stability of Thin-Walled Unstiffened Circular Cylindrical Shells Under Nonuniformly Distributed Axial Load", Stanford University, Department of Aeronautics and Astronautics, Report SUDAER No. 220, February 1965.
44. Anon., "Some Investigations of the General Instability of Stiffened Metal Cylinders, VII - Stiffened Metal Cylinders Subjected to Combined Bending and Torsion", NACA Technical Note No. 911, November 1943.
45. Peterson, J. P., "Weight-Strength Studies of Structures Representative of Fuselage Construction", NACA Technical Note 4114, October 1957.
46. Almroth, B. O., "Postbuckling Behavior of Axially Compressed Circular Cylinders", AIAA Journal, Vol. 1, No. 3, March 1963.
47. Hoff, N. J., Madsen, W. A., and Mayers, J., "The Postbuckling Equilibrium of Axially Compressed Circular Cylindrical Shells", Stanford University Department of Aeronautics and Astronautics, Report SUDAER No. 221, February 1965.

END

DATE

FILMED

AUG 21 1966